STEADY STATE ANALYSIS OF CURRENT SOURCE INVERTER FED INDUCTION MOTOR DRIVE

A DISSERTATION

submitted in partial fulfilment of the
requirement for the award of the degree
of
MASTER OF ENGINEERING
in
Power Apparatus and Electric Drives

By

OM HARI PANDE

CHECKED
1985

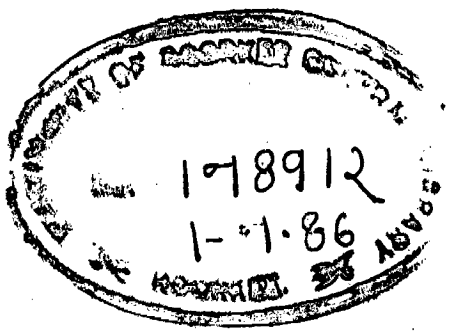

DEPARTMENT OF ELECTRICAL ENGINEERING
UNIVERSITY OF ROORKEE
ROORKEE - 247 667 (INDIA)

February, 1986

CANDIDATE'S DECLARATION

I hereby certify that the work which is being presented in the dissertation entitled, 'STEADY STATE ANALYSIS OF CURRENT SOURCE INVERTER FED INDUCTION MOTOR DRIVE', in partial fulfilment of the requirements for the degree of MASTER OF ENGINEERING IN ELECTRICAL ENGINEERING (Power Apparatus and Electric Drives) submitted in the Department of Electrical Engineering, University of Roorkee, Roorkee, is an authentic record of my own work carried out during a period of 9 months from April 1985 to Jan. 1986, under the supervision of Sri S.P. Gupta, Reader Electrical Engineering Department, University of Roorkee, Roorkee.

The matter embodied in this dissertation has not been submitted for the award of any other degree or diploma.

(OM HARI PANDE)

This is to certify that the above statement made by the candidate is correct to the best of my knowledge.

(S.P. GUPTA)
Reader
Electrical Engineering Department
University of Roorkee,
Roorkee

ROORKEE

Dated: Feb. 15 ,1986

ACKNOWLEDGEMENT

I am highly indebted to Sri S.P. Gupta, Reader in Department of Electrical Engineering, for invaluable assistance, excellent guidance, he rendered to me during the dissertation work. It was his sincere advice and highly inspiring words at most critical moments, which have enabled me to present the work in this shape. It was a pleasure to work under him during the tenure of this work.

I am very grateful to Dr. V.K. Verma, Professor in Department of Electrical Engineering for invaluable discussions which I had with him from time to time during this work.

I am thankful to Dr. P. Mukhopadhyay, Professor and Head, Electrical Engineering Department, University of Roorkee, Roorkee, for providing computer and calcomp plotter facilities.

I am also very much thankful to all the laboratory and workshop staff for their excellent co-operation during the work.

In the last, thanks are also very much due to Pramod Agrawal, my friend who helped me at various stages during the work.

(OM HARI PANDE)

ABSTRACT

This dissertation concerns an induction motor drive fed from a constant current source realized by a 3ϕ full controlled rectifier feeding a 3ϕ inverter. It describes the analytical and experimental studies of the drive in the steady-state operating condition.

The work in the beginning describes the progress made in the field of current source inverter fed induction motor drives so far. The various configurations of current-source inverter are discussed in Chapter II alongwith the current source inverter operation in auto-sequential mode.

The requirement of firing pulses for auto-sequential current source inverter are discussed in Chapter III. In this chapter a suitable firing circuit which fulfills the above requirement is also developed. The design of the different blocks of firing circuit is given and oscillograms of firing circuit are discussed. The guide lines for the selection of various components of the drive are presented in Chapter IV.

In Chapter V, the system equations in Concordia's per unit system are developed and a suitable mathematical model is formulated for steady-state analysis of the drive. Chapter VI deals with the steady-state analysis of the

drive. The system equations are written for steady-state operation and solved with the help of computer to obtain the steady-state performance of the drive with slip as independent parameter at different p.u. operating frequencies and d.c. link currents. Results of this analysis are plotted and discussed.

The results of experimental investigation of the fabricated system are presented in Chapter VII. These incorporate the experimental observations and oscillograms of current source inverter at resistive and induction motor load. The observations at induction motor load are obtained at different operating frequencies and d.c. link currents.

The experimental oscillograms incorporate the oscillograms of line voltage, line current and of voltage drop at different points of inverter circuit.

The oscillograms of line voltage and line current are compared with the ideal one and causes of discrepancies between the two are discussed. The effect of change of load and operating frequency on voltage and current waveforms is also shown with the help of oscillograms and discussed.

LIST OF SYMBOLS

H	inertia constant of induction motor in second
G	rated power output of induction motor
I_R	current in d.c. link
J	polar moment of inertia
P	number of poles
R_F	d.c. link inductor resistance
T_e	electromagnetic torque
T_L	load torque
V_{as}, V_{bs}, V_{cs}	induction motor phase voltages
V_I	inverter input voltage
V_R	output voltage of controlled rectifier
X_{CO}	commutating reactance
X_F	inductive reactance of d.c. link inductor
X_m	mutual reactance at base frequency
X_r	rotor self reactance at base frequency
X_s	stator self reactance of induction motor at base frequency
f_b	base frequency in Hertz
i_{as}, i_{bs}, i_{cs}	stator phase currents
r_r	rotor resistance per phase

r_s	stator resistance per phase
t	time in seconds
V_I	input voltage to inverter
α	firing angle of controlled rectifier
θ_e	angular position of synchronous reference frame
θ_r	angular position of rotor
ω_b	base angular frequency
ω_r	rotor speed
ω_{sl}	slip speed of induction motor
s	slip of induction motor
suffix 0	represents variables in steady-state operation
suffix b	represents base quantities
suffix d,q	direct and quadrature axis quantities
suffix r	rotor quantity
suffix s	stator quantity

CONTENTS

.....

CHAPTER I

INTRODUCTION

1.1. LITERATURE REVIEW

The aggregate of electric motor, the energy transmitting shaft and the control equipment by which the motor characteristics are adjusted and their operating conditions with respect to mechanical load varied to suit particular requirements, is called an electric drive. The drive together with the load constitutes the drive system.

From the very beginning, d.c. motors have been considered workhorses in industry for variable speed applications. Though the control principle and the converter equipment are somewhat simple, the d.c. machine has the following drawbacks [17]:

(i) increased cost for KVA and decreased power/weight ratio as compared to their a.c. counterpart due to commutator,

(ii) accentuated sparking at high currents and speeds,

(iii) limited armature voltage rating,

(iv) limited armature current rating due to commutation problem,

(v) unsuitable to operate in dusty and explosive environment and require frequent maintenance,

The above deficiencies obviously cannot be tolerated in many industrial applications. A suggested alternative is to use a cage induction motor, operating at variable frequency and supplied from a static frequency converter. The use of a cage induction motor has the following advantages:

(i) Its construction is simple and robust

(ii) Comparatively less cost per KVA as compared to d.c. counterpart

(iii) The power/weight ratio is about twice that of d.c. motor

Although the cage induction motor has the above advantages, the cost of control equipment is considerably higher and the control techniques are very complex. The research and development efforts in a c. drives technology has been focused recently on solving the above problems. As a result of availability of improved voltage and current rating thyristors and the trend of their prices to come down day by day in the recent years, people have shown considerable interest in variable speed induction motor drives and in the recent years, many new techniques, suitable for speed control of induction motor have been developed.

The basic well known techniques through which efforts are made to obtain a suitable variable speed induction motor drive are,

(a) Stator voltage/current and frequency control

(b) Rotor power control

(c) Stator voltage control

(d) Rotor impedance control

Among all the above control techniques only (a) and (c) are applicable in case of cage induction motor.

At steady-state, an induction motor may be characterised by a transformer equivalent circuit and the following approximate performance expressions can be derived.

$$I_s \simeq I_r \simeq \frac{(V_s/\omega_e)\omega_{sl}}{(R_r^2 + \omega_{sl}^2 L_{lr}^2)^{1/2}} \qquad \ldots(1.1)$$

Here $\omega_{sl} = s\,\omega_e$.

$$T_e \simeq \frac{3P}{2} \left(\frac{V_s}{\omega_e}\right)^2 \frac{\omega_{sl} R_r}{R_r^2 + \omega_{sl}^2 L_{lr}^2} \qquad \ldots(1.2)$$

$$Po \simeq 3 I_r^2 R_r \left(\frac{\omega_e}{\omega_{sl}} - 1\right) \qquad \ldots(1.3)$$

$$\phi_g \simeq K \frac{V_s}{\omega_e} \qquad \ldots(1.4)$$

Where all the symbols are in standard notation. From (1.1) and (1.2) torque per ampere may be expressed as,

$$\frac{T_e}{I_s} \approx \frac{3P}{2} \cdot \frac{V_s}{\omega_e} \cdot \frac{R_r}{(R_r^2 + \omega_{sl}^2 L_{lr}^2)^{1/2}} \qquad \ldots(1.5)$$

The various speed control techniques are now reviewed in brief.

Stator voltage control technique provide a simple and economical method of speed control of cage type induction motors. The drive system characteristics are shown in Fig. (1.1) with variable stator voltage but at constant supply frequency along with a load torque curve of a pump or blower type load. The motor with high rotor resistance is normally used in this method of speed control, which correspondingly, causes higher copper loss in the machine.

This may be expanded as below [5]. Assuming sinusoidally varying quantities, the average torque produced by the stator field reacting with rotor current is given by,

$$T_M = \frac{I_r^2 R_r}{s} \qquad \ldots(1.6)$$

where T_M is the motor developed torque.

Neglecting the magnetising current associated with the stator winding, the input current (I_s) is proportional to the rotor current. Consideration of how the rotor current varies with slip will therefore indicate how the rotor and stator I^2R losses may vary.

$$\Rightarrow T_M \alpha \frac{I_s^2 R_r}{s} \qquad \ldots(1.7)$$

Considering a fan load, the load torque will be proportional to the square of the motor speed. This

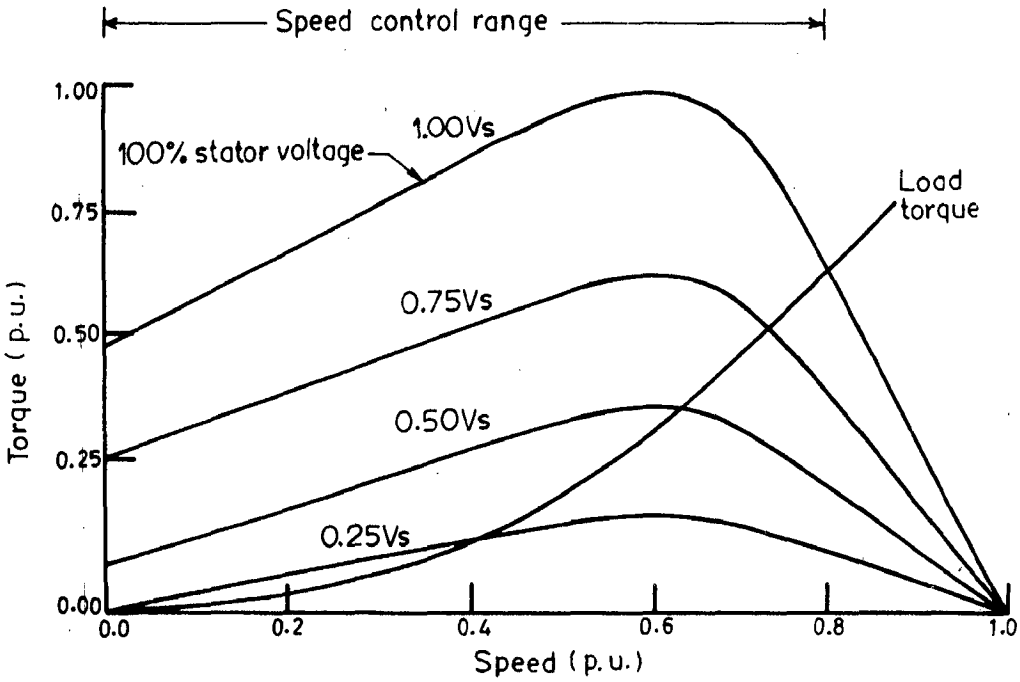

Fig.1.1_ Variable voltage torque - speed curves .

proportionality gives,

$$T_L \alpha (\text{rotor speed})^2 \alpha (1 - s)^2 \qquad \ldots(1.8)$$

where T_L is the load torque.

Now at the steady operating condition the motor and load torques will be equal. Therefore combining the equations (1.7) and (1.8) we get,

$$I_s \alpha \frac{(1 - s)\sqrt{s}}{\sqrt{R_r}} \qquad \ldots(1.9)$$

The equation (1.9) points at the following two conclusions:

(i) The input current increases as speed is reduced and becomes maximum for fan type load when $s = 1/3$.

(ii) The input current is inversely proportional to (rotor resistance)$^{1/2}$ i.e. $I_s \alpha \frac{1}{\sqrt{R_r}}$

Fig. (1.2) has been drawn to illustrate the increase to be expected in the input currents of fan motors controlled by varying the supply voltage. Using the curve in fig. (1.2), it is seen, for example, that a motor with a normal full load slip of 12 percent will have a maximum input current about 25 percent greater than the normal full load current. It can also be noted that rotor and stator losses will increase by about 56 percent..

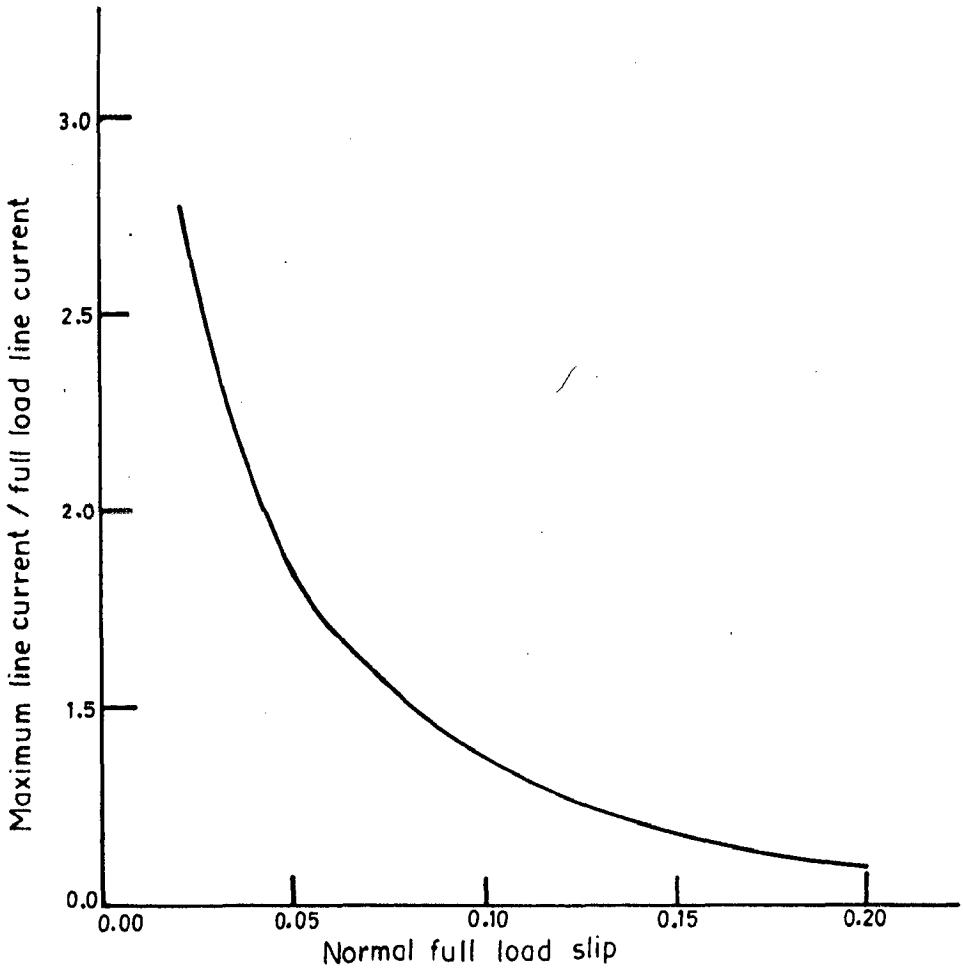

Fig. ~~13~~ 1·2 Relating motor full load slip to peak line current for fair load.

The conclusions to be drawn from the foregoing theory can be summarized as follows. If the rotor resistance is low and motor full load slip is also low, then heating problems of the stator winding may be expected as the speed is reduced because of the large increase of input current. The best practical solution to this problem is to use the machines with high resistance rotors.

One of the methods to accomplish above said type of control is the variable voltage control by thyristors [2, 3] used for sybsynchronous speed control. In this scheme, normally one pair of SCR$_s$ connected in inverse parallel are inserted in each of the three phases of stator winding and the effective voltage delivered to the motor can be varied from zero to full supply voltage by controlling the conduction periods of the SCRs. The motor is subjected to a chopped sine-wave voltage and the supply currents also have a high harmonic current, but satisfactory operation has been achieved with small and medium sized induction motors up to 100 h.p., or more. Stator voltage control is cheaper to install but operating efficiency is poor, and de-rating is necessary at low speeds to avoid over heating due to excessive current and reduced ventilation. Therefore this technique is normally used for fractional horsepower drives, and also for a.c. - powered cranes and hoists where large torque at high slip is only demanded for intermittent portions of the duty cycle.

The most versatile method giving efficient wide-range speed control is the variable frequency control of induction motor [2, 11]. The variable frequency supply alters the synchronous speed of the induction motor.

Induction motors used in the static variable frequency drive systems have the operating characteristics and features which meet the requirements of modern variable speed drive systems. Some of these are the capability of operation at very high and low speeds, at high torque and overloads, in a constant power or torque mode, and in the negative torque region for dynamic braking.

The variable frequency operation of an induction motor is obtained by the use of frequency converter. A frequency converter is a device that can convert the input supply to an a.c. supply of variable frequency and variable voltage. The rotating type of frequency converters were used previously but now they are obsolete and are replaced by the solid-state frequency converters.

The static frequency converters are divided into two categories:

(i) Cyclo converters

(ii) D.C. link converters

A cyclo converter converts a.c. supply of fixed frequency to a lower output frequency through a one step

conversion process. It can be programmed to generate variable voltage, variable frequency power to drive an induction motor. The output frequency range is limited to one third of the supply frequency and therefore the drives employing cyclo-converters are suitable only for operation at low frequency. The output voltage of cyclo-converter contains complex harmonic patterns. However one advantage of cyclo-converter drive is that regeneration is simple and the system can be easily designed for four-quadrant operation. The cyclo-converter drives are normally used in very large power applications. The cost and complexity of power and control circuits make them uncompetitive with other classes of drives in general applications.

A d.c. link converter is a two stage conversion drvice in which power from the a.c. network is first rectified to d.c. and then inverted to obtain a.c. voltage at variable frequency. This type of inverter can operate over a large frequency range and is suitable for wide-range speed control drives. However this type of inverter employing thyristors requires additional commutation circuits and is, therefore, complicated. Also for regeneration capability, it requires additional circuits and hence, the cost and complexity are increased.

In general for wide range speed control where regenerative braking is not essential a d.c. link converter fed induction motor is the best choice.

If the stator supply frequency is increased to increase speed of the machine, the airgap flux is reduced which correspondingly reduces the developed torque of the machine. If speed control is desired with full torque capability, the rated airgap flux must be maintained (as in a d.c. shunt motor), i.e., the supply voltage should increase proportional to the frequency. An advantage in rated airgap flux mode of speed control is that the torque sensitivity per ampere of current is maximum which permits fast transient response of the system. The torque-speed curves of induction motor with variable voltage, variable frequencies are shown in Fig. (1.3). The motor used in this type of drive has low slip characteristic which results in improved efficiency. Below the base speed (1.0 P.U.) the region is defined as constant torque region, where rated airgap flux is maintained by a constant volts/hertz ratio resulting in constant pull out torque capability. At very low frequency, the stator resistance dominates over the leakage reactance, and therefore, additional voltage is impressed to maintain the flux. At base speed, the full motor voltage is applied, and beyond this point, as frequency is increased, the torque diminishes due to loss of the aigrap flux. In this region the machine is said to operate in constant power mode.

Thus a control scheme in which the rotor slip frequency is directly controlled while maintaining the constant air-gap flux, the drive can exhibit a precise control and adjustment of torque at any speed. In a

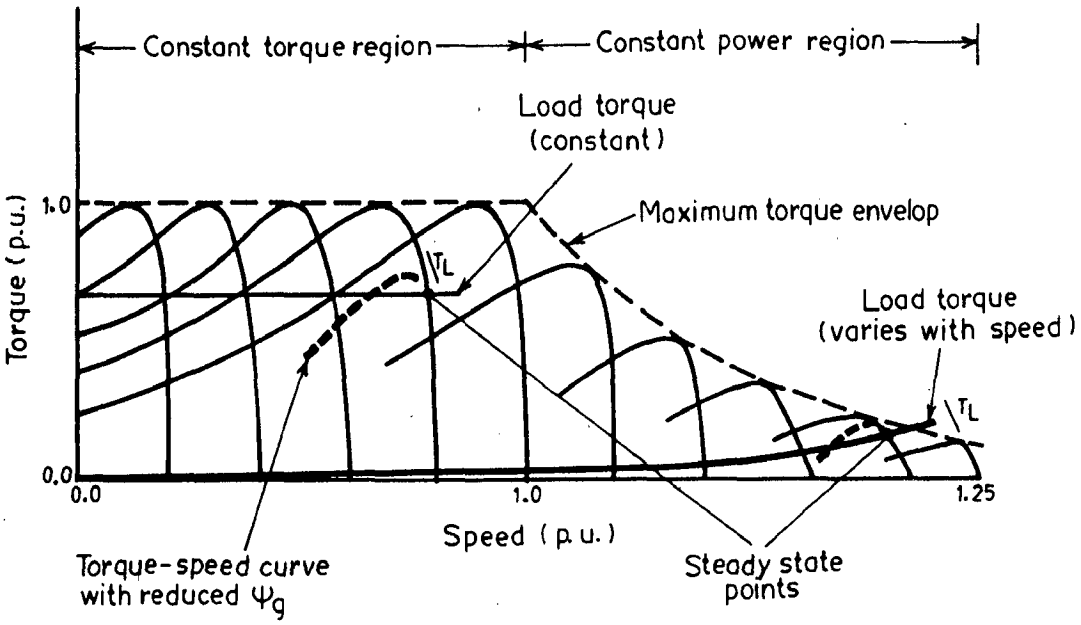

Fig.1.3 Torque - speed curves of induction motor with variable-voltage variable frequency supply.

closed loop system in which rotor slip frequency air-gap flux and stator current are held constant the drive develops a constant torque at all motor speeds [2, 11]. Thus with a control strategy in which the stator current as well as rotor frequency are controlled in order to maintain the air-gap flux constant, high torque can be obtained throughout the entire range of speed control.

Nearly all static a.c. drives built today can be described as voltage source converters, since the output terminal voltage is essentially independent of current. Recently, however, the useful features of inverters in which the current rather than voltage appears essentially as the independent variable have been recognized. In case of voltage source converters, we set the voltage and frequency which is applied to the motor. The motor is then free to respond within its speed/torque parameters as the application dictates. Unusual load variations can, and often do, push the motor to its breakdown point or cause regeneration to occur in the converter by overhauling the motor. In either case, an untimely shut-down or damage to the motor or converter results. In this respect current source converter appears to have inherent advantages. These advantages are [18, 32],

(i) Converter grade S.C.Rs can be used.

(ii) Inverter can recover from a direct short circuit across any two of its output terminals.

(iii) The inverter can also recover from occasional commutation failure.

(iv) Any fault on the inverter side causes slow rise of fault current which can be cleared by suppressing rectifier gates.

(v) The ability of the drive to continue to operate in spite of the aforementioned conditions in many cases allows the operator to repair a component failure in the unit at some later, more convenient time.

(vi) The commutation capability of the inverter is load current dependent.

(vii) The inverter-converter arrangement is capable of power regeneration.

(viii) The control circuit is simpler and more reliable.

In spite of several merits as mentioned aobve, the current fed inverter drive has also several limitations. These limitations are,

(i) The frequency range of the inverter is somewhat lower.

(ii) It is difficult to operate at no load since the commutation capability is load current dependent.

(iii) The large size of the d.c. link inductor and the commutation capacitors make the inverter somewhat bulky and expensive.

(iv) The commutation is dependent on machine sub-transient reactance which adds large transient over-voltage at the machine terminal.

(v) The response of the CSI fed drive is somewhat sluggish and tends to give a stability problem at the light load high speed conditions.

The current-source-inverters are used in single motor drives in medium to high horse power range. Although the multimotor operation is somewhat difficult, recently it is receiving considerable attention.

The current-source inverter was first introduced round about 1964[32], and as shown in Fig. (1.4), is a D.C. link system. Thenafterwards in 1972, Phillips, for the first time described in his paper [21], a combination of power and control techniques for current fed induction motor drive which achieve a.c. drive features not available until then. The current source inverter described in his paper is slip regulated for both speed and torque control. He has shown that the current source/slip regulated inverter (CS/SR) concept controls operation of the a.c. motor at its optimum torque/ampere rating point while maintaining

and enhancing its rugged simplicity to achieve torque limit, fast response, regeneration, and wide speed range.

In 1973, Farrer and Miskin [8] showed that if a cage induction motor is fed with a quasi-square sine-wave current, the motor terminal voltage is approximately sinousoidal under normal operating conditions. A simple analytical approach based on the assumption that the motor resistances and reactances do not change with frequency, is also shown to describe adequately the terminal voltage. They have also discussed the numerous advantages of current-source-inverter over the voltage-source-inverter.

State variable steady-state analysis of controlled current induction motor drive was first attempted by Lipo and Cornell is 1975 [14]. They derived the exact equations defining steady-state operation of a controlled current induction motor drive system by solving the system state equations in the stationary reference frame. They included the effects of saturation in the analysis by using the slope ratio method. They computed the electromagnetic torque and current pulsations for various load conditions and varified them experimentally. They have also discussed the similarties and differences between the torque slip characteristic of current and voltage source inverters. They have shown that normal open loop operation occurs on the unstable side of the torque-slip characteristic, if motor is to remain unsaturated. This necessiates the use of feed back control for stable operation.

After Lipo and Cormell have shown that open loop operation of current-source-inverter fed induction motor is not preferred Nelson and Radomski attempted a simple closed loop scheme in the same year [18]. Their control scheme uses two feedback loops to control motor slip frequency and torque. First loop known as slip control loop measures rotor speed, adds in slip frequency and provides the inverter with the correct synchronous frequency to maintain constant slip. This loop enables the motor to operate at constant power factor over whatever load range is desired. The second loop known as torque control loop monitors current in the d.c. link, compares it to a reference input, and controls the rectifier bridge to maintain constant current. Since motor torque is proportional to current squared, this loop effectively regulates motor torque which is determined by the reference input. The above control scheme was simulated on an analog computer and simultaneously a 100 H.P. system was built and tested in the laboratory. Due to the excellent agreement between computer and laboratory results, the above paper demonstrates computer simulation as an effective method for designing current-source inverter fed induction motor drives.

In 1977, Revankar and Bashir [22] deiscussed the effect of commutating capacitor, feed inductance and the induction motor parameters on the current-source inverter operation and presented the guide lines for

suitable choice of components. They have also given the monograms to evaluate the component ratings.

In the same year Cornell and Lipo [4] presented a paper in which they emphasised on the modelling and design of CSI fed induction motor drives. They have shown that open loop operation is unstable for most operating conditions, and control loops must be added to realize feasible operating points. They have verified the results obtained by Nelson and Radomski [17] that independent current magnitude and slip frequency control is capable of stabilizing the drive system for all operating points in the motoring and regenerating modes of operation. They have developed a dynamic model for current-controlled induction motor drives, and a transfer function approach to the transient response investigation is formulated by means of d-q variables in the synchronously rotating reference frame. They have also presented an analytical design technique for finding the transfer function between a specific input command and a controlled output variable based on small signal linearization. The frequency response corresponding to the appropriate transfer function is compared to the actual frequency response measured on a laboratory breadboard and also on a hybrid computer simulation of the system. The results demonstrate that transfer function techniques can be reliably used to synthesize the necessary slip-frequency/current and speed control strategies.

In the schemes, system slip-frequency is forced to respond to changes in current magnitude in order to maintain constant flux in the air gap during both steady-state and transient conditions. The two principle advantage of this constraint are that motor performance is optimized and operation in the saturated rectifier voltage condition is possible (rectifier full on) because the slip frequency channel coupled to d.c. link current provides a stabilizing mechanism for the system.

In 1979, Lipo developed a novel simulation of a current-source-inverter [15] which retains the effects of commutation but minimizes the number of analog computer components. He has also compared the simulation traces with tested results on actual systems.

In 1980, Yuvrajan developed in his paper [33] a mathematical model of 3ϕ induction motor fed from a CSI using the actual phase variables of the machine on a digital computer. Using the simulation, the performance of the inverter and the induction motor are obtained. Simulation is also extended to the closed loop control of induction motor and the effect of variation of parameters such as the slip, frequency on the transient performance of the drive is studied. Waveforms of the voltage, current torque and also waveforms across different components of the drive are given as obtained from the computer.

The results of the conventional analysis of the steady-state operation of an a.c. drive using a current-source inverter and a cage I.M. When compared with experimental results show a large error in the predicted and observed values of the peak commutation capacitor voltage and the commutation angles. Therefore in 1981, Joshi and Dewan presented a modified analysis [10], which takes into account the following factors that are neglected in the previous conventional analysis:

(i) the variation of the a.c. back EMF of the induction motor during the commutation interval

(ii) the phase shift of the fundamental component of the line current due to the finite commutation interval

The peak commutation voltage and commutation intervals, as predicted by the modified analysis, are closer to the experimental results than those predicted by the conventional analysis. It is also shown that a further improvement in the predicted results can be obtained if the effective value of the leakage inductance in the induction motor model is measured by a blocked rotor test using square-wave current from the inverter. The results predicted by using the effective leakage inductance are in close agreement with the experimental results.

They have also mentioned that at frequencies higher than a critical value, the series diodes are forward-biased for a short interval other than the usual conduction period of $\frac{2\pi}{3}$ radian. The conduction of diodes shunts a part of the input current through the inverter leg without passing through the machine. The above paper also gives a method of predicting the critical frequency by computing the anode to cathode voltage across the series diodes.

The heart of the current-source-inverter is the current source. A very large feed inductor in series with a voltage source can simulate such a current source. Larger is the inductor better is the current source but large feed inductor will make the system costly and the system response slower. Thus the design of the inductor is critical. The aim of the paper presented by Revankar and Pillai [24] is to investigate the effect of feed inductance on circuit operation and evolve design criterion for the choice of the feed inductance.

The upper frequency limit of the CSI operation is decided by the commutation period of the SCRs. Large commutation periods in a CSI circuit can cause overlap between successive commutations limiting the frequency of operation. Revanker and Pillai in 1982 suggested [26] that a local discharge loop can be provided for the commutating capacitors to quicken the commutating process. They have also presented the analysis of new commutation circuit

and its effect on circuit operation. The results are compared with the conventional commutation circuit and are experimentally verified.

When an induction motor is driven by a variable frequency supply, the motor current and losses increase as a direct result of the harmonics in the supply. The methods of determining these effects have been given by Douglas Scholey [6]. Venkatesan and Lindsay [31] have calculated the losses in a cage induction motor fed from six step voltage and current source inverters and compared the efficiencies of the motor when supplied from these sources. The equivalent circuit that takes into account the effect of space harmonics and the skin effect in rotor bars is used for the calculation of main and stray copper losses. They have shown that for reduced torque outputs, the motor efficiency is higher when supplied from a current-source inverter whereas for torque outputs greater than the rated torque, operation from the voltage-source inverter is more efficient.

In the same year, Manju Jain [12] working on a CSI fed I.M. drive have shown that open loop mode of operation exhibits instability in almost entire operating range. She attempted to stabilise the drive over very wide range of operating speeds by using controlled slip constant flux control scheme as suggested by Phillips and Lipo [21, 4]. She developed system characteristic equation

by employing the theory of small displacement and used D-partitioning technique for proper co-ordination of the controller parameters. She has also presented a method for predicting the drive performance as affected by the sixth order harmonics of stator current. In the end she has discussed the transient performance of the drive under various operating conditions of the drive-starting, sudden speed changes in both up and down direction and reversal in the direction of rotation of the motor.

In contrast to controlled slip constant flux control scheme suggested by Lipo and Phillips, a new controlled slip variable flux drive scheme for CSI fed induction motor was proposed by Ravankar and Havanur in 1982. The scheme [27] is based on the simple and direct relations that exist between flux, slip frequency, torque and stator current components resolved along the airgap flux and in quadrature. It provides separate and independent control of flux and torque in the motor. They also discussed the advantages of this schemes as compared to previous ones. Experimental results using the new scheme are also presented and discussed in the above paper.

With regard to less expenditure, fewer losses, and less weight, the d.c. choke in the link of current source inverters must be small. The performance of the d.c. link and special control methods for minimizing the link inductance are presented by Friedrich and Mueller in 1983 [9].

The commutation of current in a current-source inverter fed induction motor was analysed by Farrer and Miskin [8] using simplified models. Their models provide sufficiently accurate results when the frequency of operation is high. At low frequencies the results are found to be less accurate because the assumption of sinusoidal back e.m.f. is not valid. Subrahmanyam in 1984 tackled this problem and developed a simplified model [30] which provides accurate results at all operating frequencies with least computational effort and is useful in the analysis and design of CSI fed induction motor drives.

In the same year, Fekete and Szentirmai developed an automatically operated 4-quadrant drive to provide variable motor speed and torque both in motor and generator actions [7]. The main attraction of the above paper is the details of the firing scheme to obtain the 4-quadrant operation.

It is generally believed that the current-source inverter adjustable frequency controller with auto-sequential commutation cannot be easily tested without a load motor connected. But Osman have shown that the above inverter can easily be tested without a load motor by adding some simple circuits in both the regulator and power circuits and by following step by step test procedure [20]. He has also shown that the simplest form of the power circuit is not well suited to high frequency

operation at light load, because the duration of commutation is inversely proportional to the d.c. link current. He has described an improved diode ring-up circuit that accelerates commutation in the auto-sequential current-source-inverter.

One of the limitations of conventional auto-sequential current source inverter for high power induction motor drives is the high voltage that is produced in the commutation capacitors during the current commutation from one phase to another. Since the capacitor voltage appears directly across the semi-conductor components, it increases their required voltage ratings. The high voltage spikes generated at the motor terminals may also cause damage to the motor insulation. Recently Rasappa presented the solution of the above problem. In his paper [25] he has given a brief review of the literature on limiting the capacitor voltage and clamping the voltage spikes. He has also proposed two circuits suitable for achieving the above goal. The analysis and the results of digital computer simulation of the proposed circuits are also given in his paper.

1.2 SCOPE OF PRESENT WORK

The author considered a cage induction motor fed from a current-source inverter. The mathematical model of the drive in per unit system is first developed and

steady-state performance is analysed such as power output, power factor, stator voltage, efficiency, total losses e.t.c. as affected by variation in slip at different p.u. d.c. link currents and operating frequencies.

A simple firing scheme for operating the current-source-inverter in auto-sequential mode has been developed along with the power circuit of the drive.

The performance of the current-source-inverter is investigated at resistive and induction motor loads. The load test is carried out at different operating frequencies and d.c. link currents on induction motor and steady-state performance of the drive is obtained experimentally. The experimental results have been compared with the theoretical ones and the discrepancies between the two are discussed.

The oscillograms of line voltage, line current at the input of induction motor and of voltage drop across different components of the inverter circuit have been recorded and discussed. Some of the above oscillograms are also recorded at resistive load to study the effect of nature of load.

The effects of change of operating frequency and load on the line voltage and line current waveforms have also been studied.

CHAPTER II

CURRENT SOURCE INVERTER

2.1 INTRODUCTION

Inverters are used for generating variable frequency poly phase supply from a d.c. source. The voltage source inverters are voltage driven i.e. the input is a stiff d.c. voltage source with negligible input impedance. On the other hand, current-source inverter is current driven i.e. the input is a stiff d.c. current source with infinitely large input impedance. Fig. (2.1) shows a schematic diagram of current-fed inverter drive. A phase-controlled rectifier generates variable d.c. voltage which is converted to a current source by connecting a large inductor in series. A diode rectifier followed by a d.c. chopper can also constitute the variable voltage d.c. source. The thyristors of the inverter steer the source current I_d symmetrically to the three phases of the machine to generate a variable frequency, six-stepped current wave. Since the source is considered stiff, the wave is not affected by the nature of the load, i.e., it is dual to voltage wave of a voltage-fed inverter.

During the last several years, there has been a wide interest in the controlled current inverter drives due to its greater simplicity, better controllability, higher regenerative capability and ease of protection.

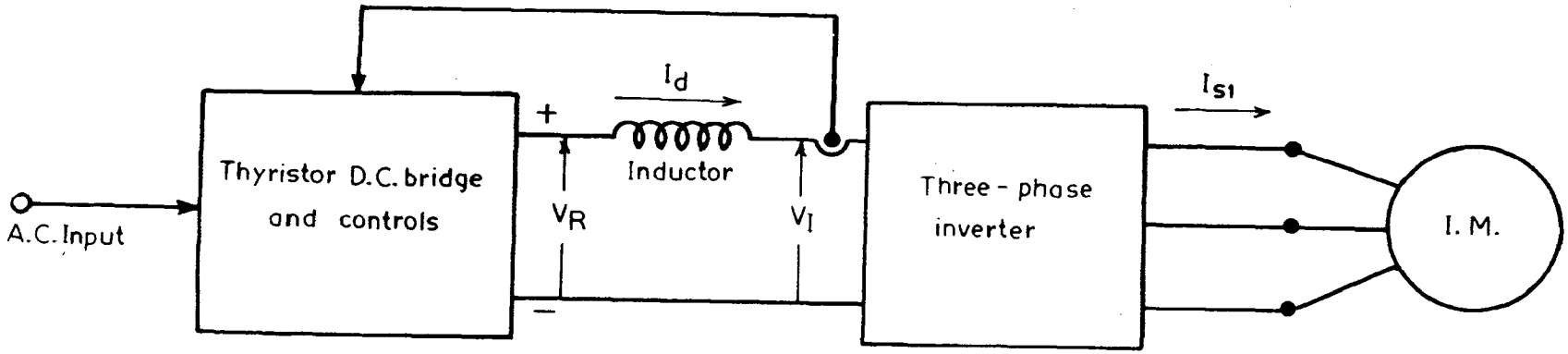

Fig. 2.1 – Basic controlled current induction motor (CCI) drive system.

2.2 VARIOUS CONFIGURATIONS OF CURRENT SOURCE INVERTER

Since the induction motor constitutes a lagging power factor load, the thyristors of the inverter need forced commutation. Three of the forced commutated inverter types are shown in Figures (2.2), (2.3), and (2.4).

The auto-sequentially commutated inverter (ASCSI), as shown in Fig. (2.2), is very commonly used with induction motor load. The six capacitors and six diodes constitute the forced commutation circuit. The diodes tend to isolate the capacitors from the load and help store energy for commutation. The commutation process causes transient overvoltages at the machine terminals. The designed capacitance value depends on the compromise of transient overvoltage and highest operating frequency of the inverter.

Fig. (2.3) shows an inverter with individual auxiliary commutation. Here, an auxiliary thyristor bridge with the help of three capacitors permits independent commutation of each thyristor of the inverter. Since the commutation takes place through the auxiliary device, the duration of commutation tends to widen causing significant torque reduction at higher frequency. That is why, this configuration is seldom used for induction motor drive.

Fig. (2.4) shows the simplest commutation circuit where a capacitor is connected between the neutral of the

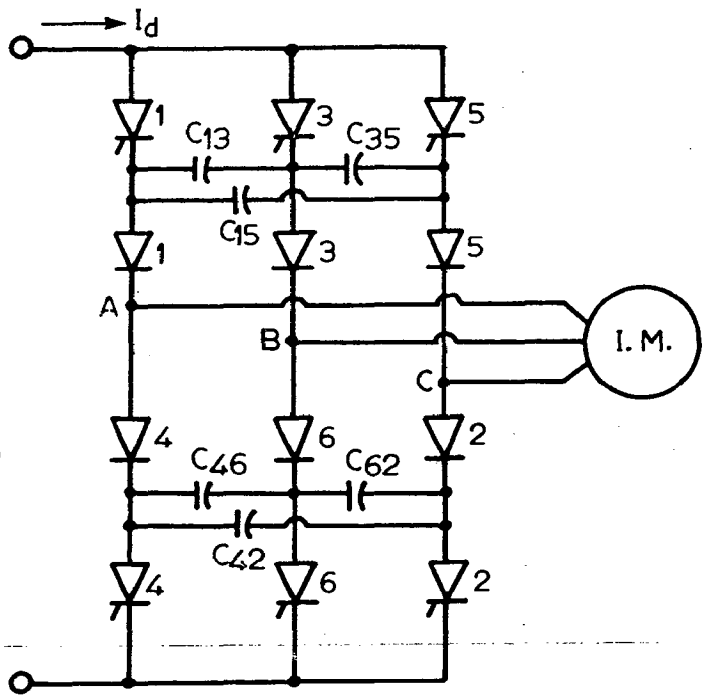

Fig.2.2:- Current inverter with autosequential commutation.

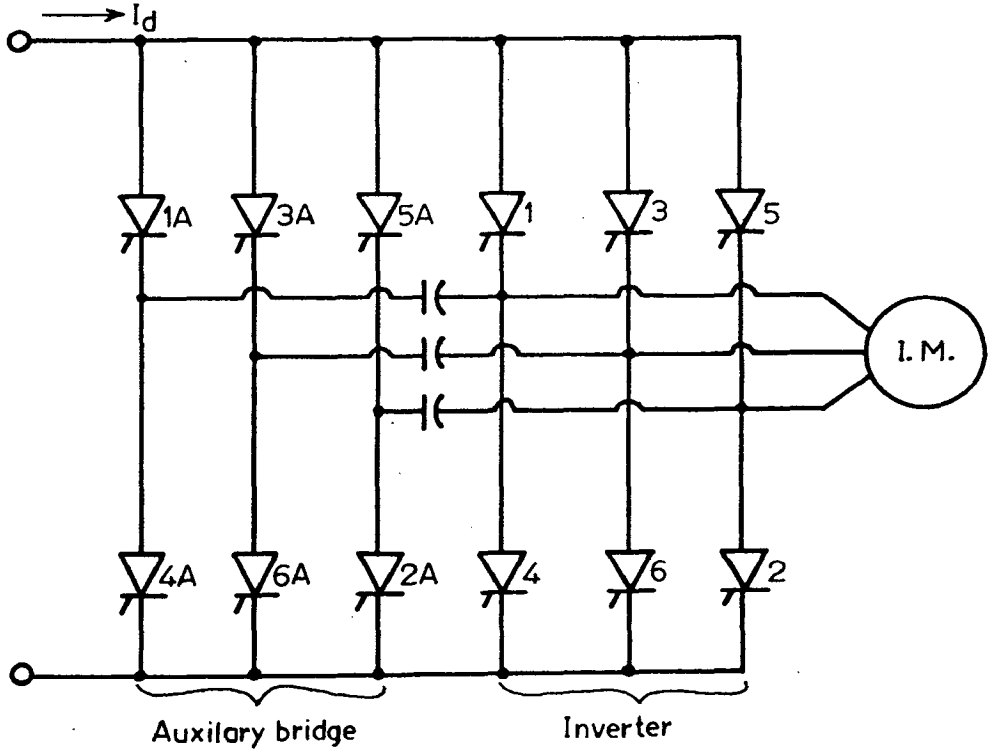

Fig.2.3_ Current inverter with individual commutation.

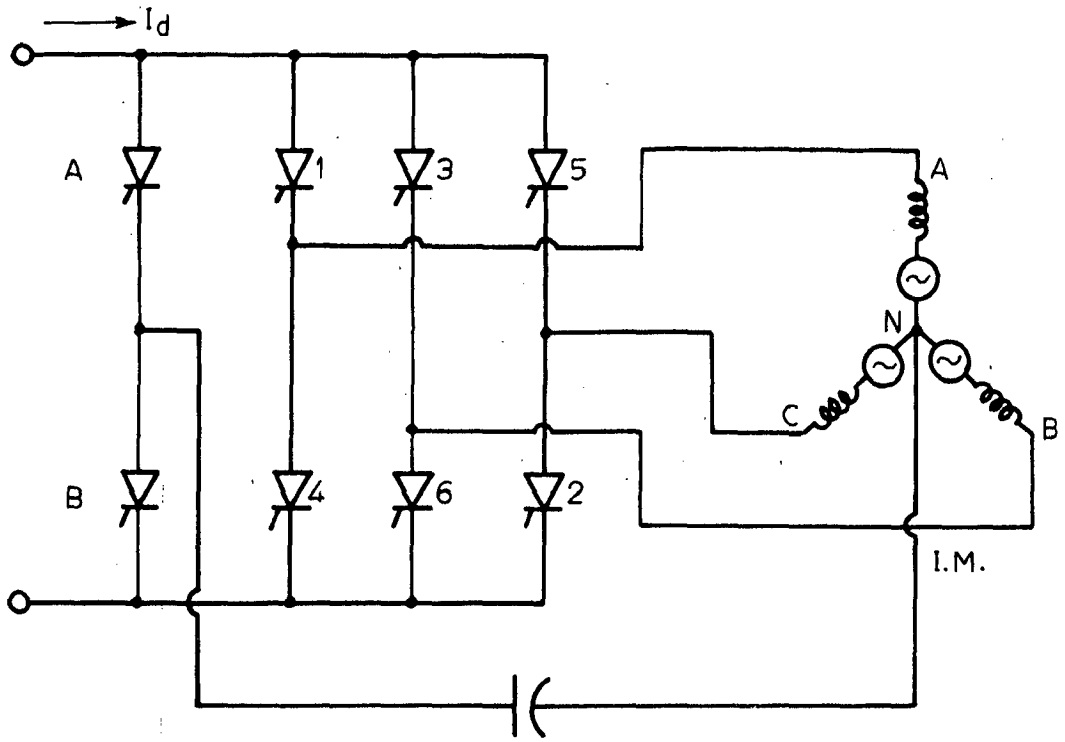

Fig.2.4_ Current inverter with fourth leg commutation.

machine and the fourth leg of the inverter. The auxiliary thyristor A is responsible for commutation of the upper half of the bridge, whereas B commutates the lower half of the bridge. In a full cycle of operation, the capacitor voltage alternates six times and that is why this circuit is called third harmonic commutated inverter. The circuit, though simple is not normally used for induction motor drive because torque reduction due to commutation is substantial at higher frequencies.

2.3 OPERATION OF CURRENT SOURCE INVERTER IN AUTO-SEQUENTIAL MODE

The configuration of current-source inverter in auto-sequential commutation mode[Fig. (2.1)]is used in the present work. In order to describe the automatic process of commutation transfer of current from phase A to phase B is discussed. The current transfer process is divided into three time intervals[Fig. (2.5)]. The approximate equivalent circuits for each interval are shown in Fig.[2.6(a)] to Fig.[2.6(d)]. It is assumed that all the semiconductor devices are ideal switches, commutation overlaps do not occur and the d.c. link current is constant and ripple free.

The begin with it is assumed that the SCR T_1 and T_2 are conducting and T_3 is fired to commutate current from T_1 to T_3 and ultimately from phase A to B. The capacitor C_{13} between SCR T_1 and T_3 will be charged with the

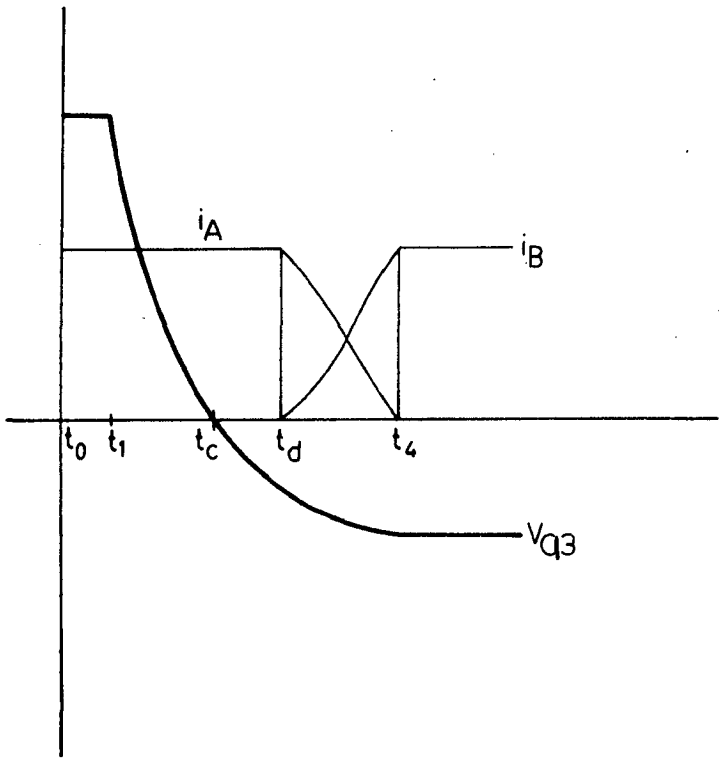

Fig.2.5_ Capacitor voltage and machine currents during commutation.

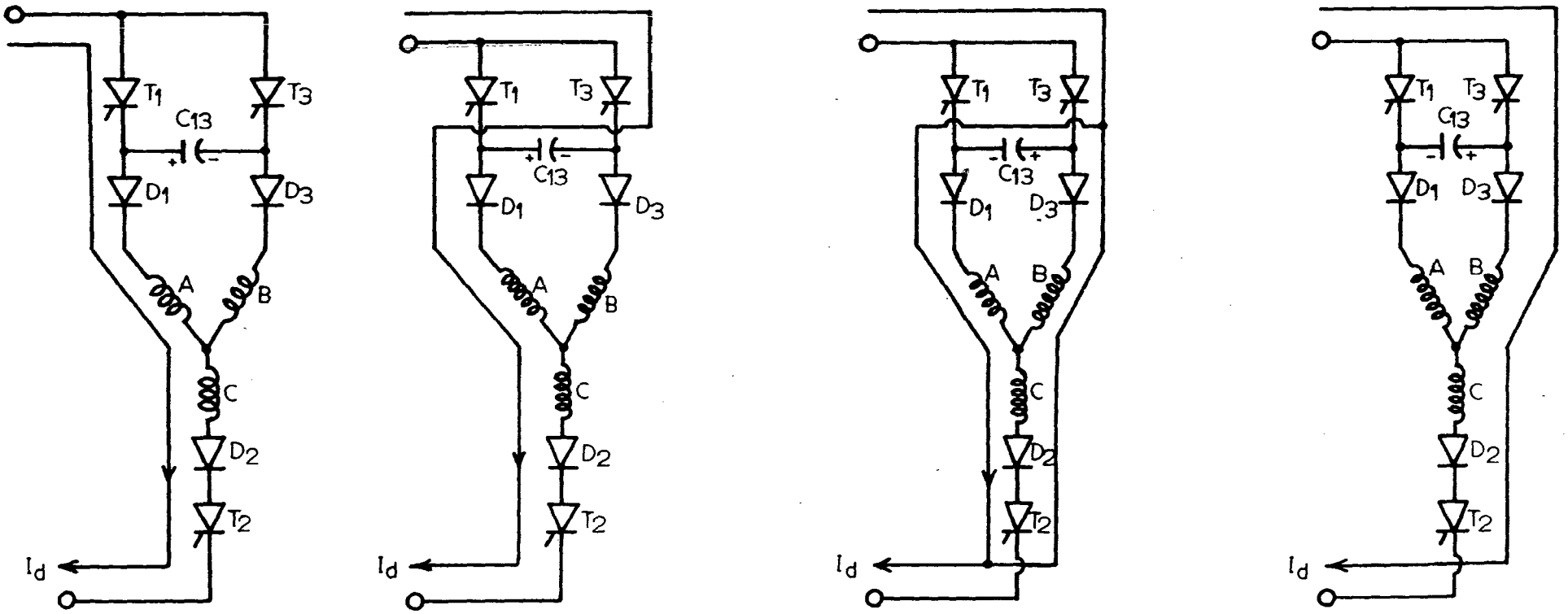

Fig. 2.6 – Current commutation from phase A to phase B.

polarity shown. In this case current I_d will flow through SCR T_1, diode D_1, motor phase A, motor phase C, diode D_2, SCR T_2 and back to supply[Fig. 2.6(a)]. After SCR T_3 is fired the commutation is complete in three stages[Fig. (2.5)].

1. In the first stage the current is commutated from the SCR T_1 to T_3 as the voltage of C_{13} acts as reverse voltage to SCR T_1. The transfer of current from T_1 to T_3 can be taken to be instantaneous. The load current path is shown in Fig. [2.6(b)].

2. In this stage of commutation the diode D_3 has a reverse voltage across it and therefore current flowing through T_3 cannot flow through D_3. This current divides itself, and flows through the capacitors (C_{13} parallel to the series combination of C_{15} and C_{35}) [Fig. (2.2)]. The current through the capacitors modifies the voltage across them. Capacitor C_{13} gets discharged linearly, the voltage across it being zero at $t = t_c$. The period t_o t_c is generally greater than the recovery time of the SCR, so that it remains in the blocked state even though the SCR gets positive voltage as the capacitor voltage reverses after $t = t_c$. The diode D_3 is still in blocked condition. The link current flowing

through the capacitors further modifies the capacitor voltages. At the instant $t = t_d$ diode D_3 gets forward biased and starts conducting. During t_c t_d only capacitor voltages change but the machine currents remain the same.

3. The third stage of commutation starts at the instant t_d when the diode D_3 starts conducting. The current divides between D_1 and D_3[Fig. 2.6(c)]. The diode current (D_1) flows through the capacitors which are now charged in the reverse direction. The current in D_1 falls gradually to zero while the current in D_3 simultaneously increases to d.c. link current. The commutation is complete when the current is completely transferred from phase A to phase B [Fig. 2.6(d)].

Table (2.1) illustrates the operation of the auto-sequential-current-source inverter for one complete cycle. It is clear that SCRs must be fired in the sequence 1 - 2 - 3 - 4 - 5 - 6 - 1 for the correct operation.

2.4 CONCLUSION

In the present chapter, current-source-inverter is shown as a dual to voltage-source-inverter. The three configurations of current-source-inverter are discussed and the commutation process in the most commonly used configuration (ASCSI) is explained.

TABLE (2.1)

TURN ON OF SCR NUMBER	COMMUTATED SCR NUMBER	CURRENT-PATH SOURCE
4	2	$T_3 - D_3 - \phi_B - \phi_A - D_4 - T_4$
5	3	$T_5 - D_5 - \phi_C - \phi_A - D_4 - T_4$
6	4	$T_5 - D_5 - \phi_C - \phi_B - D_6 - T_6$
1	5	$T_1 - D_1 - \phi_A - \phi_B - D_6 - T_6$
2	6	$T_1 - D_1 - \phi_A - \phi_C - D_2 - T_2$
3	1	$T_3 - D_3 - \phi_B - \phi_C - D_2 - T_2$

CHAPTER III

DEVELOPMENT OF FIRING SCHEME FOR CURRENT SOURCE INVERTER

3.1 INTRODUCTION

A simple firing scheme for realizing the firing requirements of an auto-sequentially commutated current source inverter is developed. The scheme uses Johnson Counter as the basic unit for generating the three phase variable frequency square wave supply. The outputs of the Johnson Counter are combined to produce six set of firing pulses with a phase difference of 60° from one another.

3.2 REQUIREMENTS OF FIRING CIRCUIT

The current source inverter is mostly used in 120° mode of operation which means that each thyristor conducts for 120° during each cycle. The firing pulses requirements of the thyristors for this mode of operation are as follows [Fig. (3.1)]:

1. The firing pulses to the thyristors of upper row i.e. 1, 3, 5 should be 120° apart.

2. The firing pulses to the thyristors 1 and 4, 3 and 6, 5 and 2 should be 180° apart.

3. In order to ensure firing of thyristors for all type of loads, pulses should be wide,

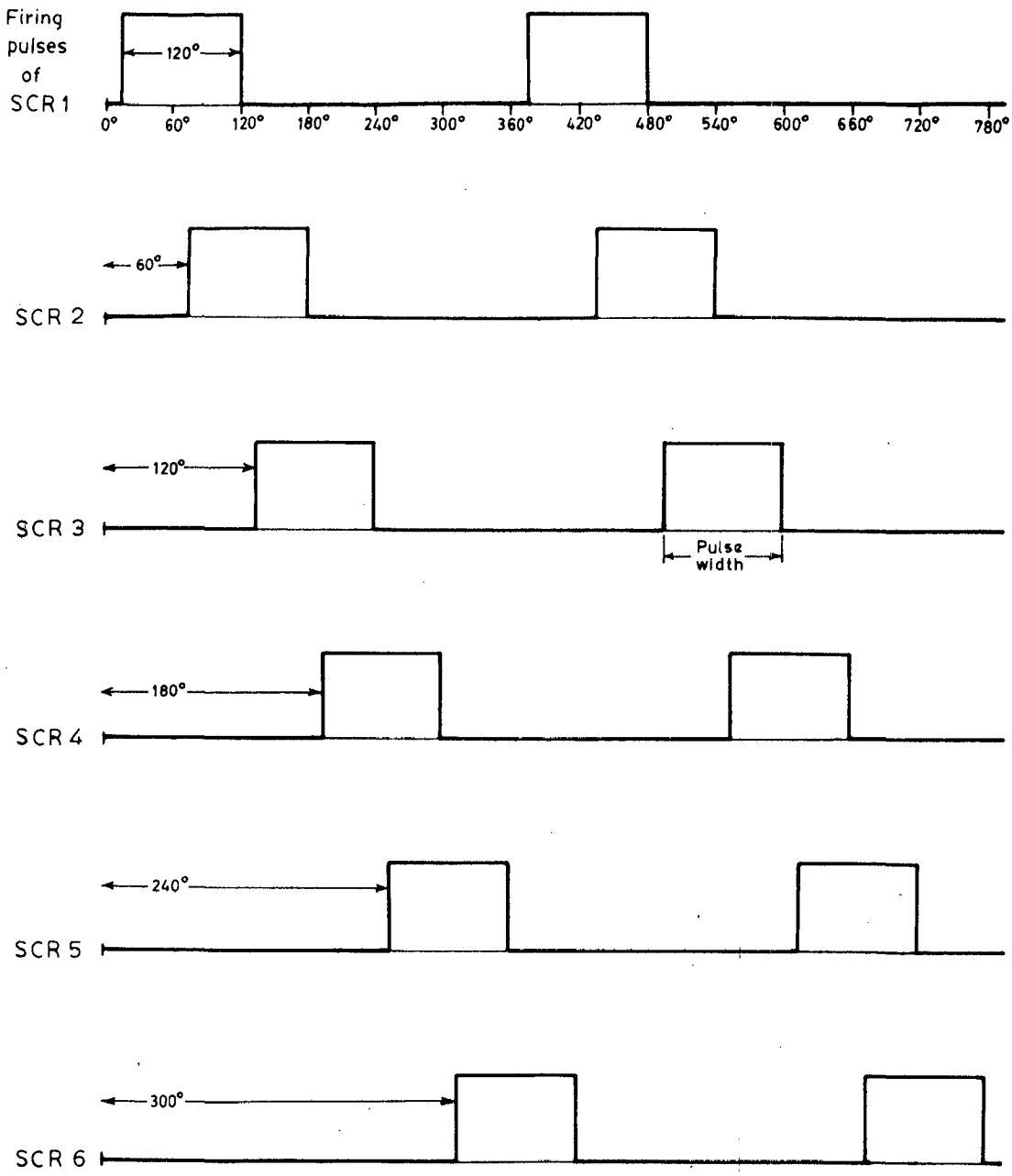

Fig.3.1_ Firing sequence of the CSI.

preferably as wide as the total conduction period of the thyristor to be fired i.e. 120°.

4. Each thyristor should get sufficient time to turn off.

3.3 REALIZATION OF THE FIRING SCHEME

Fig. (3.2) shows the firing scheme which fulfills all the four conditions stated above. Block 1 is a Johnson Counter whose input is clock pulses (Block 2) and output is a three phase square wave as is clear from Table (3.1) which indicates the state (high or low) of each output pin and its time diagram [Fig. (3.3)]. The frequency of the three phase square wave will be one sixth of the frequency of the clock pulses.

When the output of the Johnson Counter are ANDED as in block 5 of Fig. (3.2) with one another in a particular way [refer also Table (3.2)], six pulses of 120° duration but shifted by 60° from one another are obtained [Fig. (3.4)]. When these 120° duration square pulses are ANDED with high frequency pulses obtained from the oscillator (Block 4) we get continuous pulses for 120° duration [Fig. (3.5)].

In order to fulfill condition (4) there should be a delay in the begining of each pulse. This delay should be of the order of the turn-off time of the thyristor.

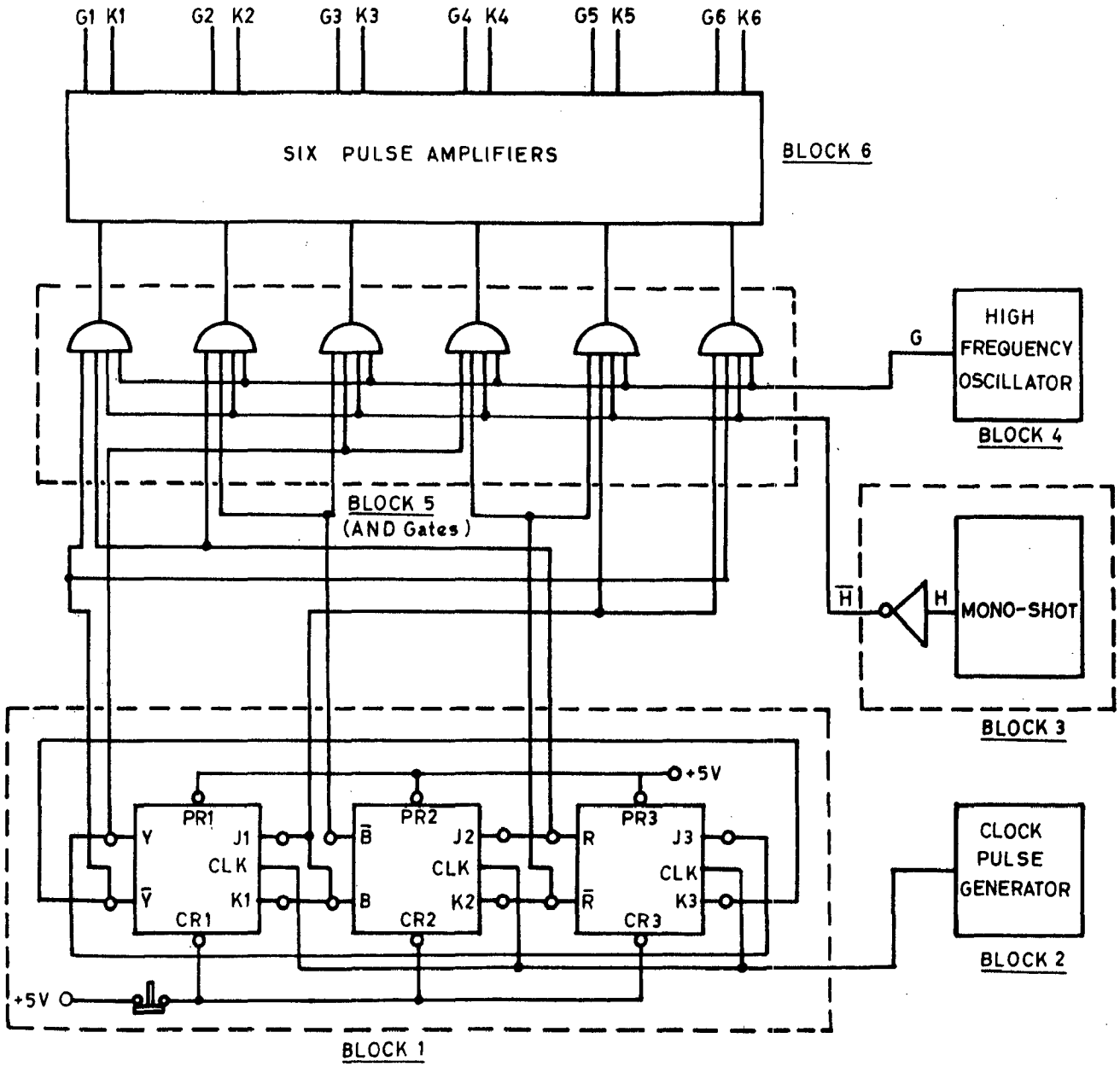

Fig. 3.2 – Block diagram of firing scheme for current source inverter.

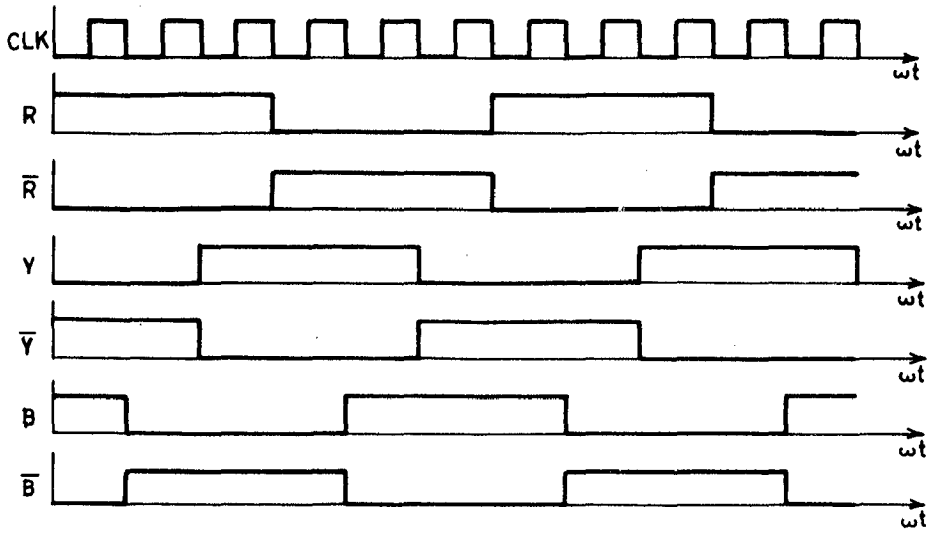

Fig.3.3_ Output of Johnson counter.

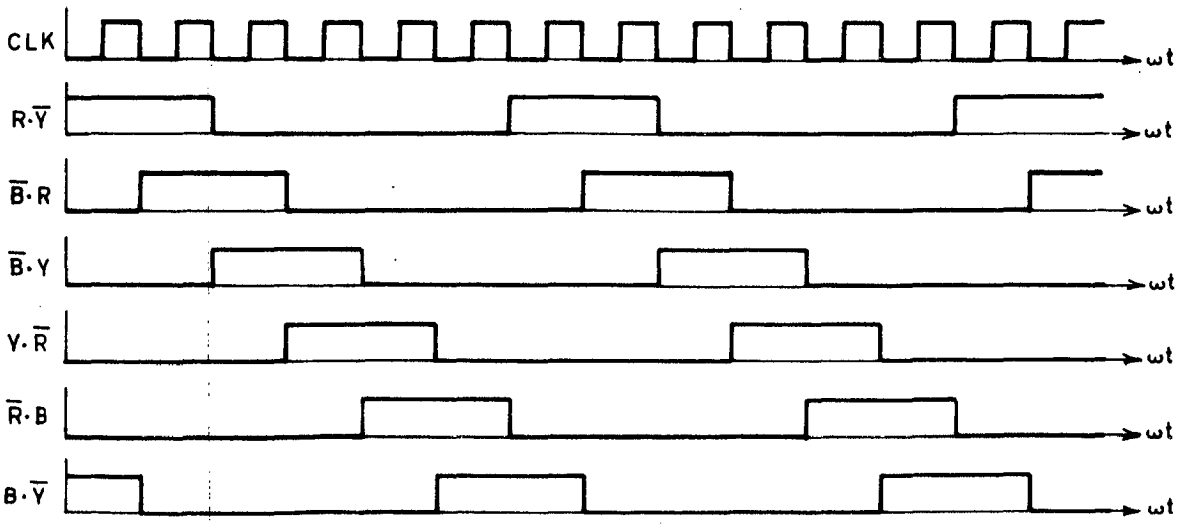

Fig.3.4_ Six pulses of 120° duration with 60° phase shift.

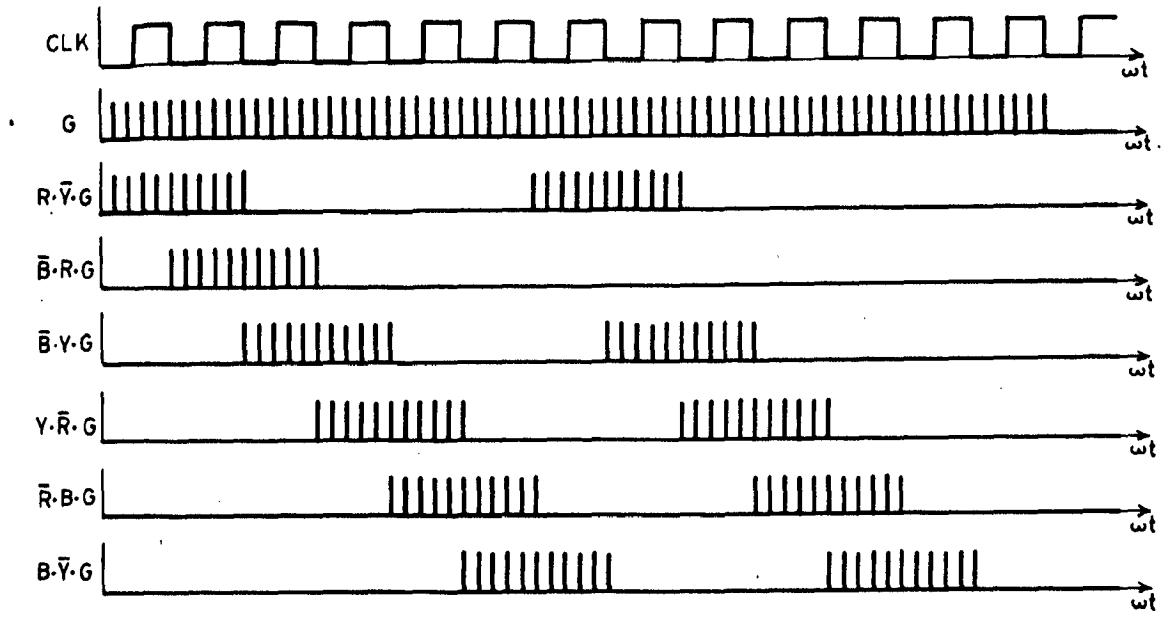

Fig. 3.5_ Continuous pulses for 120° duration.

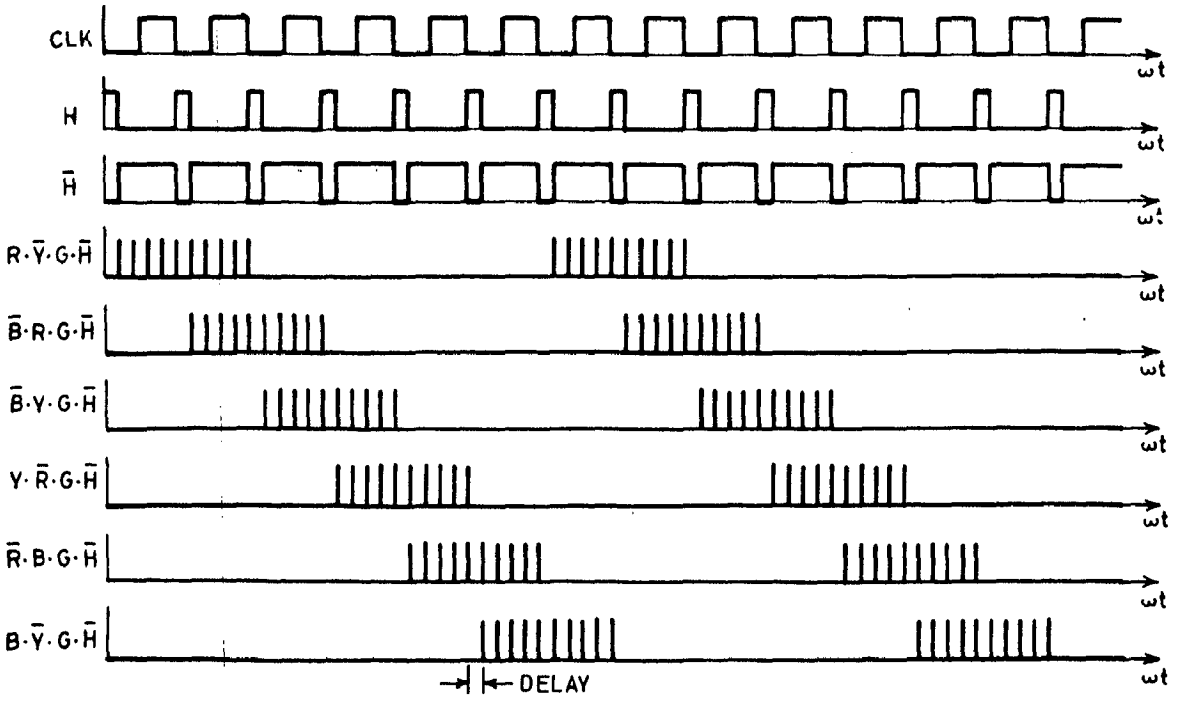

Fig. 3.6_ Continuous pulses with delay in starting.

TABLE (3.1)

PULSE NUMBER	R	$\overline{R}$	Y	$\overline{Y}$	B	$\overline{B}$
1	1	0	0	1	1	0
2	1	0	0	1	0	1
3	1	0	1	0	0	1
4	0	1	1	0	0	1
5	0	1	1	0	1	0
6	0	1	0	1	1	0

TABLE (3.2)

PULSE NUMBER	$B.\overline{Y}$	$\overline{B}.R$	$\overline{B}.Y$	$Y.\overline{R}$	$\overline{R}.B$	$B.\overline{Y}$
1	1	0	0	0	0	1
2	1	1	0	0	0	0
3	0	1	1	0	0	0
4	0	0	1	1	0	0
5	0	0	0	1	1	0
6	0	0	0	0	1	1

It is clear from the time diagram [Fig. (3.6)] that if we AND the pulses $\bar{H}$ with each of Fig. (3.5), we will get the desired delay in the begining of each pulse. To obtain $\bar{H}$ we trigger a mono-shot at the falling edge of each clock pulse and then invert it [Block (3), Fig. (3.2)].

Now we amplify the pulses as shown in Fig. (3.2) with the help of pulse amplifiers (Block 6).

3.4 DESIGN OF FIRING CIRCUIT

The firing circuit consists of Johnson Counter, oscillator, mono-shot, inverter, 4-input AND gates and the pulse amplifiers. The description of these components is as follows:

3.4.1 Johnson Counter

Johnson Counter is realised using IC 7476 which is dual master-salve JK flip-flop. The pin details of IC 7476 are given in Appendix 'A'.

3.4.2 Oscillator

IC 555 has been used as an oscillator. The details of IC 555 are given in Appendix 'A'.

The connections are shown in Appendix 'B'. The external capacitor C_T charges through R_A and R_B and discharges through R_B only. Thus the duty cycle may be set precisely by the ratio of these two resistances.

In free running mode of operation the capacitor charges and discharges between $\frac{1}{3}$ VCC and $\frac{2}{3}$ VCC. The charging and discharging time and hence, the frequency is independent of the supply voltage. The charging time (output high) is given by,

$$t_1 = 0.693\ (R_A + R_B)C_T$$

The discharging time (output low) is given by,

$$t_2 = 0.693\ R_B\ C_T$$

Thus the total time period is given by,

$$T = t_1 + t_2 = 0.693\ (R_A + 2R_B)C_T$$

Frequency of oscillation is therefore,

$$f = \frac{1}{T} = \frac{1.44}{(R_A + 2R_B)C_T}$$

For the inverter frequency from 20Hz to 100Hz the frequency of the clock pulses should be 120Hz to 600 Hz.

for $f = 120$ Hz

$R_A = 1$ K , $C_T = 0.1\,\mu f$, $R_B \simeq 60K$

for $f = 600$ Hz

$R_A = 1K$, $C_T = 0.1\,\mu f$, $R_B \simeq 12K$

Therefore R_A is taken as 100 ohm, C as 0.1 μF and 100K pot is used for R_B to adjust the desired frequency accurately.

For high frequency pulses, oscillator frequency is selected as 500 Hz. For this frequency R_A, R_B and C are selected as 1.0K ohms, 6.80K ohms and 0.02 μF respectively.

3.4.3 AND GATE

The 180° duration outputs of Johnson counter are ANDED with one another [Table (3.2)] and with Fig. (3.6) and high frequency pulses using 4 input AND gates in order to get 120° continuous pulses with small amount of initial delay. IC 7421 is used for this purpose which is dual 4-input AND gate. The pin details of IC 7421 are given in Appendix 'A'

3.4.4 MONO SHOT

IC 74121 has been used as mono-shot. The pin details of IC 74121 are given in Appendix 'A'. In order to trigger the mono shot at negative going edge of clock pulse, the circuit is connected as shown in Appendix 'B'. The duration of the output pulse is determined by the timing resistor Rex. connected between pin 14 and 11. The timing resistance Rex. must be in the range of 1.4K ohm to 40K ohm. The maximum allowable value of timing capacitor is 1000 μf. The duration of the output pulse in seconds is given by,

$$T_{ON} = 0.7 \text{ Rex Cex}$$

T_{ON} is selected as 350 μ Sec (approximately) so that reliable turning off time for thyristor is assured.

Hence,

$$C_{ex} R_{ex} = \frac{350 \times 10^{-6}}{0.7} = 500 \times 10^{-6}$$

Therefore, values of R_{ex} and C_{ex} selected are 4.7K ohm and 0.1 μf respectively.

3.4.5 INVERTER

IC 7404 has been used as inverter. The details of IC 7404 which is hex-inverter chip are given in Appendix 'A'

3.4.6 PULSE AMPLIFIER

The pulse output from AND gate may not be strong enough to turn ON thyristor. Therefore, the output of AND gate is amplified through an amplifier as shown in Fig. (3.7). A transistor SL 100 is used for this purpose. The load resistance R_c is taken as 10 ohm and base resistance R_{base} as 1K to achieve the desired amplification. The gate and cathode terminals are at higher potentials of the power circuit, therefore the control circuit should not be directly connected to the power circuit. A pulse transformer is used for electrical isolation between control circuit and power circuit. A diode IN 4001 is connected across R_c and pulse transformer primary winding to avoid the

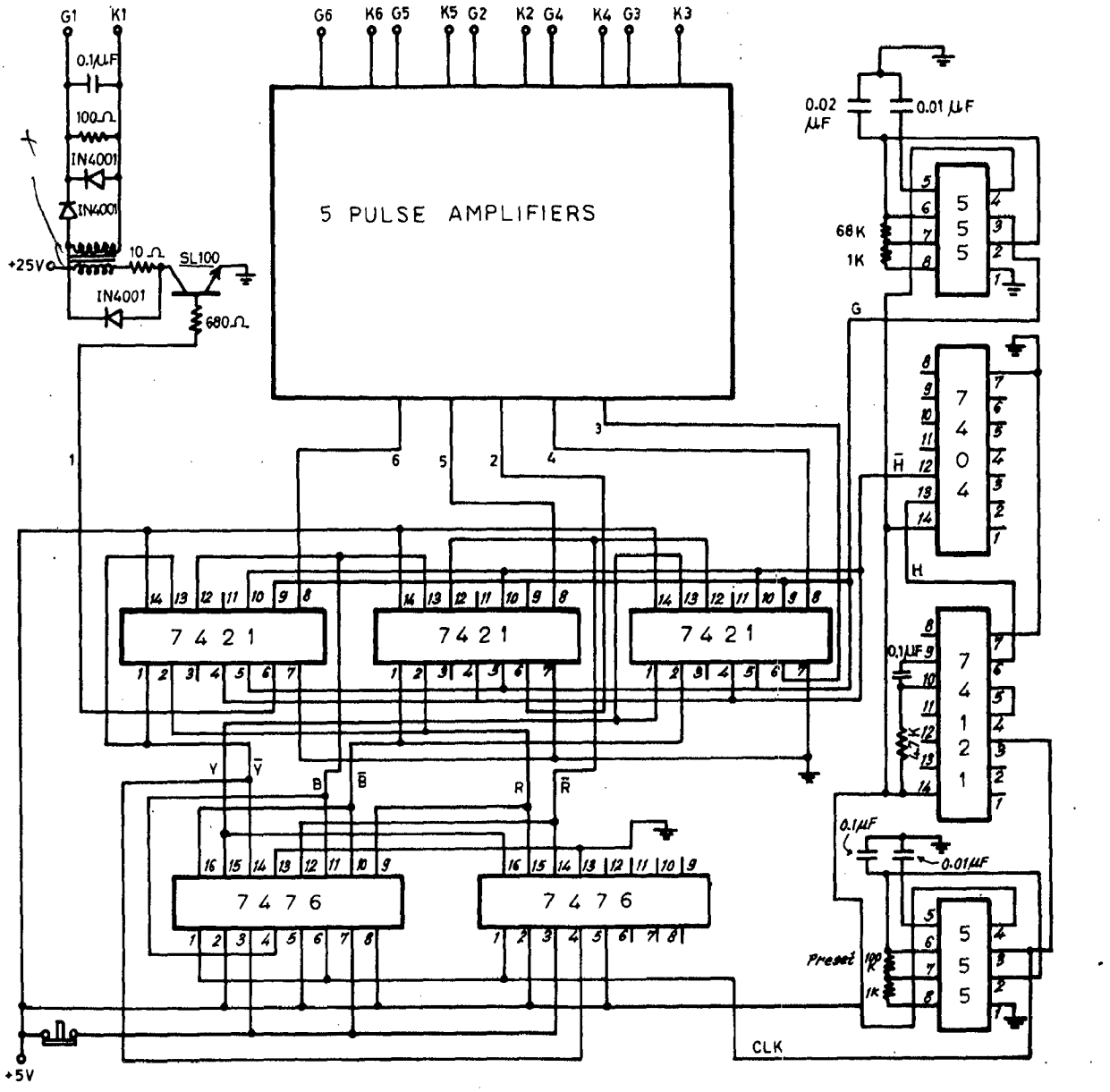

Fig.3.7_ Firing scheme for current source inverter.

saturation of pulse transformer core. A diode IN 4001 is connected in series with secondary of pulse transformer to block the negative pulses. Gate should also be protected against over voltages. This is achieved by connecting a diode IN 4001 across gate to cathode.

A common problem encountered in the SCR circuitary is spurious firing of the thyristors. Trigger pulses may be induced at the gates due to turn ON or turn OFF of a neighbouring SCR or terminals in the power circuit. These undesirable pulses may turn ON the thyristor thus causing improper operation of the circuit. The SCR gates are protected against such spurious signals by connecting a capacitor (0.1 μF) and a resistance (100 ohm) across the gate to cathode to bypass the noise pulses [28].

3.5 OSCILLOGRAMS OF THE FIRING CIRCUIT

The oscillograms recorded at the different points of firing circuit Fig. (3.7) are shown in the bigures (3.8) to (3.13).

Fig. (3.8) shows the input clock pulses of the Johnson Counter and one of its three outputs. The oscillogram closely matches with the ideal waveform of time diagram Fig. (3.3). It can be seen that the frequency of output square wave is one sixth of the frequency of clock pulses.

Oscillograms Of The Firing Circuit

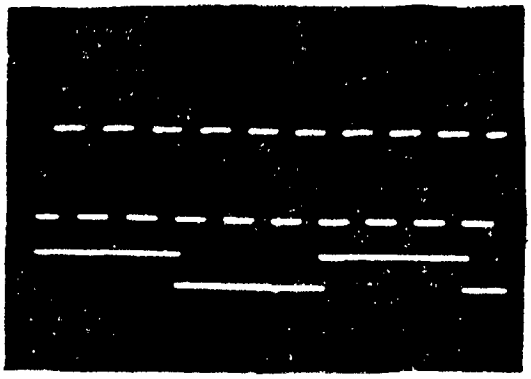

Fig. 3.8

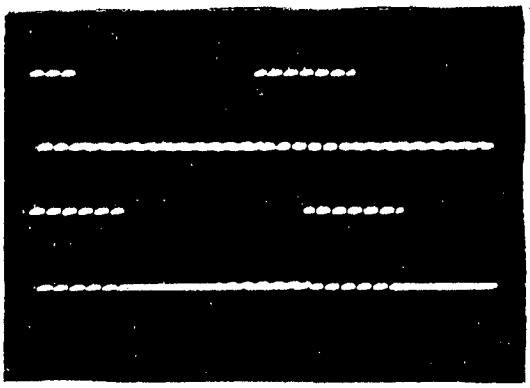

Fig. 3.11

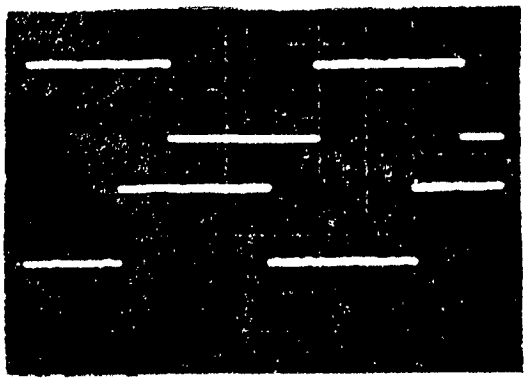

Fig. 3.9

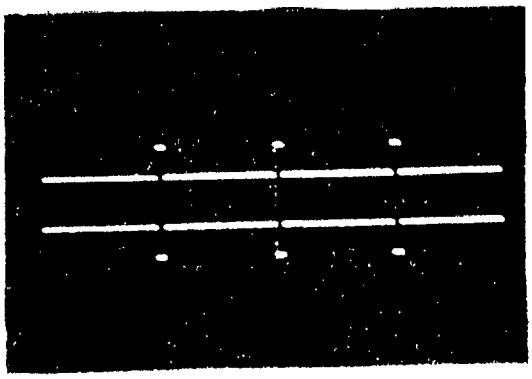

Fig. 3.12

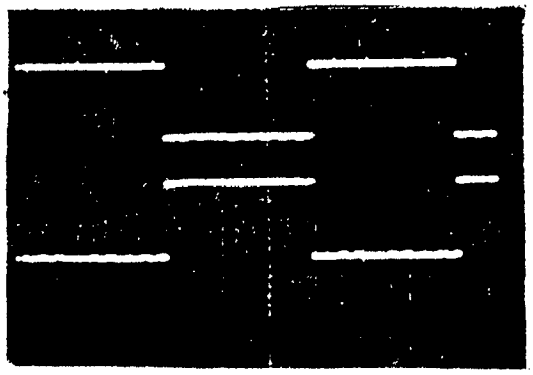

Fig. 3.10

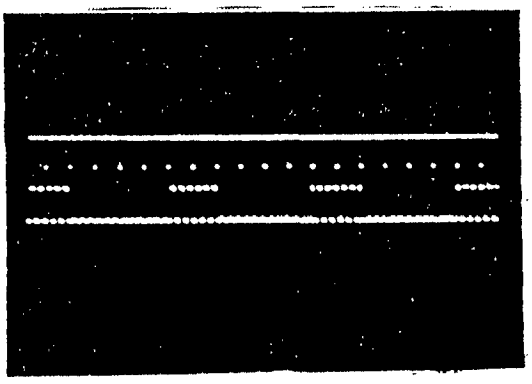

Fig. 3.13

Fig. (3.9) shows the R and Y phases of the Johnson Counter output. The 120^{o} phase difference between the two can be seen clearly. Fig. (3.10) shows the R phase and its inverted waveform. Both the oscillograms are identical to the ideal waveforms shown in Fig. (3.3).

Fig. (3.11) shows two continuous pulses of 120^{o} duration which form the firing pulses of two consequtive S.C.Rs after a minor modification. The phase shift between the two is of 60^{o}.

These pulses are obtained by ANDING 120^{o} square pulses of Fig. (3.4) with high frequency oscillator pulses [Block(5), Fig. (3.2)]. These waveforms are in close agreement with that of Fig. (3.5).

Fig. (3.12) shows the output of the mono-shot [Block(3), Fig. (3.2)] and its inverted waveform ($\overline{H}$). Fig.(3.13) shows the inverted output of monoshot ($\overline{H}$) and one of the 120^{o} continuous pulses of Fig. (3.11). It can be understood from the Fig. (3.13) and Fig. (3.6) that the ANDING of two waveforms will result in a very small time delay equal to the duration of mono-shot output in the begining of 120^{o} continuous pulse.

3.6 CONCLUSION

The Fig. (3.7) shows the complete firing scheme of Fig. (3.2) in terms of actual pin connections and

component values. This firing scheme has been found satisfactory for operating current-source-inverter made of 16A, 1200 PIV rating S.C.Rs, feeding a 3ϕ cage induction motor of 375 Watt size.

CHAPTER IV

SELECTION OF VARIOUS COMPONENTS OF THE DRIVE

4.1 INTRODUCTION

In this chapter, the criteria for the selection of various components of the drive is presented. This includes selection of motor, d.c. link inductor, commutating capacitors, diodes and thyristors.

4.2 SELECTION OF MOTOR AND THE LOADING ARRANGEMENT

The criteria for selecting the motor for the present work was to go for a 3-phase cage induction motor of small rating to enable use of inductor, capacitors, diodes and thyristors of moderate rating. The motor with following specifications was selected:

3-phase, 50 Hz cage induction motor	
No	S.L. 50
Rated Power	375 Watts
Rated Voltage	220 Volts
Rate Current	2.0 Ampere
No load Current	1.1 Ampere
Synchronous speed	1500 RPM

The loading arrangement comprises of a d.c. machine which is coupled with the above induction motor. This d.c. machine has been used as a separately excited generator for loading purpose. The specifications of this machine are:

No	S.L. 51
POWER OUTPUT	300 W
RATED VOLTAGE	125 V
RATED SPEED	1725 RPM

4.3 SELECTION OF SCRs FOR CONTROLLED RECTIFIER

The SCRs of the controlled rectifier must be able to withstand the maximum voltage coming across them and carry maximum current corresponding to any operating condition.

SCR Voltage Rating

The supply voltage input to the controlled rectifier is 220 volts, line to line a.c., therefore, the peak inverse voltage (PIV) across each arm of the SCR bridge will be given by,

$$PIV = \frac{\pi}{3} V_{do}$$

where $V_{do} = \frac{3\sqrt{2}}{\pi} V_{L-L}$

$$= \frac{3\sqrt{2}}{\pi} \times 220$$

$$\simeq 293 \text{ Volts}$$

Therefore $PIV = \frac{\pi}{3} \times 293$

$$\simeq 308 \text{ Volts.}$$

Allowing a safety factor of about 2.0 so that the SCR can easily take a reasonable transient over voltage, SCR with 600 Volts PIV rating are used.

SCR Current Rating

The full load current of the induction motor is 2.0 amperes.

Therefore current in the d.c. link corresponding to full load current of the motor will be,

$$I_R = \frac{\pi}{2\sqrt{3}} \times 2.0$$

$$= 1.81 \text{ ampere.}$$

Allowing a safety factor of about 2.0, SCRs of 5 amperes rating can easily take the motor full load current. The SCRs used are of 10 amperes current rating.

The SCRs selected for controlled rectifier have following specifications:

SCR Type OE 1006

Current Rating 10A

Maximum Reverse Repetitive Voltage 600 Volts

These SCRs have been mounted firmly on heat sinks because the heat developed, caused almost entirely by forward current and forward voltage drop, greatly

exceeds what the device can itself dissipate at normal working temperature. SCR bridge is protected against over current by providing proper fuses in its circuit.

4.4 SELECTION OF D.C. LINK INDUCTOR

The analysis of the current source inverter is arried out on the basis of constant-current-source at its input. A very large inductor in series with a d.c. voltage source can simulate such a current source, but such a inductor will make the system response slower. With regard to less expenditure, fewer losses and less weight also the inductor should be kept small. A medium size inductor with a current loop will ideally suit to our system. For the present work an inductor of 800mH is used in the d.c. link.

4.5 SELECTION OF COMMUTATING CAPACITORS

In the CSI fed drives, high voltage is developed across the commutating capacitors during the current commutation from one phase to another. Since the capacitor voltage appears directly on the semi-conductor components, the commutating capacitors are designed to limit peak voltage on devices rather than to provide adequate turn-off time for the SCRs. It has been found [18, 30] that the voltage developed across the capacitor is inversely proportional to the square root of the commutating

capacitance. Consequently the commutating capacitors should be selected large enough to enable use of SCRs and diodes of moderate voltage rating.

In the present work, variable capacitors are used and best performance of the system is obtained at $C = 30 \mu F$.

4.6 SELECTION OF SCRs FOR CURRENT-SOURCE INVERTER

Since the commutating capacitors are sufficiently large, the turn-off time available is sufficient to permit the use of normal SCRs instead of special fast turn-off SCRs.

SCR Voltage Rating

The voltage rating of the SCRs is decided by the maximum voltage developed across the commutating capacitors during the current commutation. This voltage is directly proportional to the d.c. link current and inversely proportional to the square root of the commutating capacitance.

For the present work, since the d.c. link current is very small and the commutating capacitors selected are quite large, therefore SCRs with 1200 PIV rating are

SCR Current Rating

Since the d.c. link current alone is steered by the SCRs symmetrically to the three phase, therefore current rating of the inverter SCRs is also decided by the d.c. link current. Allowing a safety factor of 2.0, SCRs with 5 amperes rating can easily carry the full load current. The SCRs used with 1200 PIV are of 16 amperes rating.

The SCRs selected for current-source inverter have following specifications:

SCR Type SS 1012

Current Rating 16 A

Maximum Reverse Repetitive Voltage 1200 V

Similarly to the SCRs of controlled rectifier, these have also been mounted on heat sinks but instead of snubber circuit, a small value of inductance in series with each SCR to limit di/dt to a safe value is used.

4.7 SELECTION OF DIODES FOR CURRENT SOURCE INVERTER

The function of diodes is to isolate the capacitors from the load and thus to prevent their discharging. The criteria for the voltage rating of the diodes is also the maximum voltage developed across the commutating capacitors. Since these diodes are used in series with SCRs therefore their current rating should be same as that of SCRs.

For the present work diodes with the following specifications are selected.

Diode Type	SPR 16 PB
Current rating	16 Ampere
Maximum Reverse Repetitive Voltage	1200 V

These diodes are also mounted on the heat sinks for the proper heat dissipation.

4.8 CONCLUSION

The guide lines for the selection of various components of the power circuit are discussed and the power circuit is designed for the speed control of 375 Watts cage induction motor.

CHAPTER V

DEVELOPMENT OF MATHEMATICAL MODEL

5.1 INTRODUCTION

An a.c. employing current source inverter consists of controlled rectifier, a d.c. link inductor and a current mode inverter. The controlled rectifier and d.c. link inductor combine to form a d.c. current source which supplies a regulated d.c. current to the current mode inverter. A rectifier controlled constant current source inverter fed induction motor drive is considered here. The induction motor is mathematically modelled in its synchronously rotating reference frame. The mathematical equations of whole drive are systematically developed in concordia's per unit system.

5.2 SYSTEM STUDIED

The system schematic diagram for a rectifier controlled constant current source inverter fed induction motor is shown in fig. (5.1). The system comprises of a three phase controlled rectifier bridge, a d.c. link smoothing inductor, a current-controlled inverter and a three phase squirrel cage induction motor. The loading arrangement comprises of a separately excited d.c. generator which is coupled to I.M. The current-source-inverter is typically the auto-sequential type described earlier in Chapter 2. The output voltage of controlled rectifier is controlled by

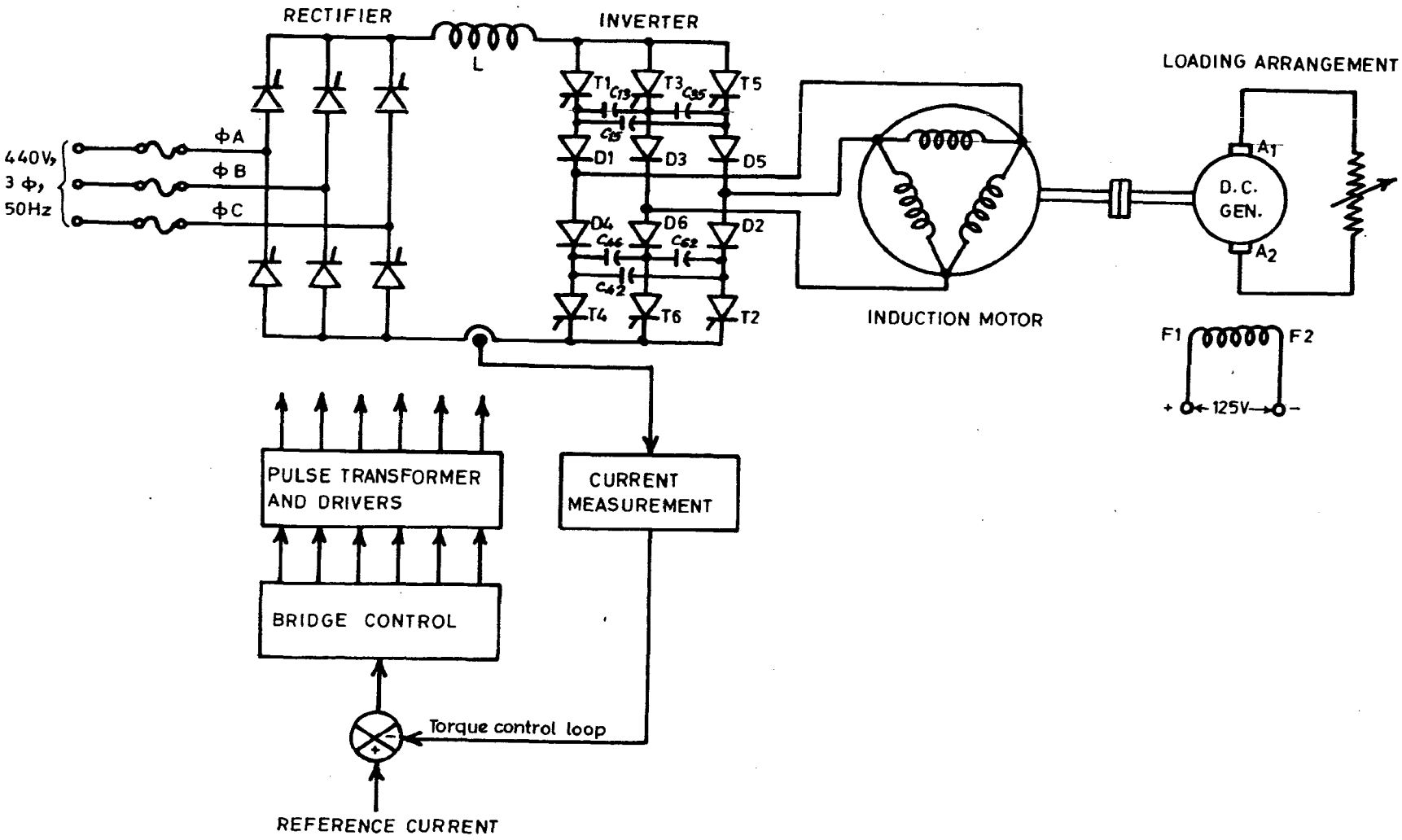

Fig. 5.1 _ System schematic diagram .

proportional controller working on the d.c. link current error. D.C. link current reference is set by adjusting the firing angle initially.

5.3 SYSTEM EQUATIONS (IN M.K.S. SYSTEM)

5.3.1. Induction Motor

The induction motor can be modelled using a two axis representation developed from the generalized machine theory. Several assumptions are required in order to use this representation. These assumptions are as follows:

(i) The three phase stator winding of the motor are balanced and sinusoidally distributed in space.

(ii) Rectifier output voltage is pure d.c.

(iii) No saturation occurs and thus superposition is applicable.

(iv) The switching transients in the inverter are ignored i.e. the commutation period is negligible.

(v) There are no core losses in the induction machine and all solid-state devices are assumed to be losses free.

We will describe the three phase squirrel cage induction motor in the synchronously rotating reference frame with the angular relationship between the q-axis and the magnetic axis of the stator and rotor phases is so selected that these axis coincide at time t = 0 [Fig. (5.2)].

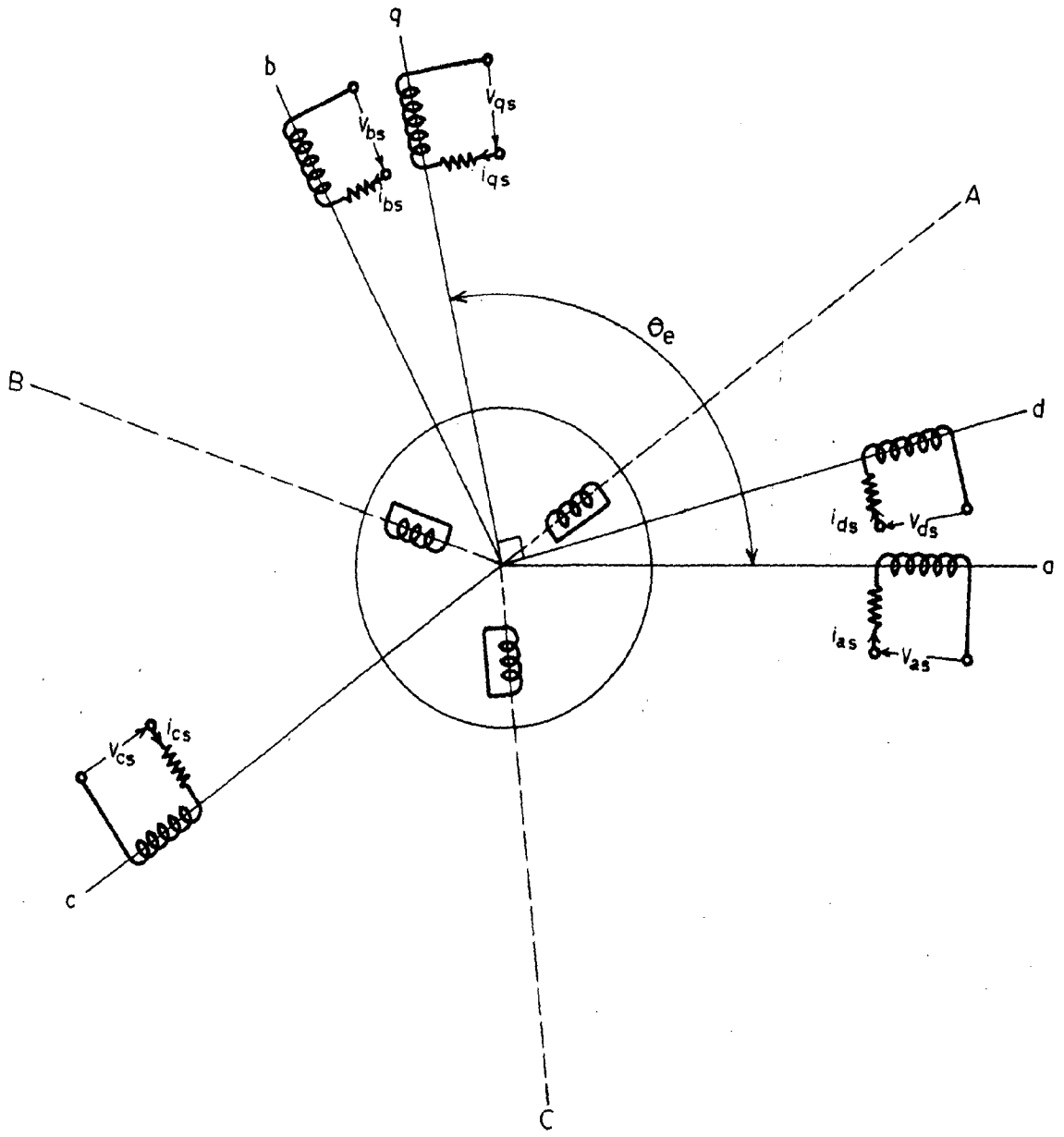

Fig. 5.2 – Reference frames.

Based on the above assumptions, the motor can then be described by the following fourth order matrix equation.

$$\begin{bmatrix} V_{ds} \\ V_{qs} \\ 0 \\ 0 \end{bmatrix} = \begin{bmatrix} (r_s+pL_s) & -\omega_e L_s & pM & -\omega_e M \\ \omega_e L_s & (r_s+pL_s) & \omega_e M & pM \\ pM & -\omega_{sl} M & (r_r+pL_r) & \omega_{sl} L_r \\ \omega_{sl} M & pM & \omega_{sl} L_r & (r_r+pL_r) \end{bmatrix} \begin{bmatrix} i_{ds} \\ i_{qs} \\ i_{dr} \\ i_{qr} \end{bmatrix} \quad \ldots(5.1)$$

Here ω_e denotes the angular velocity of the synchronously rotating reference frame and is equal to the fundamental component of applied voltage.

5.3.2 Current-Source Inverter

When a squirrel cage induction motor is supplied from a current-source inverter, the motor phase currents are not sinusoidal but are rectangular in nature for star connected motor[Fig.(5.3)]. The current flows for only 120 degrees of each half cycle (neglecting commutation effects). Ideally only two phase conduct at any instant of time resulting in six distinct modes of operation of the inverter.

The stepped currents shown in Fig.(5.3) exciting the three stator phases can be represented by the Fourier series expansions as given below:

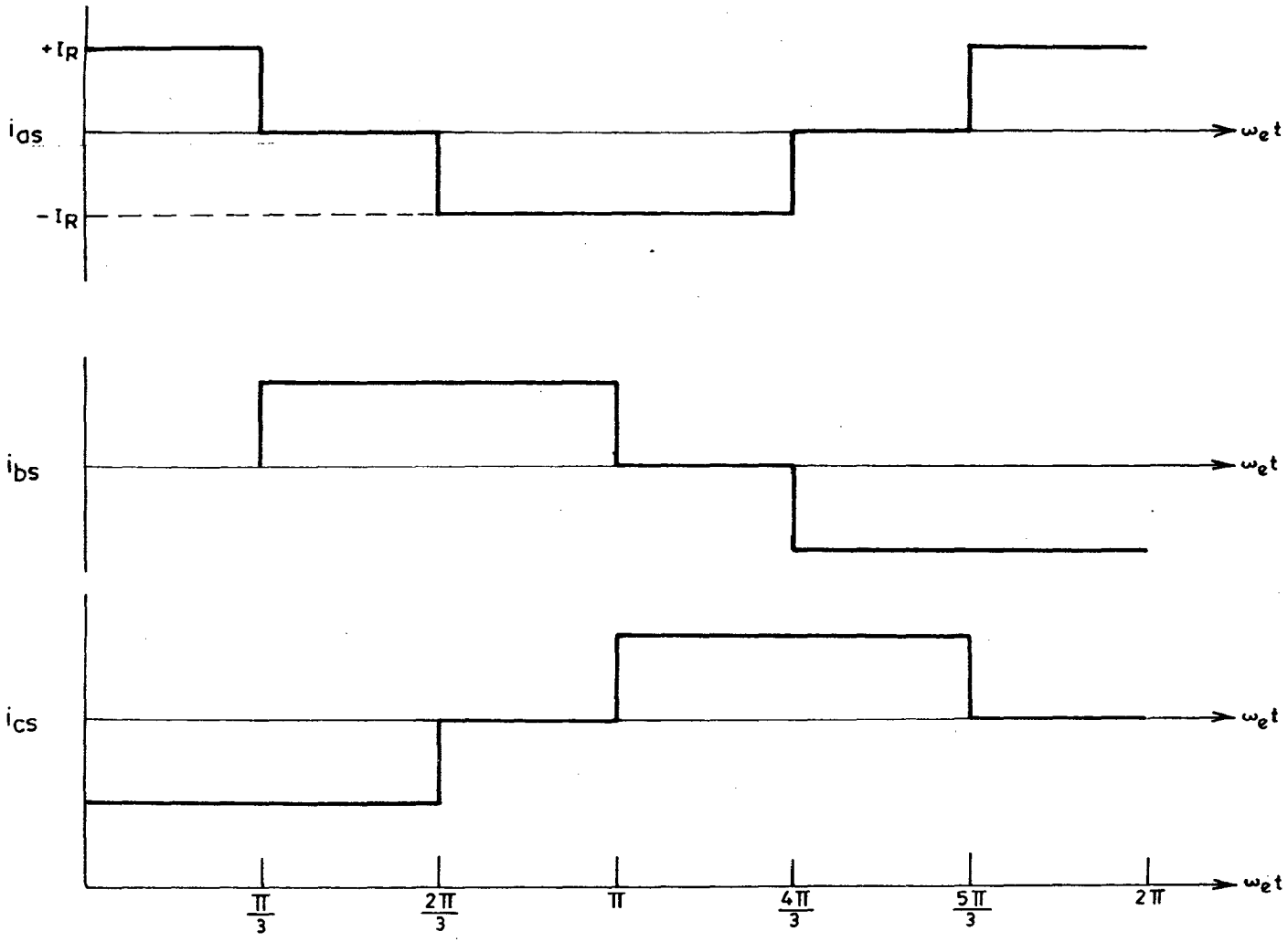

Fig. 5.3_ Idealized motor line currents.

$$i_{as} = \frac{2\sqrt{3}}{\pi} I_R \left[\cos \omega_e t - \frac{1}{5} \cos 5\,\omega_e t + \frac{1}{7} \cos 7\,\omega_e t - \frac{1}{11} \cos 11\,\omega_e t + \ldots\right]$$

$$i_{bs} = \frac{2\sqrt{3}}{\pi} I_R \left[\cos\left(\omega_e t - \frac{2\pi}{3}\right) - \frac{1}{5} \cos\left(5\,\omega_e t + \frac{2\pi}{3}\right) + \frac{1}{7} \cos\left(7\,\omega_e t - \frac{2\pi}{3}\right) - \frac{1}{11} \cos\left(11\,\omega_e t - \frac{2\pi}{3}\right) \ldots\right]$$

$$i_{cs} = \frac{2\sqrt{3}}{\pi} I_R \left[\cos\left(\omega_e t + \frac{2\pi}{3}\right) - \frac{1}{5} \cos\left(5\,\omega_e t - \frac{2\pi}{3}\right) + \frac{1}{7} \cos\left(7\,\omega_e t + \frac{2\pi}{3}\right) \ldots\right] \quad \ldots\ldots (5.2)$$

The above phase currents expressions can be transformed to a d-q reference frame running at synchronous electrical angular velocity of the fundamental component of the current applied to the induction machine stator.

The q-axis of the reference frame is assumed to coincide with the stator a-phase axis (a_s) at t=0 [Fig.(5.2)]. This condition gives the following equations of transformation:

$$i_{qs} = \frac{2}{3} \left[i_{as} \cos\theta + i_{bs} \cos\left(\theta - \frac{2\pi}{3}\right) + i_{cs} \cos\left(\theta + \frac{2\pi}{3}\right)\right]$$

$$i_{ds} = \frac{2}{3} \left[i_{as} \sin\theta + i_{bs} \sin\left(\theta - \frac{2\pi}{3}\right) + i_{cs} \sin\left(\theta + \frac{2\pi}{3}\right)\right]$$

$$i_{os} = \frac{1}{3} \left[i_{as} + i_{bs} + i_{cs}\right] \quad \ldots\ldots (5.3)$$

where $\theta = \omega_e t$.

Substitution of i_{as}, i_{bs} and i_{cs} from equations (5.2) in equations (5.3) yields,

$$i_{os} = 0$$

$$i_{qs} = \frac{2\sqrt{3}}{\pi} I_R \left[1 - \frac{2}{35} \cos 6\omega_e t - \frac{2}{143} \cos 12\omega_e t \ldots\right]$$

$$i_{ds} = \frac{2\sqrt{3}}{\pi} I_R \left[- \frac{12}{35} \sin 6\omega_e t - \frac{24}{143} \sin 12\omega_e t \ldots\right] \quad \ldots(5.4)$$

Equations (5.4) may also be written as

$$i_{qs} = \frac{2\sqrt{3}}{\pi} I_R g_{qs}$$

$$i_{ds} = \frac{2\sqrt{3}}{\pi} I_R g_{ds} \quad \ldots(5.5)$$

where,

$$g_{qs} = \left[1 - \frac{2}{35} \cos 6\omega_e t - \frac{2}{143} \cos 12\omega_e t \ldots\right]$$

$$g_{ds} = \left[- \frac{12}{35} \sin 6\omega_e t - \frac{24}{143} \sin 12\omega_e t \ldots\right] \quad \ldots(5.6)$$

If it is assumed that no power is lost in the inverter then,

$$V_I I_R = (V_{as} i_{as} + V_{bs} i_{bs} + V_{cs} i_{cs})$$

$$= \frac{3}{2} (V_{qs} i_{qs} + V_{ds} i_{ds}) \quad \ldots(5.7)$$

Substituting the values of i_{qs}, i_{ds} from equations (5.4) in equation (5.7) the inverter voltage can be expressed as,

$$V_I = \frac{3\sqrt{3}}{\pi} \left[V_{qs}\, g_{qs} + V_{ds}\, g_{ds} \right] \qquad \ldots(5.8)$$

The differential equation for the d.c. link is given by,

$$V_R = V_I + (R_F + pL_F)\, I_R \qquad \ldots(5.9)$$

The output of the controlled rectifier is given by,

$$V_R = \frac{3\sqrt{3}}{\pi} V_s \cos\alpha - \frac{3}{\pi} X_{co}\, I_R$$

where

V_s = peak phase voltage

X_{co} = commutating reactance in ohms

α = firing angle

defining,

$$\frac{3\sqrt{3}}{\pi} V_s \cos\alpha = V_{RX}$$

Then,

$$V_R = V_{RX} - \frac{3}{\pi} X_{co}\, I_R \qquad \ldots(5.10)$$

Substituting the expression of V_R from equation (5.9) in equation (5.10), we get,

$$V_{RX} = V_I + (R_F + \frac{3}{\pi} X_{co} + pL_F)\, I_R \qquad \ldots(5.11)$$

The electromagnetic torque of the induction motor is given by the expression,

$$T_e = \frac{3}{2} \cdot \frac{P}{2} \cdot L_{12} [i_{qs} i_{dr} - i_{ds} i_{qr}] \qquad ...(5.12)$$

where P = number of poles.

5.4 EQUATIONS IN CONCORDIA'S PER UNIT SYSTEM

From equation (5.2), the expression of the line current is given as,

$$i_{as} = \frac{2\sqrt{3}}{\pi} I_R [\cos \omega_e t - \frac{1}{5} \cos 5 \omega_e t + \frac{1}{7} \cos 7 \omega_e t - \frac{1}{11} \cos 11 \omega_e t \ ...]$$

Let the r.m.s. value of base current on machine side be I_b amperes per phase. The maximum value of this base current will be $\sqrt{2}\ I_b$ amperes. We define 1.0 p.u. d.c. link current (I_{Ib}) as one which gives 1.0 p.u. machine phase currents.

Thus from the above equation,

$$\sqrt{2}\ I_b = \frac{2\sqrt{3}}{\pi} I_{Ib}$$

$$\Rightarrow I_{Ib} = \frac{\sqrt{2}\pi}{2\sqrt{3}} I_b \qquad ...(5.13)$$

Unit power on inverter side (P_I) = $V_{Ib}\ I_{Ib}$.

Unit power on machine side (P_M) = $3\ V_b\ I_b$ (under unit p.f. condition).

where V_b = machine base voltage.

Equating power on inverter side to power on machine side to find out inverter base voltage,

$$V_{Ib}\ I_{Ib} = 3\ V_b\ I_b$$

Hence
$$V_{Ib} = \frac{3V_b\ I_b}{I_{Ib}} \qquad \ldots(5.14)$$

The inverter has been assumed loss less.

Substituting the expression for I_{Ib} from equation (5.13) in equation (5.14),

$$V_{Ib} = \frac{3V_b\ I_b}{\sqrt{2}\pi\ I_b}\ 2\sqrt{3} = \frac{3\sqrt{6}}{\pi}\ V_b \qquad \ldots(5.15)$$

Base impedance on machine side

$$= \frac{V_b}{I_b} = Z_b \text{ ohms per phase} \qquad \ldots(5.16)$$

Base impedance on inverter side $= \frac{V_{Ib}}{I_{Ib}}$

$$= \frac{\frac{3\sqrt{6}}{\pi}\ V_b}{\sqrt{\frac{2}{3}}\pi\ I_b} = \frac{18}{\pi^2}\ Z_b \text{ ohms.} \qquad \ldots(5.17)$$

$$\text{Base torque (N - m)} = T_{base} = \frac{G}{2\pi\ f_b/P/2} \qquad \ldots(5.18)$$

where f_b is base frequency in Hz.

Rewriting equation (5.11),

$$V_{RX} = V_I + (R_F + \frac{3}{\pi} X_{co} + pL_F)\ I_R$$

We will define all the reactances at base frequency. So the above equation becomes,

$$V_{RX} = V_I + (R_F + \frac{3}{\pi} X_{co} + \frac{p}{\omega_b} X_F)\ I_R \qquad \ldots(5.19)$$

Dividing both sides of equation (5.19) by V_{Ib},

$$\frac{V_{RX}}{V_{Ib}} = \frac{V_I}{V_{Ib}} + (R_F + \frac{3}{\pi} X_{co} + \frac{p}{\omega_b} X_F) \frac{I_R}{I_{Ib}} \cdot \frac{I_{Ib}}{V_{Ib}}$$

$$\text{or } V'_{RX} = V'_I + (R'_F + X'_{co} + p^* X'_F)\ I'_R \qquad \ldots(5.20)$$

where operator $p^* = \frac{d}{d\tau}$ and $p = \frac{d}{dt}$

since τ is defined as $\omega_b . t$, therefore $d\tau = \omega_b . dt$

$$\Rightarrow p^* = \frac{d}{d\tau} = \frac{d}{\omega_b . dt} = \frac{p}{\omega_b} \qquad \ldots(5.21)$$

In equation (5.19) dash shows various quantities in p.u. Considering equation (5.2),

$$i_{as} = \frac{2\sqrt{3}}{\pi} I_R \left[\cos \omega_e t - \frac{1}{5} \cos 5\ \omega_e t + \frac{1}{7} \cos 7\ \omega_e t \ldots\right]$$

Dividing both sides by $\sqrt{2}\ I_b$,

$$\frac{i_{as}}{\sqrt{2}\ I_b} = \frac{2\sqrt{3}}{\pi} \cdot \frac{I_R}{\sqrt{2}\ I_b} \left[\cos \omega_e t - \frac{1}{5} \cos 5\ \omega_e t + \frac{1}{7} \cos 7\ \omega_e t \ldots\right]$$

or

$$i'_{as} = I'_R \left[\cos \omega_e t - \frac{1}{5} \cos 5\ \omega_e t + \frac{1}{7} \cos 7\ \omega_e t \ldots\right] \qquad \ldots(5.22)$$

Similarly other equations can be written in p.u. and are as follows:

$$V'_I = V'_{qs}\, g_{qs} + V'_{ds}\, g_{ds} \qquad \ldots(5.23)$$

$$i'_{qs} = I'_R\, g_{qs} \qquad \ldots(5.24)$$

$$i'_{ds} = I'_R\, g_{ds} \qquad \ldots(5.25)$$

$$\begin{bmatrix} V'_{qs} \\ V'_{ds} \\ 0 \\ 0 \end{bmatrix} = \begin{bmatrix} (r'_s + p^* X'_s) & \omega'_e X'_s & p^* X'_m & \omega'_e X'_m \\ -\omega'_e X'_s & (r'_s + p^* X'_s) & -\omega'_e X'_m & p^* X'_m \\ p^* X'_m & \omega'_{sl} X'_m & (r'_r + p^* X'_r) & \omega'_{sl} X'_r \\ -\omega'_{sl} X'_m & p^* X'_m & -\omega'_{sl} X'_r & (r'_r + p^* X'_r) \end{bmatrix} \begin{bmatrix} i'_{qs} \\ i'_{ds} \\ i'_{qr} \\ i'_{dr} \end{bmatrix} \qquad \ldots(5.26)$$

In the equation (5.26), all reactances are defined at base frequency i.e. f_b and $p^* = \frac{p}{\omega_b}$. Now considering equation (5.12),

$$T_e = \frac{3}{2} \cdot \frac{P}{2} \cdot \frac{1}{\omega_b} X_m \left[i_{qs}\, i_{dr} - i_{ds}\, i_{qr}\right]$$

Dividing both sides by T_{base}, i.e. $\frac{3V_b\, I_b}{2\pi f_b / P/2}$

$$T'_e = X'_m [i'_{qs}\, i'_{dr} - i'_{ds}\, i'_{qr}] \qquad \ldots(5.27)$$

5.5 EQUATION OF MOTION

Equation of motion is given by the following expression (in M.K.S. unit)

$$\frac{2J}{P}\frac{d\omega_r}{dt} = T_e - T_L \qquad \ldots(5.28)$$

where T_e = Electromagnetic torque in N – m.

T_L = Load torque in N – m.

Dividing both sides of equation (5.28) by T_{base} [equation (5.18)],

$$\frac{J}{P^2/4} \cdot \frac{2\pi f_b}{G}\frac{d\omega_r}{dt} = T_e' - T_L' \qquad \ldots(5.29)$$

where T_e' and T_L' are in p.u.

The inertia constant of the machine H in seconds is given by,

$$H = \frac{1}{2} J \frac{(w_b/P/2)^2}{P_M}$$

where $\omega_b = 2\pi f_b$ = base angular speed in electrical radians per sec.

Rewriting equation (5.29)

$$\frac{2 \cdot \frac{1}{2} \cdot J(\frac{\omega_b}{P/2})^2}{G}\frac{d}{dt}(\frac{\omega_r}{\omega_b}) = T_e' - T_L'$$

or

$$4\pi f_b H p(\omega_r') = T_e' - T_L' \qquad \ldots(5.30)$$

where $\omega_r' = \frac{\omega_r}{\omega_b}$

From here onwards, the star on the operator p and the dashes used in the equations (5.20) to (5.30) to differentiate between p.u. system and M.K.S. system quantities will be dropped out for the sake of notational convenience and it will be remembered that all equations are in p.u. system with motoring convention.

Now combining the equations derived above, we will develop the model of the whole drive shown in Fig. (5.1).

It is well known that machine stability is determined primarily by the fundamental component of machine variables. Therefore we will neglect the effect of harmonics. Thus only fundamental component of a.c. is considered. Therefore from equations (5.6),

$$g_{ds} = 0,\ g_{qs} = 1 \qquad \ldots(5.31)$$

Rewriting equation (5.26),

$$\begin{bmatrix} V_{qs} \\ V_{ds} \\ 0 \\ 0 \end{bmatrix} = \begin{bmatrix} (r_s+pX_s) & \omega_e X_s & p\,X_m & \omega_e\,X_m \\ -\omega_e\,X_s & (r_s+pX_s) & (\omega_e\,X_m) & p\,X_m \\ p\,X_m & \omega_{sl}\,X_m & (r_r+pX_r) & \omega_{sl}\,X_r \\ -\omega_{sl}\,X_m & p\,X_m & -\omega_{sl}\,X_r & (r_r+pX_r) \end{bmatrix} \begin{bmatrix} i_{qs} \\ i_{ds} \\ i_{qr} \\ i_{dr} \end{bmatrix} \qquad \ldots(5.32)$$

Substituting values of g_{ds} and g_{qs} from equation (5.31) in equation (5.32) to (5.25) yields,

$$\begin{aligned} V_I &= V_{qs} \\ i_{qs} &= I_R \\ i_{ds} &= 0 \end{aligned} \qquad \ldots(5.33)$$

Now we rewrite equation (5.31) after omitting the ds equation since i_{ds} is identically zero.

$$\begin{bmatrix} V_{qs} \\ 0 \\ 0 \end{bmatrix} = \begin{bmatrix} (r_s+pX_s) & p\,X_m & \omega_e\,X_m \\ p\,X_m & (r_r+pX_r) & \omega_{sl}\,X_r \\ -\omega_{sl}\,X_m & -\omega_{sl}\,X_r & (r_r+pX_r) \end{bmatrix} \begin{bmatrix} i_{qs} \\ i_{qr} \\ i_{dr} \end{bmatrix} \qquad \ldots(5.34)$$

Rewriting equation (5.20),

$$V_{RX} = V_I + (R_F + X_{co} + pX_F)\, I_R \qquad \ldots(5.35)$$

Substituting the values of V_I and I_R from equation (5.34), the above equation results in,

$$V_{RX} = V_{qs} + (R_F + X_{co} + pX_F)\, i_{qs} \qquad \ldots(5.36)$$

Substituting the expression for V_{qs} from equation (5.30) in equation (5.32) and rearranging the terms we get,

$$\begin{bmatrix} V_{XX} \\ 0 \\ 0 \end{bmatrix} = \begin{bmatrix} \{r_s+R_F+X_{co}+p(X_s+X_F)\} & p\,X_m & \omega_e\,X_m \\ p\,X_m & (r_r+pX_r) & \omega_{sl}\,X_r \\ -\omega_{sl}\,X_m & -\omega_{sl}\,X_r & (r_r+pX_r) \end{bmatrix} \begin{bmatrix} i_{qs} \\ i_{qr} \\ i_{dr} \end{bmatrix} \quad \ldots(5.37)$$

Now the equation of motion is rewritten,

$$4\pi\, f_b H(\omega_r) = T_e - T_L \quad \ldots(5.38)$$

From equation (5.27),

$$T_e = X_m\,(i_{qs}\, i_{dr} - i_{ds}\, i_{qr}) \quad \ldots(5.39)$$

Substituting the values of i_{ds} from (5.33) into (5.39) we get,

$$T_e = X_m\, i_{qs}\, i_{dr} \quad \ldots(5.40)$$

Substituting values of T_e from (5.40) into equation (5.38) gives,

$$(4\pi\, f_b\, H\, p\, \omega_r) = (X_m\, i_{qs}\, i_{dr}) - (T_L) \quad \ldots(5.41)$$

5.6 CONCLUSION

The mathematical model comprising of equations (5.37) and (5.41) completely represents the current-source-inverter fed variable speed induction motor drive shown in

figure (5.1). The induction motor equations are written in synchronously rotating reference frame under quasi-steady state conditions in its stator circuit.

Using this mathematical model, the steady-state performance of the drive is investigated in the following Chapter.

CHAPTER VI

STEADY-STATE ANALYSIS OF THE DRIVE

6.1 INTRODUCTION

In this chapter the steady-state equations of the system are derived using the mathematical model developed in the previous chapter. They are simulated on a digital computer to compute steady state performance for several values of stator frequency and d.c. link current. The results, so obtained, are discussed.

6.2 STEADY-STATE EQUATIONS

Under steady-state conditions, the machine variables in q-d reference frame and d.c. link variables are constants. Hence in this case, substituting differential terms as zero and using relations (5.33), equations (5.35) and (5.37) and (5.41) can be expressed in the following form,

$$V_{RXo} = V_{qso} + (R_F + X_{CO})\, I_{Ro} \qquad \ldots(6.1)$$

$$\begin{bmatrix} V_{RXo} \\ 0 \\ 0 \end{bmatrix} = \begin{bmatrix} (r_s+R_F+X_{CO}) & 0 & \omega_e X_m \\ 0 & r_r & \omega_{slo} X_r \\ -\omega_{slo} X_m & -\omega_{slo} X_m & r_r \end{bmatrix} \begin{bmatrix} i_{qso} \\ i_{qro} \\ i_{dro} \end{bmatrix} \qquad \ldots(6.2)$$

$$T_e = X_m\, i_{qso}\, i_{dro} = T_L \qquad \ldots(6.3)$$

Subscript o is used to define steady-state variables. ω_e is the ratio of applied electrical frequency to the base frequency. It can be interpreted as per unit operating frequency.

From equation (6.2)

$$V_{XO} = (r_s + R_F + X_{CO})i_{qso} + \omega_e\, X_m\, i_{dro} \qquad \ldots(6.4)$$

$$0 = r_r\, i_{qro} + \omega_{slo}\, X_r\, i_{dro} \qquad \ldots(6.5)$$

$$0 = -\omega_{slo}\, X_m\, i_{qso} - \omega_{slo}\, X_r\, i_{qro} + r_r\, i_{dro} \qquad \ldots(6.6)$$

From equation (6.5),

$$i_{qro} = -\frac{\omega_{slo} X_r}{r_r} i_{dro} \qquad \ldots(6.7)$$

Substituting value of i_{qro} from equation (6.7) in (6.6) and solving for i_{dro},

$$i_{dro} = \left[\frac{\omega_{slo}\, X_m\, r_r}{(\omega_{slo} X_r)^2 + (r_r)^2}\right] i_{qso} \qquad \ldots(6.8)$$

Substituting the value of V_{RXo} from equation (6.4) in equation (6.1),

$$V_{qso} = r_s\, i_{qso} + \omega_e\, X_m\, i_{dro} \qquad \ldots(6.9)$$

Substitution of the expression for i_{dro} from equation (6.8) in equation (6.9), (6.3), and (6.7) respectively, gives the following:

$$V_{qso} = \left[r_s + \frac{\omega_e \, \omega_{slo} \, X_m^2 \, r_r}{(\omega_{slo} \, X_r)^2 + (r_r)^2} \right] i_{qso} \quad \ldots(6.10)$$

$$T_e = \left[\frac{\omega_{slo} \, (X_m)^2 \, r_r}{(\omega_{slo} \, X_r)^2 + (r_r)^2} \right] (i_{qso})^2 \quad \ldots(6.11)$$

$$i_{qro} = - \left[\frac{(\omega_{slo}) \, X_r \, X_m}{(\omega_{slo} \, X_r)^2 + (r_r)^2} \right] i_{qso} \quad \ldots(6.12)$$

Rewriting equation for V_{dso} from equation (5.32),

$$V_{dso} = - \omega_e \, X_s \, i_{qso} - \omega_e \, X_m \, i_{qro} \quad \ldots(6.13)$$

Substituting the value of i_{qro} from equation (6.12) in (6.13),

$$V_{dso} = \left[-\omega_e \, X_s + \frac{\omega_e \, \omega_{sl} \, X_r \, (X_m)^2}{(\omega_{sl} \, X_r)^2 + (r_r)^2} \right] i_{qso} \ldots(6.14)$$

Since the q-axis is assumed to coincide with a-phase at $t = 0$, referring fig. (5.2),

$$\theta_e = \omega_e t$$

Also,

$$i_{as} = i_{qso} \cos\theta_e$$

$$V_{as} = V_{qso} \cos\theta_e + V_{dso} \sin\theta_e$$

$$= |V_{as}| \cos(\theta_e + \phi_e)$$

where

$$|V_{as}| = [(V_{qso})^2 + (V_{dso})^2]^{1/2} \qquad \ldots(6.15)$$

$$\text{Power factor (lagging)} = \cos[\tan^{-1}(-\frac{V_{dso}}{V_{qso}})] \qquad \ldots(6.16)$$

Rewriting equation (6.1),

$$V_{RXo} = V_{qso} + (R_F + X_{CO})\, i_{qso} \qquad \ldots(6.17)$$

since $i_{qso} = I_{Ro}$.

Copper losses of the drive

Copper losses in induction motor stator

$$= r_s (i_{qso})^2 \qquad \ldots(6.18)$$

Copper losses in induction motor rotor

$$= r_r[(i_{dro})^2 + (i_{qro})^2] \qquad \ldots(6.19)$$

Substituting expression for i_{qro} from equation (6.12) and expression for i_{dro} from equation (6.8) in equation (6.19),

$$\text{Copper losses in rotor} = \left[\frac{r_r\,\omega_{slo}^2\,X_m^2}{(\omega_{slo}X_r)^2 + (r_r)^2}\right](i_{qso})^2 \qquad \ldots(6.20)$$

$$\text{Losses in the d.c. line} = R_F\,I_{Ro}^2$$

Since $I_{Ro} = i_{qso}$,

$$\text{Losses in d.c. link} = R_F(i_{qso})^2 \qquad \ldots(6.21)$$

Ignoring the iron, friction and windage losses, total losses are determined as follows.

Total Losses in Drive = Losses in induction motor stator
+ Losses in induction motor rotor
+ Losses in d.c. link inductor

$$= \left[r_s + R_F + \frac{r_r\,\omega_{slo}^2\,X_m^2}{(\omega_{slo}X_r)^2 + (r_r)^2}\right](i_{qso})^2 \qquad \ldots(6.22)$$

$$\text{Power output} = T_e \times \omega_{ro} = T_e\,(\omega_e - \omega_{slo}) \qquad \ldots(6.23)$$

$$\text{Efficiency of the drive} = \frac{\text{Power output}}{\text{Power output} + \text{Total Losses in the drive.}}$$

$$\text{Efficiency} = \frac{T_e\,(\omega_e - \omega_{slo})}{T_e\,(\omega_e - \omega_{slo}) + \text{Total losses in the drive}} \qquad \ldots(6.24)$$

6.3 ANALYTICAL RESULTS AND DISCUSSIONS

In this section, the equations developed in the previous sections in terms of d - q variables of the motor have been used to determine the steady-state behaviour of the current-source inverter fed induction motor drive. P.U. parameters of the machine used in the investigations are given in the Appendix 'E'.

The torque-slip curve of the induction motor fed from current source at rated current (I_s = 1.0 P.U.) and rated frequency (f = 1.0 P.U.) is shown in Fig. (6.1). This curve is compared with the torque-slip curve of the same motor fed from voltage source at rated voltage (V_s = 1.0 P.U.) and rated frequency (f = 1.0 P.U.). The build up of induction motor stator voltage (for current source operation) and stator current (for voltage source operation) with respect to slip are shown in Fig. (6.2). Comparison of torque-slip curves of voltage-fed and current-fed induction motor shows that, for current-source operation, starting as well as maximum developed torque are very low, also the slips at which maximum torque occurs in both case are quite different. The difference in the level of flux in both cases of operation is mainly responsible for the above difference. As is clear from Fig. (6.2) that, for rated current operation, stator terminal voltage will be very low in the

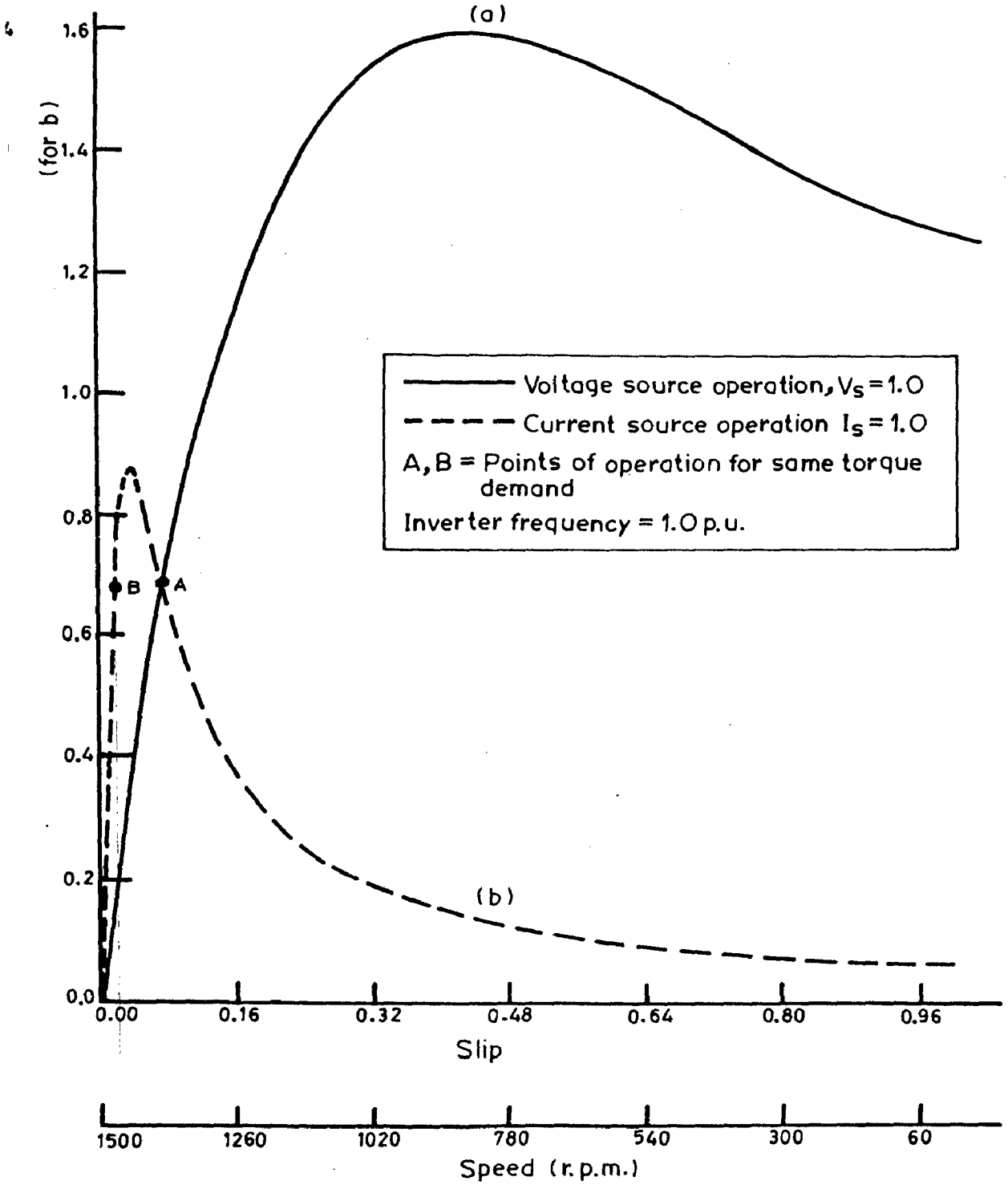

.1_ Comparison of torque-slip curves of voltage-fed and current-fed induction motor at rated frequency.

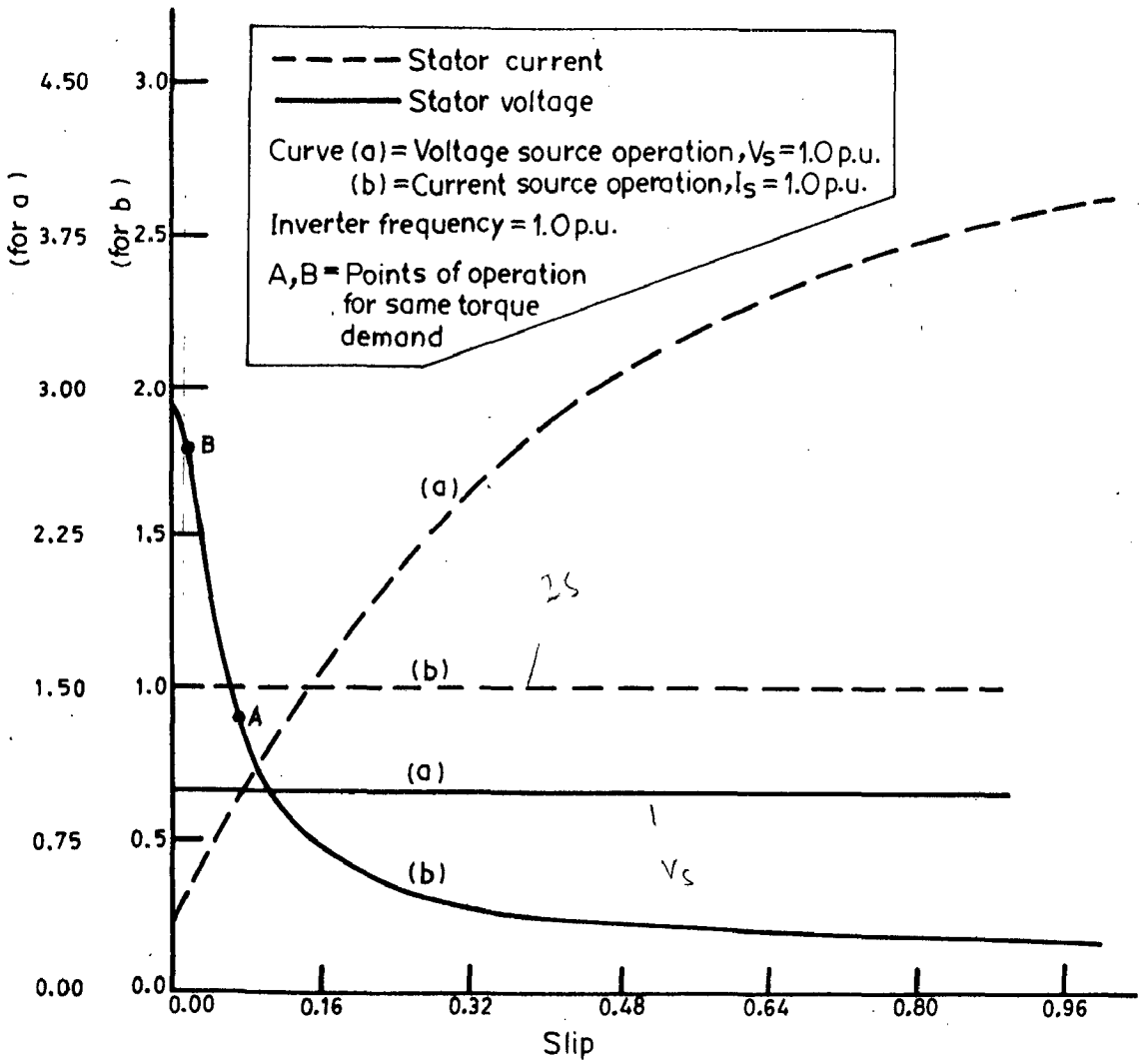

Fig. 6.2 Stator voltage build up for current-fed and stator current build up for voltage-fed induction motor at rated frequency.

starting (s = 1.0) due to low machine impedance resulting in very low airgap flux (since frequency is constant) and hence the torque. As the speed increases, the machine terminal voltage rises, resulting in the increase of airgap flux and hence the torque. In the absence of saturation in the machine, the torque rises to very high values. In a practical machine, however, the saturation will limit the developed torque. For voltage source operation terminal voltage always remains constant at 1.0 P.U. [Fig. (6.2)] resulting in the constant (rated) airgap flux in the machine for all the slips. Therefore starting torque is very large and since full saturation never occurs, maximum torque is also quite large.

For determining the steady-state performance of the current-source-inverter-fed induction motor drive, the values of stator voltage, power output, efficiency, torque, total losses, power factor are calculated in the full range of the slip (i.e. s = 0.0 to 1.0) for different values of d.c. link current and operating frequencies. The flow chart and the computer program for calculating the steady-state performance are given in Appendix C and D, respectively.

All the theoretical results of steady-state performance are plotted with respect to slip as well as speed with the help of calcomp plotter and discussed.

6.3.1 Torque-Slip Characteristics

The torque-slip curves of the drive at different d.c. link currents and operating frequencies are shown in Fig. [6.3(a)] and [6.3(b)]. It is noted from the curves that developed torque at starting (s = 1.0) is low. As the speed increases, the torque rises to high value near synchronous speed and after attaining the maximum value decreases to zero with steep slope at synchronous speed. The variable flux level in the machine is responsible for the above nature of the curve, as explained earlier.

The examination of characteristics of Fig. (6.1) for current source operation indicates two regions of operation - one on positive slope and the other on negative slope of the curve. The positive slope region is well known as unstable. However, the steady-state operating point will occur in both the regions for the same torque demand. For example machine can be operated at point A or B [Fig. (6.1)] for the same torque demand. Slip corresponding to point A is higher than B, which means that machine impedance corresponding to point A will be lower than B. Since machine is being fed from a constant current source therefore stator voltage and flux level in the machine will be higher at point B than A [Fig. (6.2)], resulting in partial saturation with

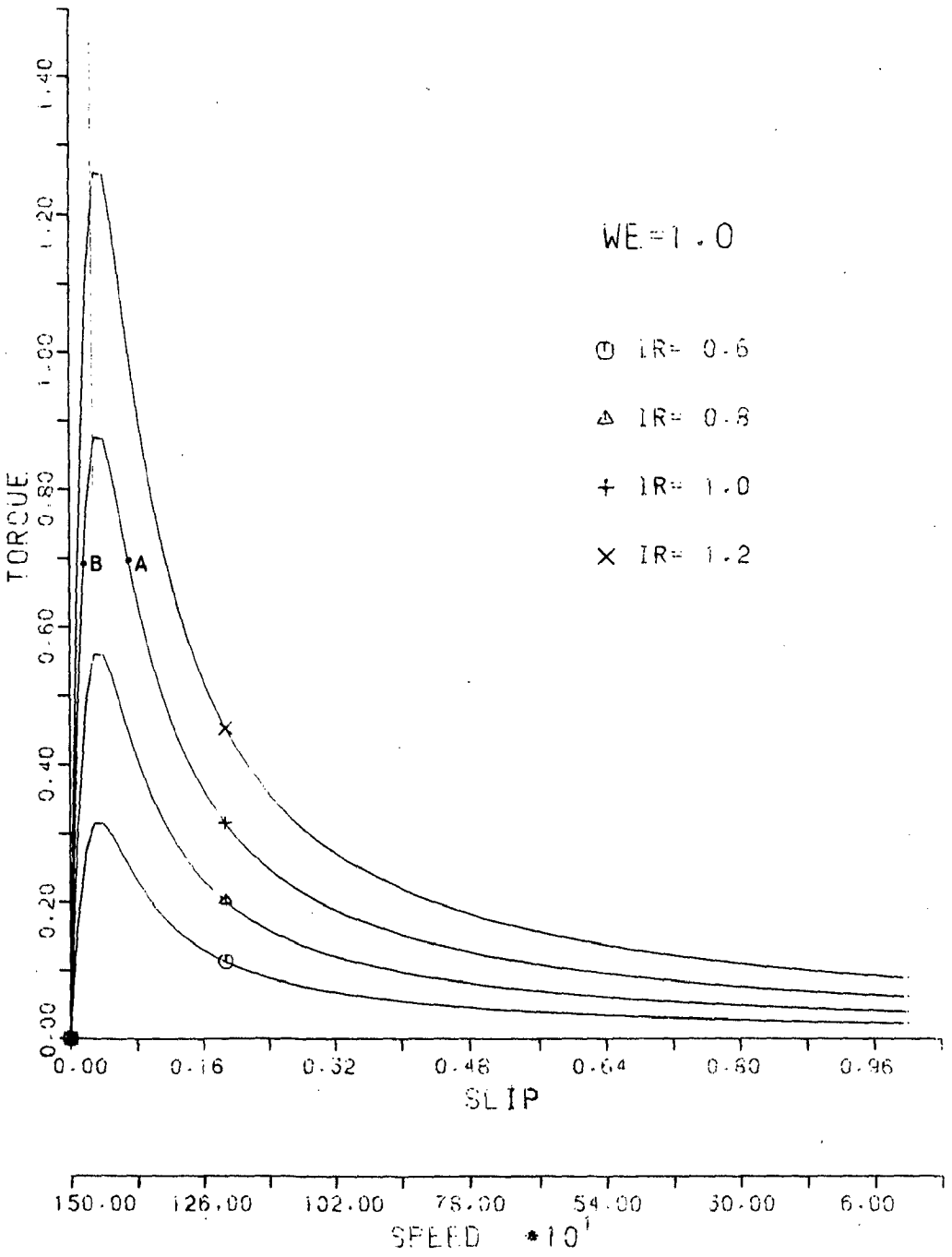

Fig.6.3(a)_ Motor torque vs. slip curves at different D.C.link currents.

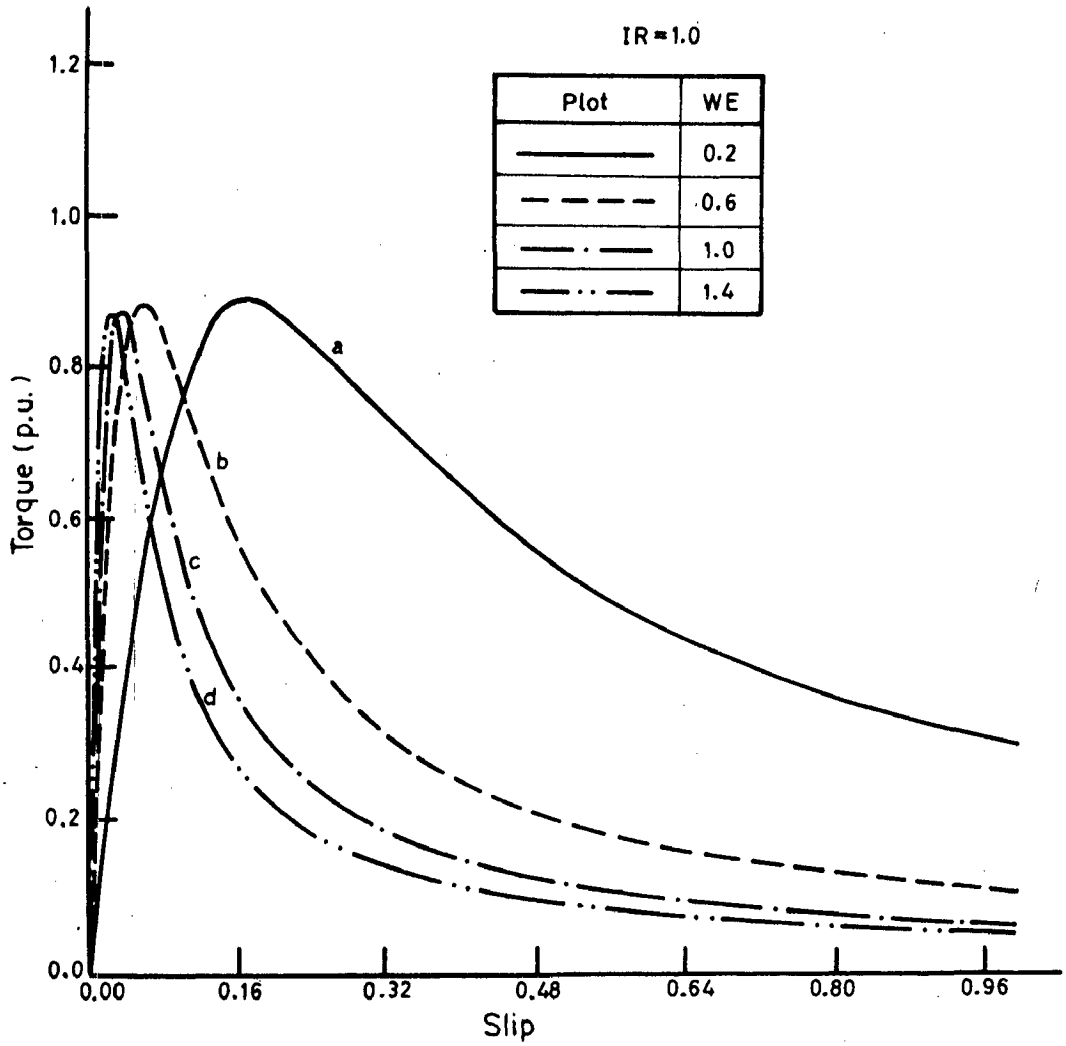

Fig.6.3(b)_ Motor torque vs. slip curves at different frequencies.

higher iron loss and torque pulsation effect at B. The stator copper losses will be same at A and B but the rotor copper losses will be somewhat higher at A on account of increase in rotor current. Point A, being point of intersection of V_s = 1.0 and I_s = 1.0 curves, corresponds to normal flux level in the machine, therefore operation should be preferred at A. However A lies in the unstable zone of operation therefore closed loop operation is mandatory.

It is seen from the curves [Fig. 6.3(a)] that increment in the d.c. link current results in the increased torques resulting in upward shift of the whole characteristic. This is because the motor torque is proportional to square of the d.c. link current. The slip at which maximum torque occurs remains almost unchanged.

As the operating frequency increases, developed torque remains the same for the given value of d.c. link current but slip corresponding to maximum torque progressively decreases, as shown in Fig. [6.3(b)].

6.3.2 Power Output Vs Slip

The power output variation with slip for different d.c. link currents (f = 1.0 P.U.) and different operating frequencies (I_R = 1.0 P.U.) are shown in Fig. [6.4(a)] and [6.4(b)]. Power output is zero at s = 0.0 and 1.0 and its variation between these extremes

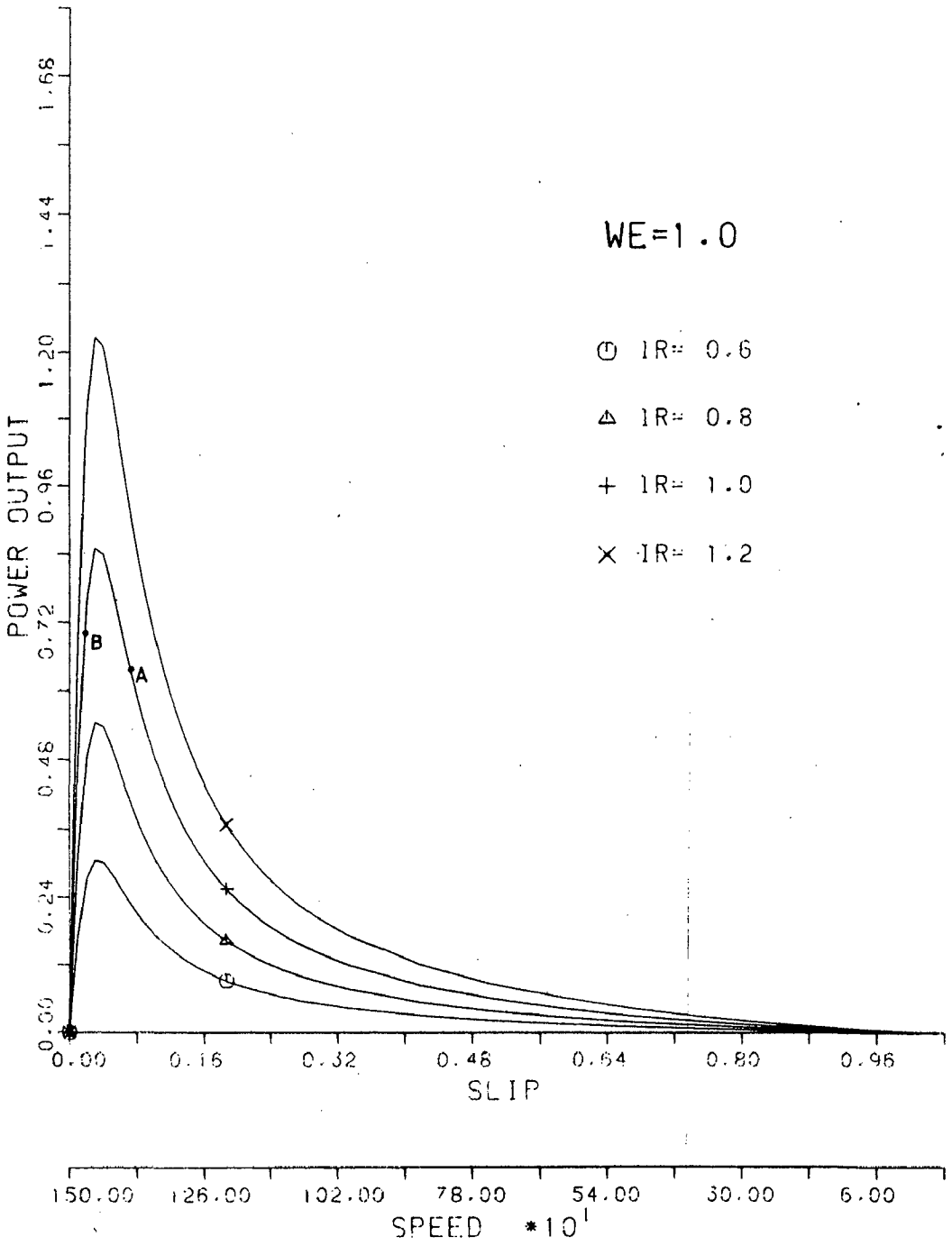

Fig. 6.4(a)_ Power output vs. slip curves at different D.C. link currents.

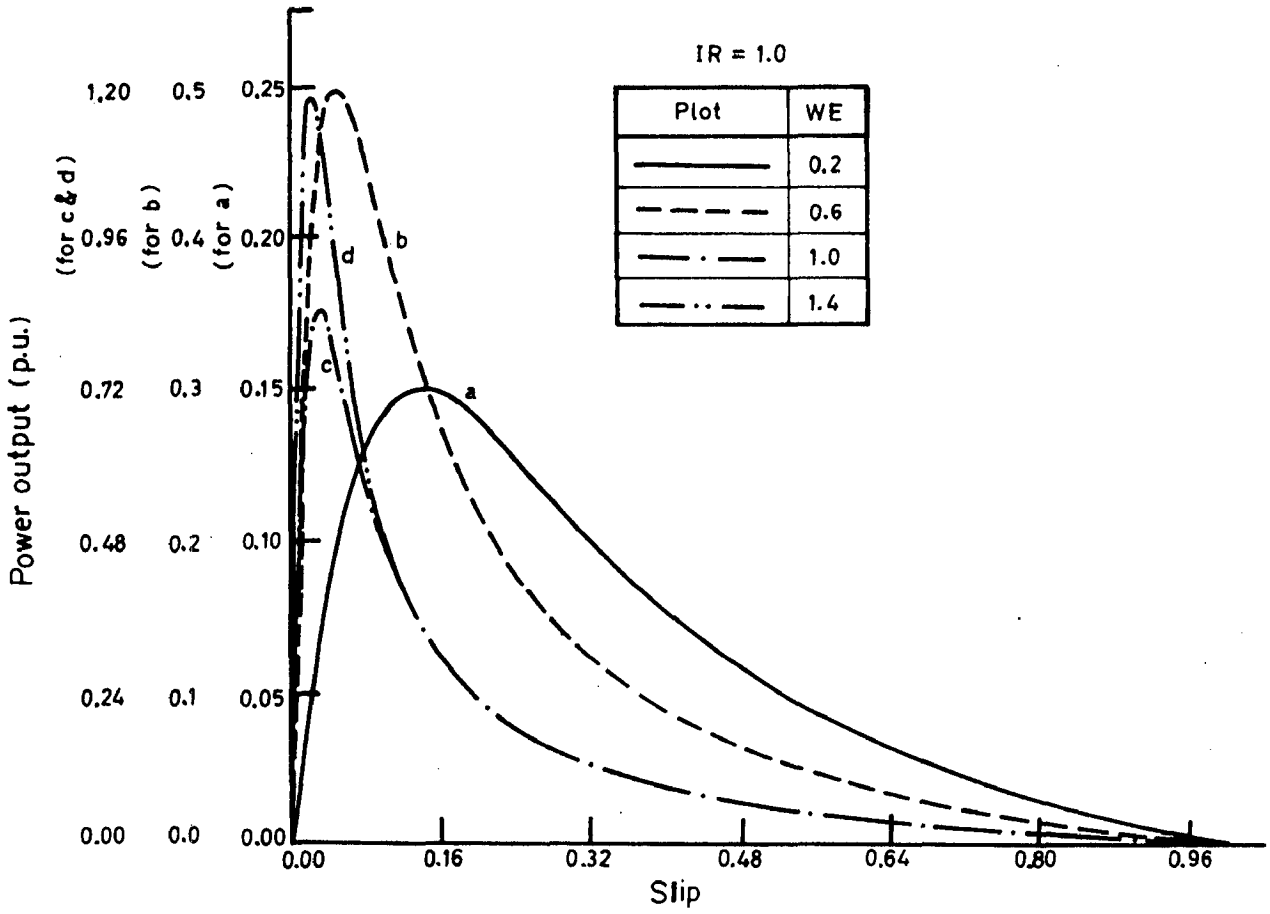

Fig.6.4(b)_ Power output vs. slip at different frequencies.

follows the pattern observed in the case of corresponding torque-slip curves. The points A, B corresponding to same torque demand, as in previous case, are also marked. It is seen that power developed at point B is higher than at A. This is only because B belongs to higher speed than A.

Maximum power output increases with increase in operating frequencies [Fig. 6.4(b)]. Power output also increases with increase in d.c. link current due to increased torque resulting in upward shift of the characteristic. [Fig. 6.4(a)].

6.3.3 Total Losses Vs Slip

These characteristics are shown in Fig. [6.5(a)] and [6.5(b)] for variation in d.c. link current and frequency, respectively. The mathematical model accounts only for copper loss in the d.c. link inductor, stator and rotor of the motor. The characteristics show that the total losses in the drive are nearly constant for a very large range of operating slips. At a given d.c. link current, stator copper loss and d.c. link inductor copper loss are constant irrespective of slip. Rotor copper loss are proportional to square of rotor current which is very nearly equal to stator current at all slips except near 0.0, where it decreases sharply, becoming zero at s = 0.0. The points of operation

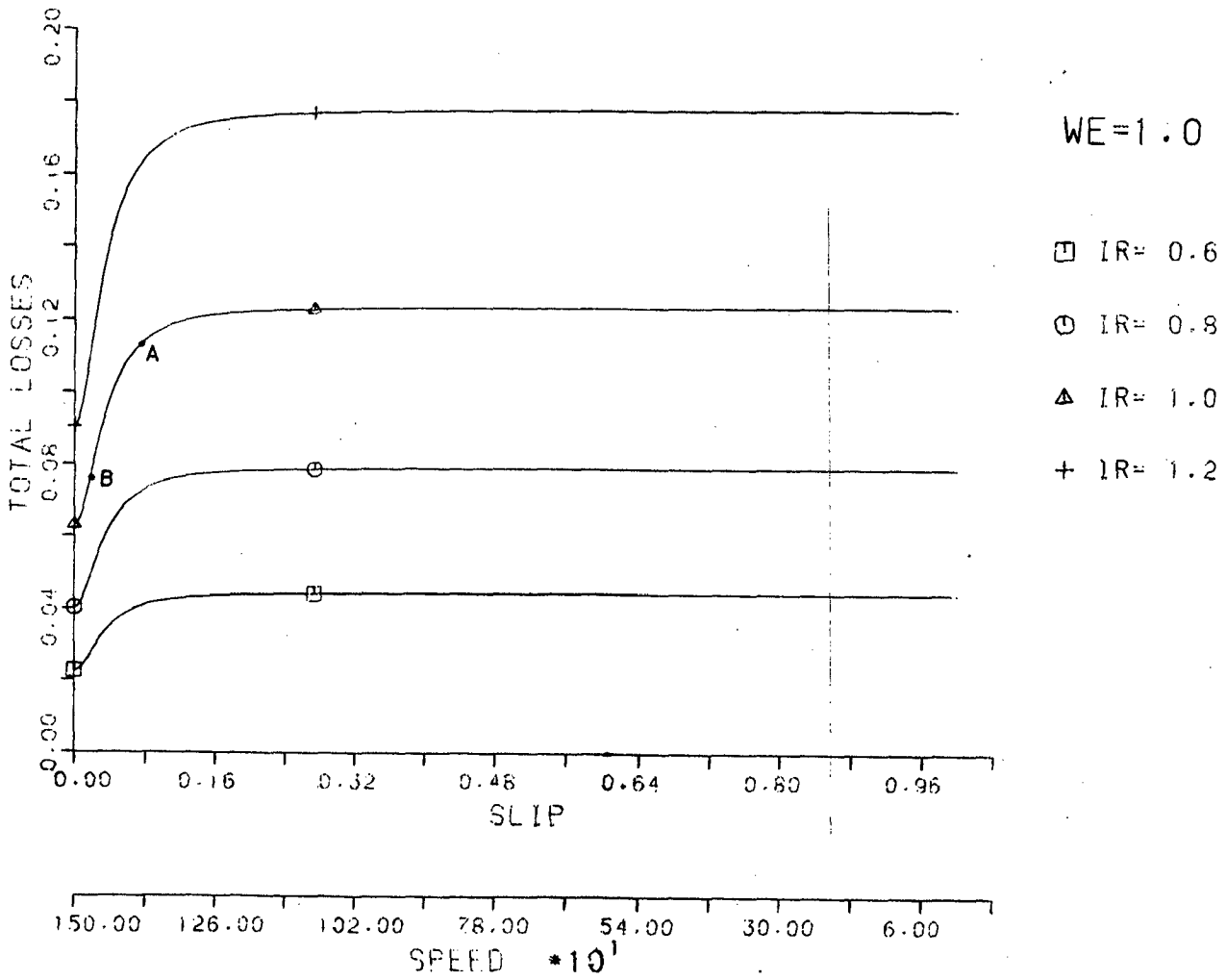

Fig. 6.5(a) – Total losses vs. slip curves at different D.C. link currents.

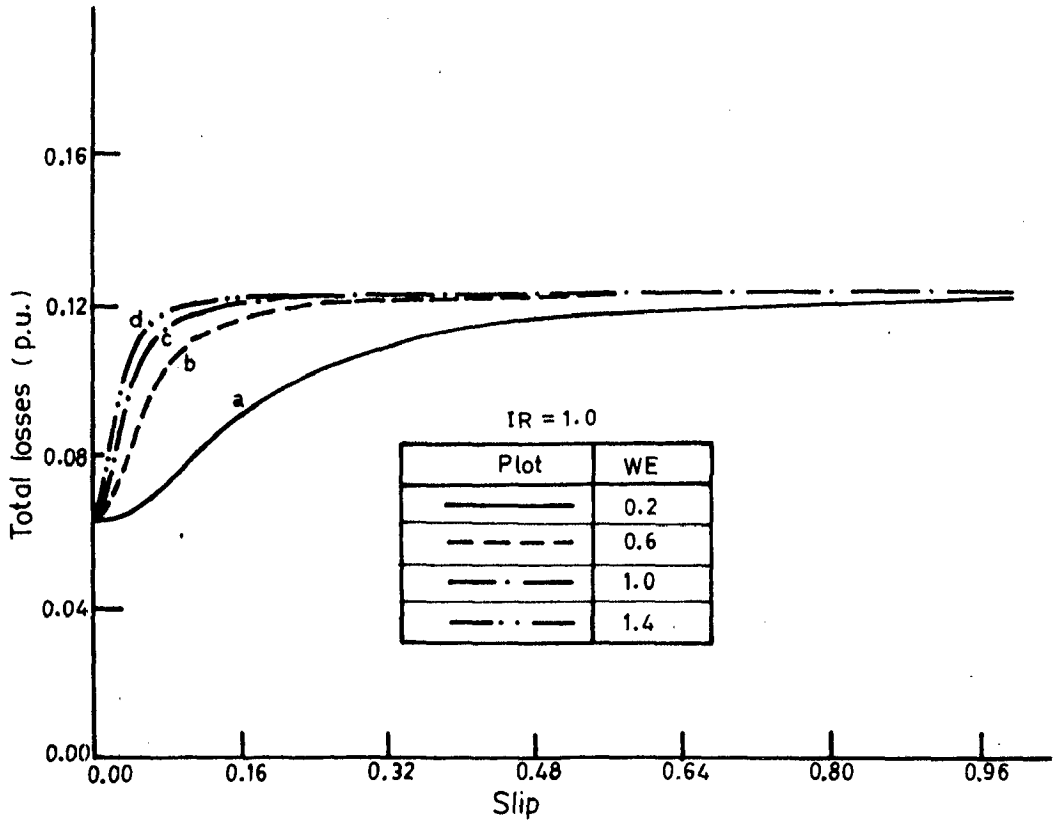

Fig.6.5(b)_ Total losses vs. slip at different frequencies.

A and B corresponding to [Fig. (6.1)] are also marked here. It is seen that losses are higher at point A than B on account of higher rotor copper losses at A. The losses at s = 0.0 are therefore d.c. link and stator copper losses only.

The increase in d.c. link current also results in the increase of total losses at all slips because copper losses are directly governed by it [Fig. 6.5(a)].

The increment in the operating frequency increase marginally the amount of copper losses in the drive but slope of the dropping part becomes more and more sharp as the frequency increases. This shows that rotor current and hence rotor copper loss start decreasing at higher slip when frequency is reduced.

6.3.4 Efficiency Vs Slip

The relevent curves are shown in Fig. [6.6(a)] and [6.6(b)] for different sets of operating conditions. It is evident from the curves that the efficiency is independent of the value of d.c. link current. This is so because both power input to induction motor and total losses of induction motor are function of square of d.c. link current. Thus ratio of motor losses and input power becomes independent of d.c. link current and so is the efficiency. The efficiency is zero

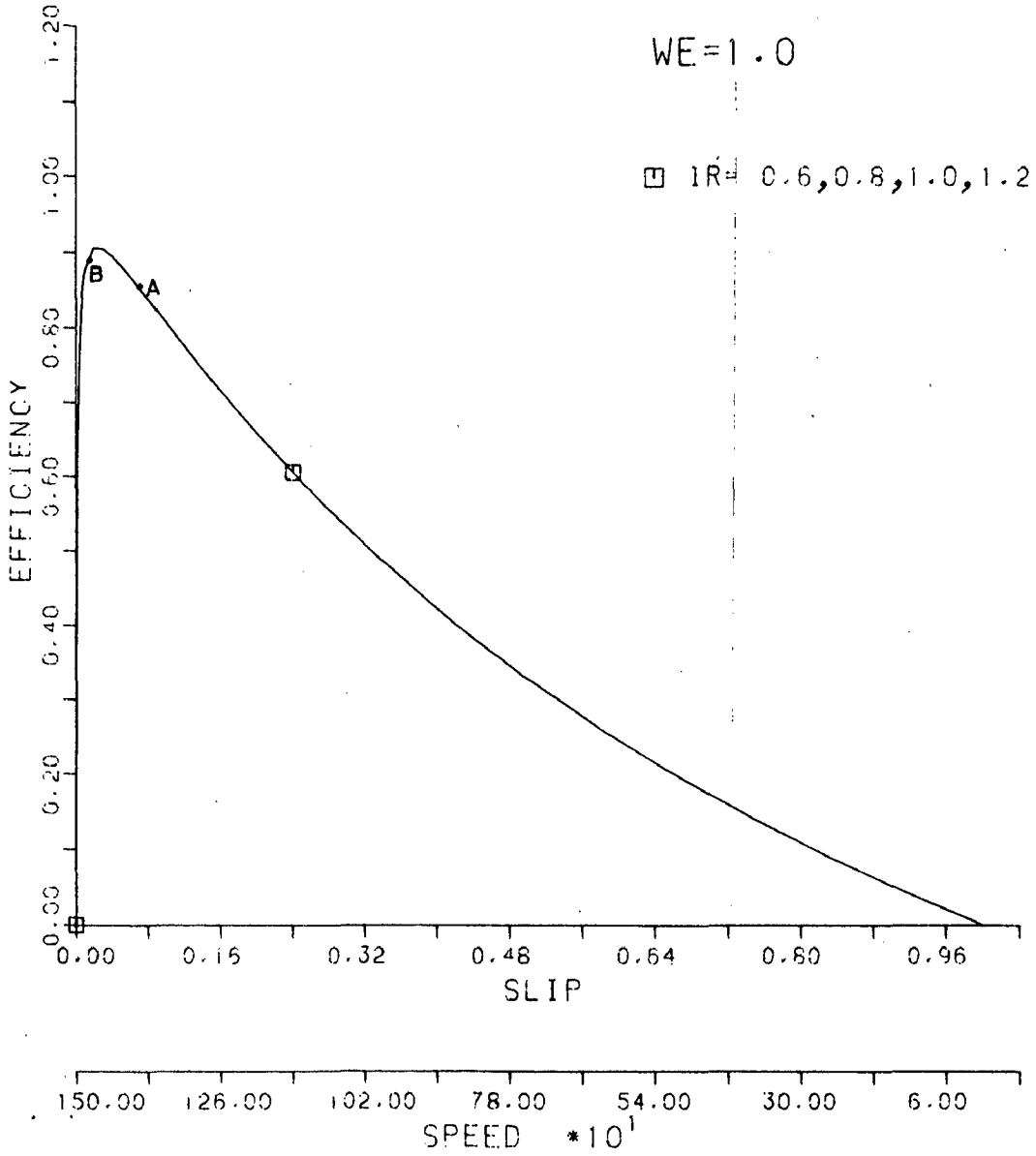

Fig. 6.6(a) _ Efficiency vs. slip curves at different D.C. link currents.

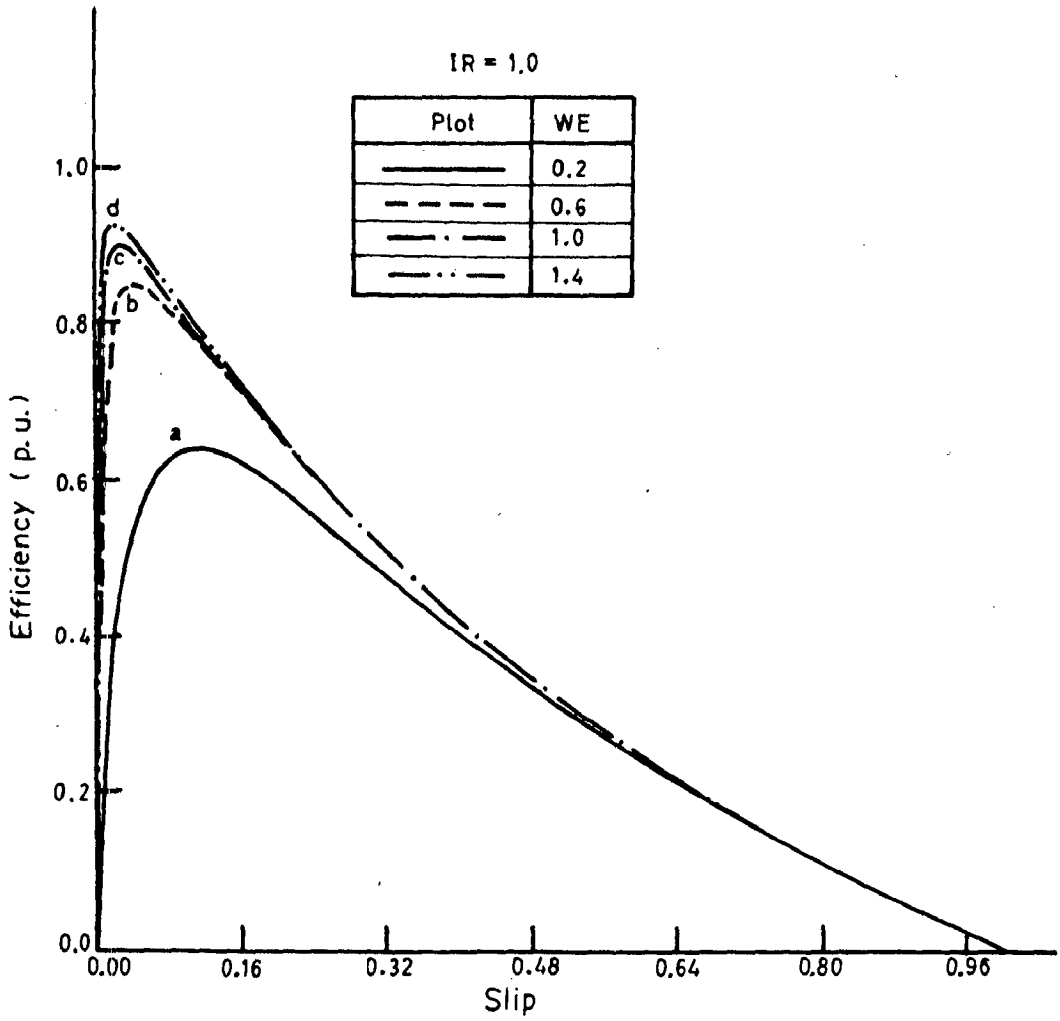

Fig. 6.6(b)_ Efficiency vs. slip at different frequencies.

at s = 1.0 and s = 0.0 since power output is zero at these slips. As the motor picks up speed, efficiency increases and after attaining a maximum value near synchronous speed falls to zero at synchronous speed. Point A and B of Fig. (6.1) are also marked here on the curve [Fig. 6.6(a)]. The efficiency is little higher at point B as compared to A, as copper losses are more at A.

The efficiency increases with increase in the p.u. operating frequency [Fig. 6.6(b)]. It happens because for a given d.c. link current and slip, power input increases with supply frequency whereas losses in the rotor remain unchanged.

6.3.5 Power Factor Vs Slip

The relationship between power factor and slip for the above said set of operating conditions are shown in Fig.[6.7(a)] and [6.7(b)]. Like the efficiency curve, power factor is also independent of the d.c. link current under the present assumptions [Fig. 6.7(a)]. The power factor curve starts from a finite value at standstill condition (slip = 1.0). It improves as the speed increases and after reaching the maximum value it starts decreasing with minimum value at synchronous speed. Points A and B are marked on the curve Fig.[6.7(a)]. It is noted that power factor at point A is far better than at point B. It is so because motor is being fed

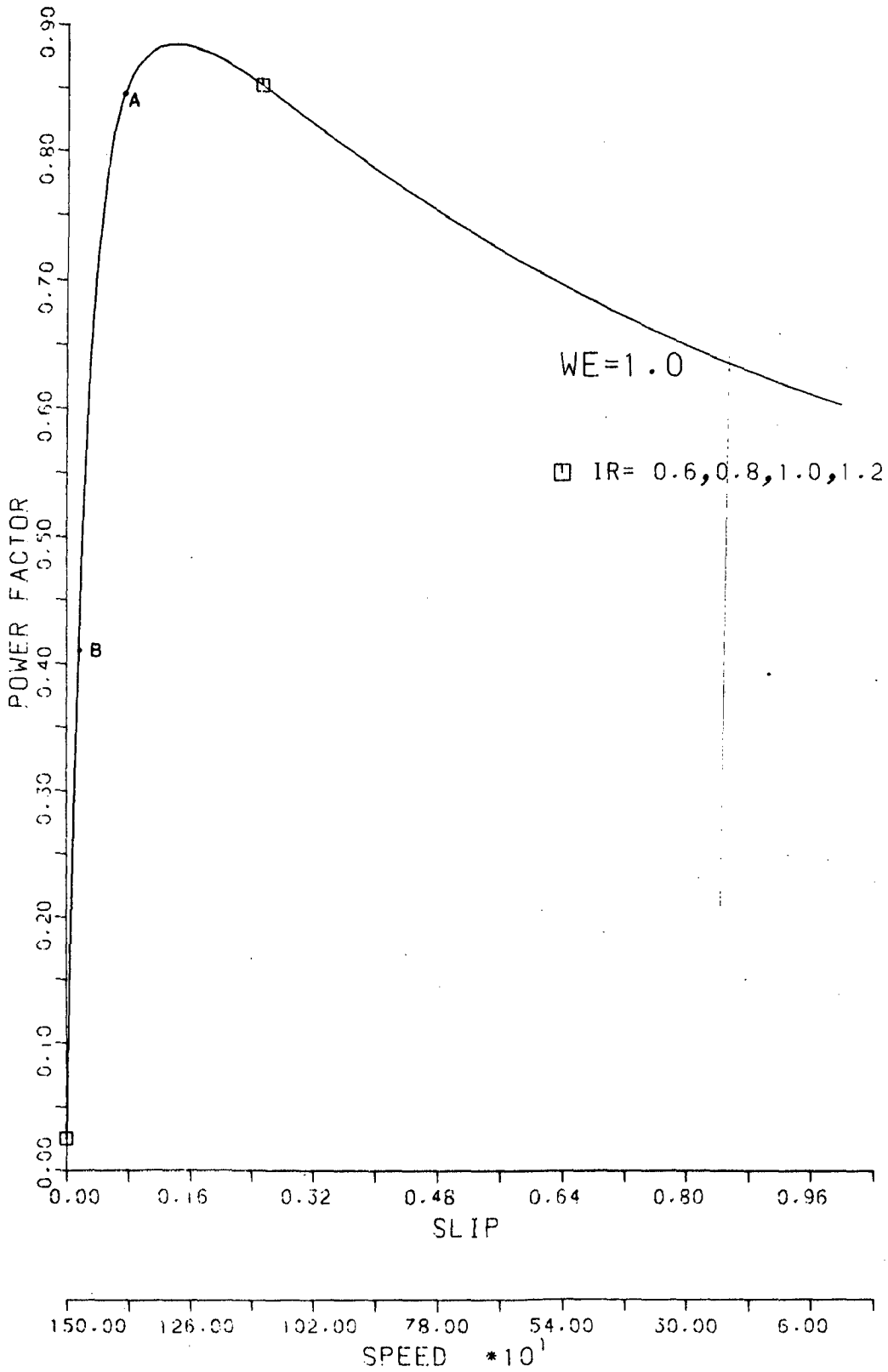

Fig. 6.7(a) _ Power factor vs. slip curves at different D.C. link currents.

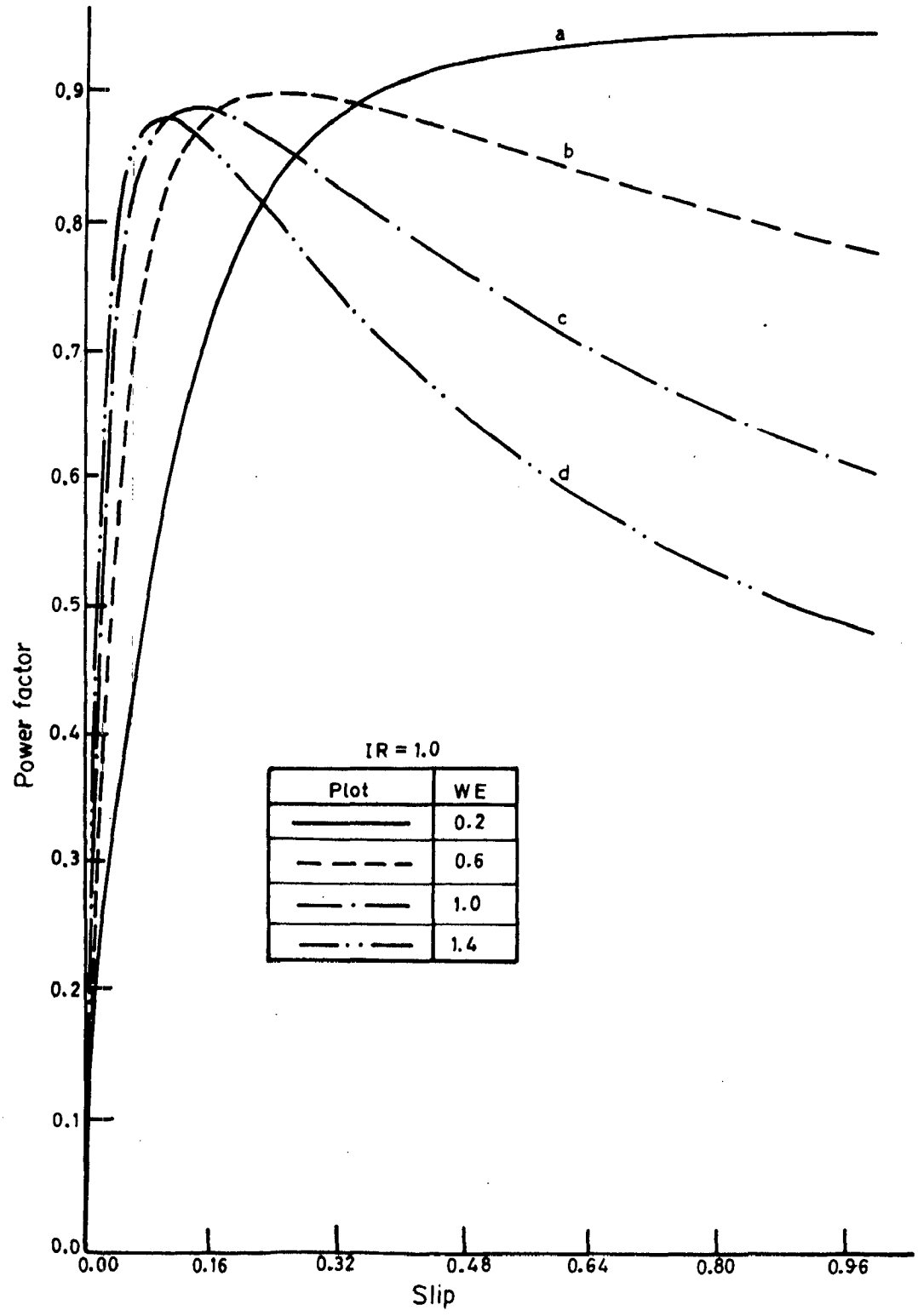

Fig. 6.7(b)_ Power factor vs. slip at different frequencies.

from a constant current source. At point A slip is higher therefore V_{dso} component (equation 6.14) reduces whereas V_{qso} component (equation 6.10) increases at A with respect to B, resulting in improvement in power factor (equation 6.16).

The variation in power factor with variation in supply frequency is shown in Fig.[6.7(b)]. It may be noted that as supply frequency increases, power factor improves near synchronous speed region but decreases progressively as slip approaches standstill value.

6.3.6 Stator Voltage Vs Slip

The stator voltage Vs slip characteristics of the induction motor for different p.u. d.c. link current and operating frequencies are shown in Fig.[6.8(a)] and [6.8(b)]. At low speeds (high slips) the stator voltage is very low and as the speed increases (slip decreases) stator voltage rises slowly. When motor approaches synchronous speed stator voltage rises sharply and assumes very high value. The above nature of the characteristic is due to variable flux level in the motor at different slips. At low speeds (high slips) motor impedance will be low resulting in lower flux and hence the lower stator voltage. As the machine picks up speed, the machine impedance increases giving rise to higher flux and hence the higher stator voltage.

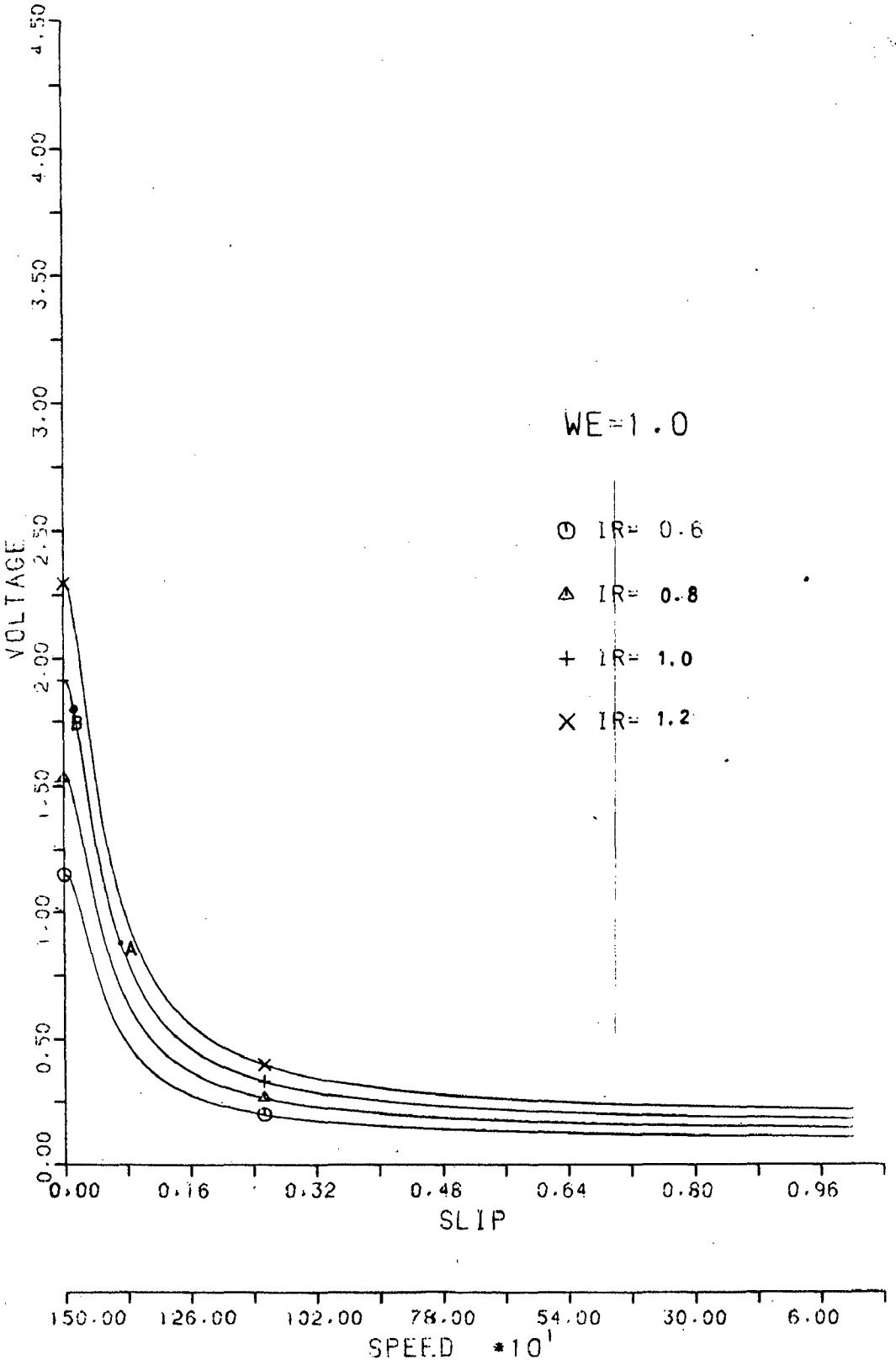

Fig. 6.8(a)_ Stator voltage vs. slip curves at different D.C.link currents.

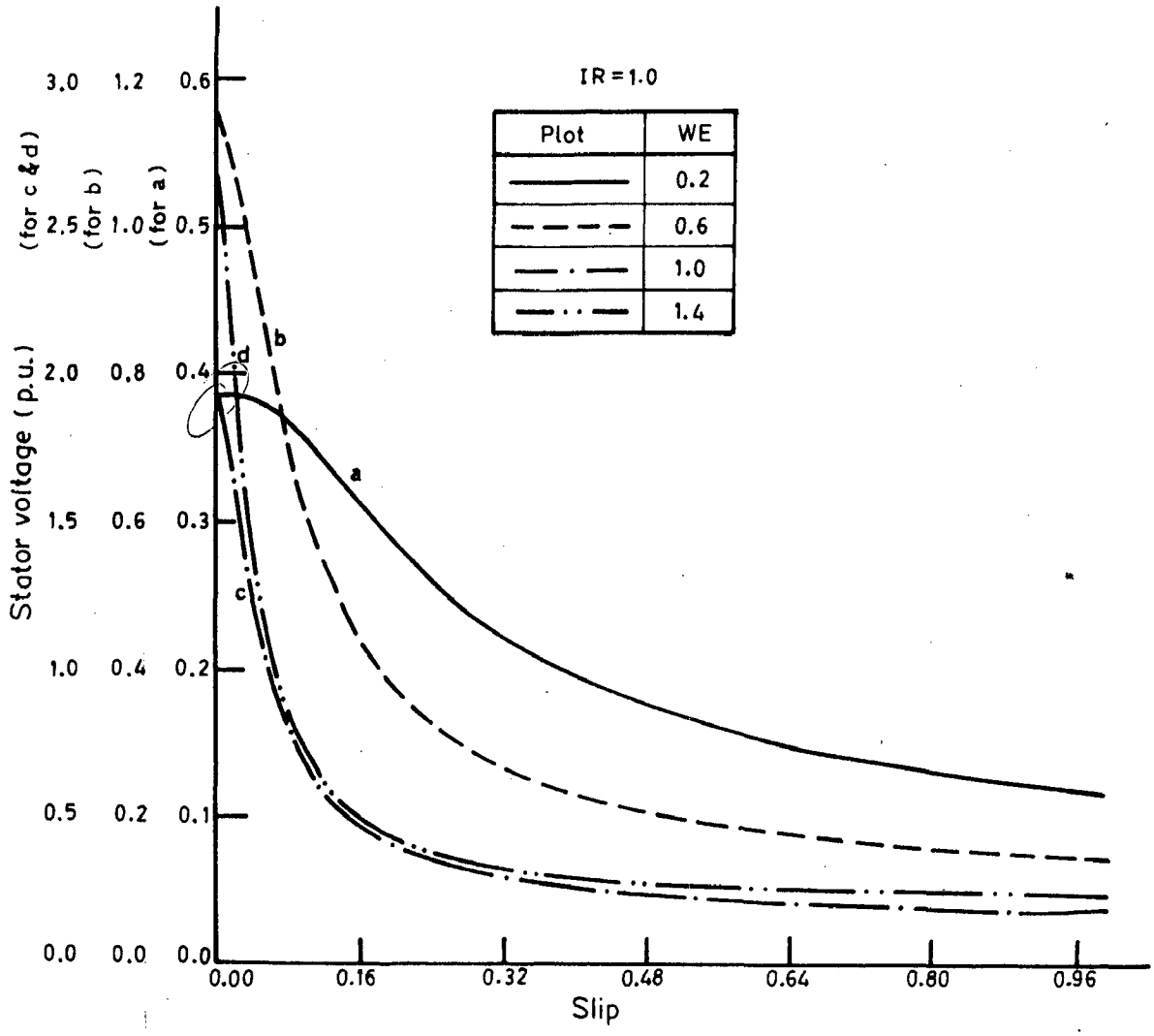

Fig.6.8(b)_ Stator voltage vs. slip curves at different frequencies.

The points A and B which corresponds to the same developed torque are also marked in the present characteristic [Fig. 6.8(a)]. It seems from the characteristic that operation at B will give rise to dangerously high stator voltage while operation at A will not. However in practical machine, saturation limits the rise of stator voltage beyond a certain limit. Therefore if open loop operation is attempted, stator voltage will never rise to such high values but motor will run in a highly saturated condition resulting in high iron losses and poor power factor. This is why operation is always preferred at A. Since A lies in the unstable zone of torque Vs slip characteristic, therefore closed loop is a must.

As d.c. link current is increased, the voltage Vs slip characteristic shifts to upper side resulting in even higher stator voltage [Fig. 6.8(a)]. It shows that flux level in the machine is directly governed by the d.c. link current.

Fig.[6.8(b)] shows that higher operating frequency results in the higher stator voltage, as for a given d.c. link current and slip, machine impedance increases with frequency.

6.4 CONCLUSION

An analytical method for determining the steady-state performance of the constant-current source inverter

fed induction motor drive has been set forth in this chapter. The motor performance at rated operating frequency and rated d.c. link current are shown with respect to slip in Fig.[6.9(a)] and with respect to torque in Fig.[6.9(b)] which summarises the complete motor performance studied so far.

The torque Vs slip characteristic can be divided into two zones, one with a positive slope and the other with a negative slope. The positive sloped zone is known to be unstable therefore operation in this zone is possible only with the help of feed back loop. However the negative sloped zone is inherently stable and machine can operate in this zone without any feed backs. Since the maximum torque occurs at very small slips, the negative sloped zone is very small.

We can always find two operating points, (A and B), one in each zone for the same torque demand. The various characteristics show that in stable zone (point B), power output will be more, losses will be less and efficiency will be better as compared to operation in the unstable zone. However power factor will be poor and stator voltage will be dangerously high while operating in the stable zone. Since the flux level in the machine will be very high when operating in the stable zone therefore saturation is bound to play an important role in the

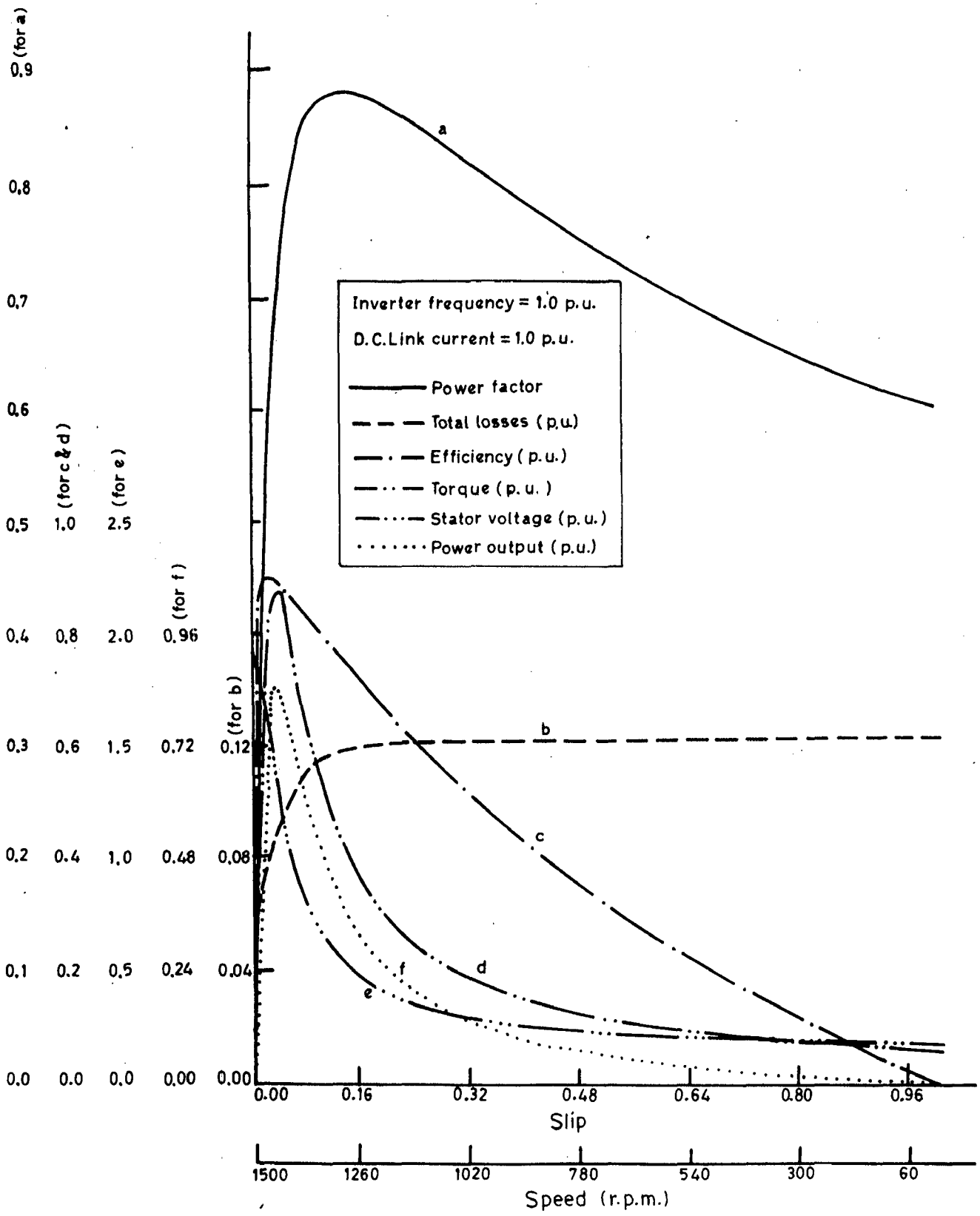

Fig. 6.9(a)_ Motor performance at a glance.

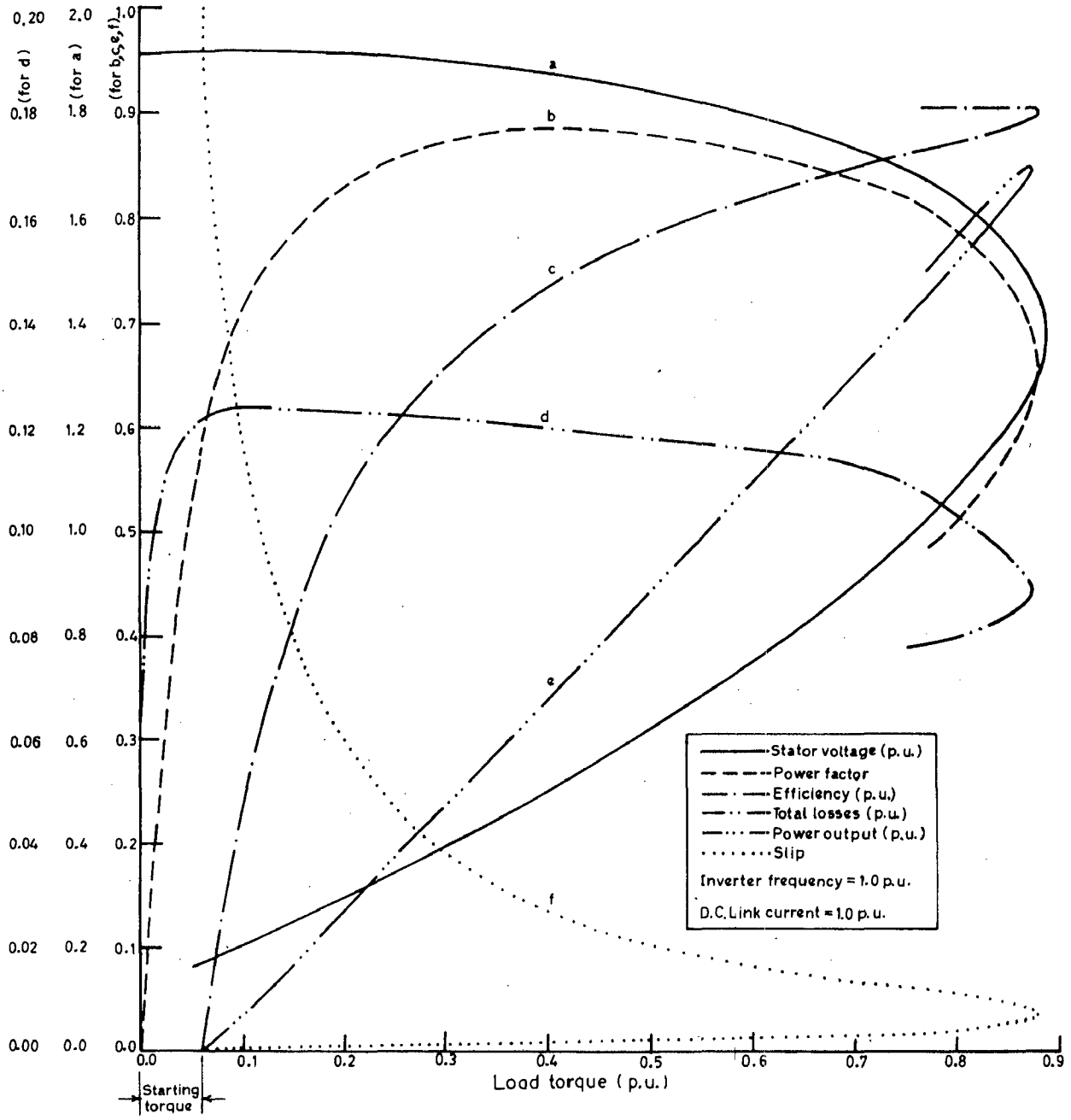

Fig. 6.9(b)_ Motor performance at a glance.

motor performance which is neglected in the present analysis. Thus it is apparant that above results of operation in stable zone are highly in error because saturation effect is not properly accounted for. In the practical case operation in stable zone (point B) will result in higher iron losses, poor power factor, poor efficiency and torque pulsations due to excessive saturation. Therefore it is never advisable to operate in the stable zone. On the other hand operation in unstable zone (point A) corresponds to normal flux level in the machine, resulting in a much improved performance. This is why, operation in the unstable zone with the help of feedback loops is always preferred.

CHAPTER VII

EXPERIMENTAL INVESTIGATION

7.1 INTRODUCTION

The performance of constant current source inverter fed induction motor is investigated experimentally in this chapter.

The observations of the load test on induction motor at different d.c. link currents and operating frequencies are presented. Results of the steady-state analysis obtained from the above observations are plotted with respect to load torque and discussed.

The oscillograms of line voltage, line current and voltage drops across different components of power circuit at resistive and I.M. load are presented and discussed. The effect of change of load and frequency on line voltage and line current waveforms is also studied.

7.2 EXPERIMENTAL SET-UP

The schematic diagram of the experimental drive is shown in Fig. (5.1). A 3ϕ delta connected cage induction motor coupled with a separately-excited d.c. generator, which acts as load, is fed from a constant current-source-inverter. The current-source is realized by connecting an inductor in series with a 3ϕ controlled

bridge rectifier. The firing pulses for the 3ϕ converter are obtained from a three phase six SCR converter Bridge Firing Unit. For keeping the current in the d.c. link constant, a current loop is used. The current loop monitors current in the d.c. link through a sampling resistor, compares it to a reference input, and controls the rectifier bridge triggers to maintain constant current. The controller used in the current loop is of proportional type and is inbuilt in the firing unit. Reference input to current loop is obtained from a 5 volt supply through a potentiometer.

The firing circuit for the auto-sequential current-source-inverter has been already discussed in chapter III. It uses Johnson Counter as the basic unit, output of which are combined to produce six sets of firing pulses.

All the components of the power circuit are mounted on the heat sinks for proper heat dissipation. Snubber circuit is used for the protection of converter SCRs against high $\frac{dV}{dt}$ and a small value of inductance is used in series with each SCR of inverter to limit $\frac{di}{dt}$ to a safe value. In addition to above protections, H.R.C. fuses are also provided in the d.c. link and the converter input.

The complete experimental set up is shown in Fig. (7.1) to Fig. (7.4). Fig.(7.1) shows the controlled rectifier, current-source-inverter and their firing circuits. Fig. (7.2) shows the resistance in the d.c. link which

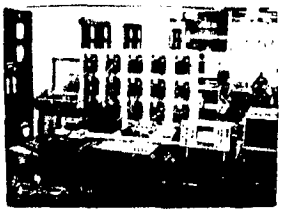

Fig. 7.1

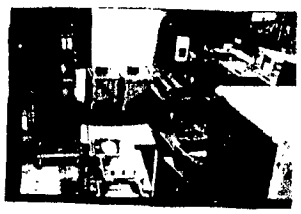

Fig. 7.2

Fig. 7.3

Fig. 7.4

Photographs Of The Experimental Set up

monitors d.c. link current and the auto-transformer whose one winding is used as d.c. link inductor. Fig. (7.3) and (7.4) show the 3ϕ cage induction motor coupled to a separately excited d.c. generator and its loading arrangement.

7.3 EXPERIMENTAL OBSERVATIONS OF CURRENT-SOURCE-INVERTER

Having successfully tested the control circuit, the current-source-inverter is tested. In first instance, it is ensured that the pulses obtained from the control circuit are capable of triggering the SCRs used in the inverter. The CSI configuration is now tested in a circuit similar to that of Fig.(5.1) with a difference that controlled rectifier is replaced by a constant d.c. source and induction motor is replaced by a 3ϕ variable resistance.

The auto-sequential commutation process of the configuration Fig. (2.2)] is checked as follows:

1. Pulses are given to SCR1 and SCR 2 and voltage across capacitor C_{13} is checked.

2. Capacitor C_{13} is found to be charged with the polarity shown in Fig. [2.6(a)].

3. Now SCR 3 is turned ON by giving pulse at its gate and voltage across C_{13} is checked again.

4. Polarity of voltage across capacitor C_{13} is reversed but the magnitude remains almost same[Fig. 2.6(d)].

This confirms that SCR T_1 is automatically commutated as soon as SCR T_3 is triggered. Similarly all the possible combinations of three SCRs are checked for automatic commutation.

7.3.1 Experimental Observations At Resistive Load

First of all d.c. voltage source is replaced by a controlled rectifier. Now the pulses are applied to all the SCRs and waveforms of current and voltage at different points of the circuit are checked. These waveforms are shown in Fig. (~~7.5~~ 7.47) to (~~7.10~~ 7.52). Now resistances in all the three phases are increased in small steps and performance of the inverter is found to be affected as follows:

1. As the resistances in all the three phases are increased, the d.c. link current nearly remains constant initially but falls sharply as the resistance is progressively increased. On the other hand voltage at the input of the inverter goes on increasing.

2. The distortion in the line current waveform increases with increase in load resistance.

3. If we go on increasing the resistance then at a particular value, the commutation is lost and CSI stops functioning.

4. The critical value of resistance at which commutation is lost, is found proportional to the d.c. link current.

7.3.2 Experimental Observations At Induction Motor Load in Open Loop

Before replacing the resistive load by induction motor, 100 K pot in the circuit of clock pulse generator [Fig. (3.7)], which is a 10 turn potentiometer with a dial is calibrated in terms of frequency [Table (7.1)]. Now resistive load is replaced by a 3ϕ cage induction motor and supplies to the control circuit and controlled rectifier are switched on with the current in the d.c. link set at minimum value. As we decrease the firing angle of controlled rectifier, current in the d.c. link increases. Torque developed in the motor with 1 p.u. current in the d.c. link is not sufficient to start the motor at no load. As the d.c. link current is increased to 1.5 p.u., motor starts and settles at speed corresponding to operating frequency. Once motor attains steady-state, d.c. link current is decreased and adjusted around 1.0 p.u. Now waveforms of motor line current and voltage are observed with the help of an oscilloscope and found to be matching with the theoretical waveforms shown side by side. These waveforms are shown in the Figs. (7.11) and (7.12). Now motor is operated without a current loop in d.c. link at different frequencies

TABLE 7.1 (~~4.7~~)

CALIBERATION OF TEN-TURN POT DIAL IN TERMS OF INVERTER FREQUENCY

	100K POT POSITION	OPERATING FREQUENCY (Hz)		100K POT POSITION	OPERATING FREQUENCY
1	1.0	83.3	15	4.5	21.3
2	1.5	64.1	16	5.0	18.9
3	2.0	49.0	17	5.5	17.3
4	2.1	46.2	18	6.0	16.0
5	2.2	41.6	19	6.5	14.8
6	2.3	39.5	20	7.0	13.8
7	2.4	38.4	21	7.5	12.8
8	2.5	37.8	22	8.0	11.9
9	2.6	36.2	23	8.5	11.5
10	2.7	34.7	24	9.0	10.7
11	2.9	33.3	25	9.5	10.4
12	3.0	32.0	26	10.0	9.8
13	3.5	27.7			
14	4.0	24.5			

Motor Current And Voltage Waveforms At

Induction Motor Load Without Current Feed Back

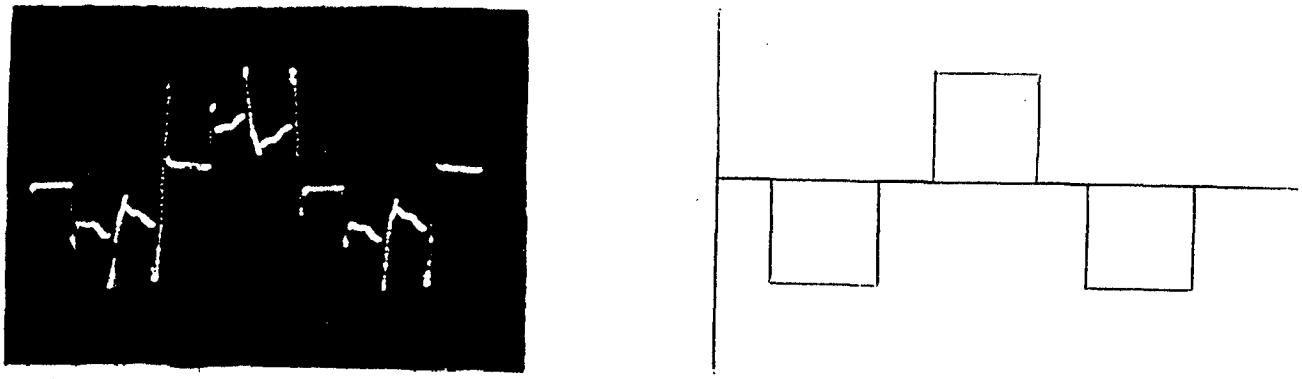

Fig. 7.11

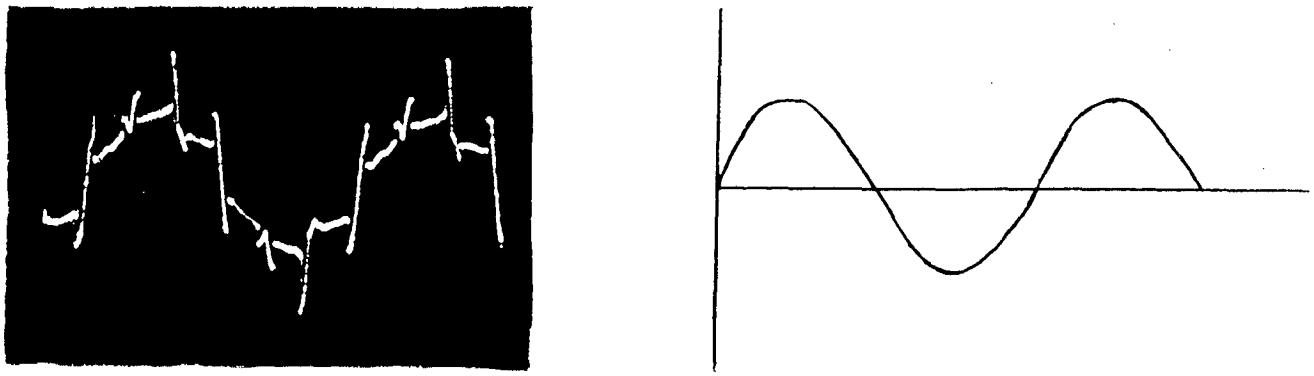

Fig. 7.12

and different d.c. link currents and following investigations are made.

1. Induction motor running only with inertia load of d.c. generator and of itself is stable in open loop, although small torque pulsations are there.

2. Motor response to change in operating frequency is very good. It adjusts its speed corresponding to operating frequency quickly.

3. The frequency range in which CSI works satisfactorily is found to be 10 to 47 Hz. As we cross the upper frequency limit, commutation is lost and motor stops.

4. As we try to load the motor in open loop with rated current flowing in the motor lines, d.c. link current falls sharply and so is the motor line current and motor becomes unstable instantaneously and stops.

5. When the motor line currents are adjusted to about 1.5 p.u., then motor is stable at very light loads but it becomes unstable as soon as the load is increased.

6. All other conditions same as in (5) but at lower operating frequencies, motor is able to carry a little more load.

7. Motor becomes hot very soon even when motor is operating at no load with rated current.

7.3.3 Experimental Observations at Induction Motor Load With Current Loop

After examining the open loop performance of the drive, a current loop is incorporated in the system as shown in Fig. (5.1). This current loop monitors current in the d.c. link through a sampling resistor and adjusts the firing angle of the controlled rectifier such as to maintain constant current in the d.c. link. Motor is started as in the open loop case and current in the d.c. link is adjusted so as to keep the current in the motor lines at rated value. Then d.c. generator, coupled to induction motor, is separately excited to give rated voltage at its armature terminals. Afterwards load connected to armature of the d.c. generator is increased in steps and the observations of motor line current, motor line voltage, input power to motor, d.c. link current, operating frequency, armature current and voltage of d.c. generator are recorded at each step. The same are tabulated in Table (7.2). The same exercise is repeated for different sets of d.c. link currents and operating frequencies. From the observations of load test

TABLE (7.2)

Operating Frequency = 24.5 Hz

a) D.C. Link Current = 3.0 A

I.M. STATOR VOLTAGE (VOLTS)	I.M. LINE CURRENT (AMPS.)	WATTMETER READING W_1 (WATTS)	WATTMETER READING W_2 (WATTS)	D.C. GENERATOR ARMATURE VOLTAGE (VOLTS)	D.C. GENERATOR ARMATURE CURRENT (AMPS.)	SPEED (R.P.M.)
1	2	3	4	5	6	7
66.0	2.75	100.0	-40.0	0.0	0.0	670
66.0	2.65	108.0	-36.0	56.0	0.22	660
66.0	2.62	112.0	-24.0	55.0	0.40	650
66.0	2.58	116.0	-20.0	53.0	0.60	648
66.0	2.53	120.0	-12.0	51.0	0.80	648
66.0	2.50	120.0	- 4.0	49.0	1.00	645
66.0	2.45	120.0	4.0	48.0	1.20	640
66.0	2.42	120.0	20.0	46.0	1.40	640
66.0	2.40	132.0	20.0	44.0	1.60	630
				UNSTABLE BEYOND THIS LOAD		
b) D.C. Link Current = 4.0 A						
76.0	3.85	160.0	-60.0	0.0	0.0	670
76.0	3.85	172.0	-56.0	57.0	0.22	665
76.0	3.81	172.0	-44.0	56.0	0.40	660

contd...

1	2	3	4	5	6	7
76.0	3.77	176.0	-40.0	54.0	0.6	660
76.0	3.60	180.0	-36.0	52.0	0.8	655
76.0	3.58	184.0	-32.0	50.0	1.0	650
76.0	3.58	188.0	-20.0	49.0	1.2	650
76.0	3.58	192.0	-16.0	47.0	1.4	645
76.0	3.55	188.0	- 4.0	45.0	1.6	645
76.0	3.55	192.0	0.0	43.0	1.8	645
76.0	3.55	184.0	16.0	41.0	2.0	645
76.0	3.55	208.0	24.0	37.0	2.5	640
76.0	3.55	200.0	40.0	35.0	2.7	620
76.0	3.35	200.0	56.0	30.0	3.05	600
				UNSTABLE BEYOND THIS LOAD		
c) D.C. Link Current = 5.0 A						
84.0	4.45	220.0	-72.0	0.0	0.0	670
84.0	4.45	232.0	-64.0	58.0	0.2	665
84.0	4.40	240.0	-56.0	57.0	0.4	665
84.0	4.40	248.0	-52.0	56.0	0.6	665

contd...

1	2	3	4	5	6	7
84.0	4.40	256.0	-52.0	54.0	0.8	660
84.0	4.40	260.0	-48.0	52.0	1.0	660
84.0	4.40	268.0	-48.0	50.0	1.2	660
84.0	4.40	272.0	-36.0	49.0	1.4	655
84.0	4.40	280.0	-32.0	47.0	1.6	655
84.0	4.40	284.0	-24.0	35.0	1.8	655
84.0	4.40	284.0	-12.0	43.0	2.0	655
84.0	4.40	288.0	-4.0	41.0	2.2	655
84.0	4.40	280.0	16.0	39.0	2.4	650
84.0	4.40	288.0	24.0	36.0	2.65	645
84.0	4.40	292.0	32.0	32.0	3.0	640
84.0	4.40	296.0	40.0	27.0	3.50	640
84.0	4.40	296.0	48.0	22.0	3.8	635
84.0	4.40	300.0	60.0	20.0	4.0	630
				UNSTABLE BEYOND THIS LOAD		

TABLE (7.3)

a) D.C. Link Current = 5.0 A

Operating Frequency = 27.7 Hz

I.M. STATOR VOLTAGE (VOLTS)	I.M. LINE CURRENT (AMPS.)	WATTMETER READING W_1 (WATTS)	W_2 (WATTS)	D.C. GENERATOR ARMATURE VOLTAGE (VOLTS)	ARMATURE CURRENT (AMPS.)	SPEED (R.P.M.)
1	2	3	4	5	6	7
96.0	4.40	256.0	-88.0	0.0	0.0	770
96.0	4.40	256.0	-76.0	62.0	0.25	765
96.0	4.40	268.0	-72.0	61.0	0.4	765
96.0	4.40	272.0	-64.0	60.0	0.5	760
96.0	4.40	272.0	-60.0	60.0	0.6	760
96.0	4.40	280.0	-60.0	58.0	0.8	760
96.0	4.40	280.0	-44.0	56.0	1.0	755
96.0	4.40	284.0	-40.0	54.0	1.25	750
96.0	4.38	288.0	-40.0	53.0	1.4	750
96.0	4.38	296.0	-36.0	51.0	1.6	750
96.0	4.35	300.0	-20.0	50.0	1.85	750
96.0	4.34	300.0	-16.0	48.0	2.0	745
96.0	4.34	308.0	- 4.0	45.0	2.25	740
				UNSTABLE BEYOND THIS LOAD		

contd....

b) D.C. Link Current = 5.5 A

1	2	3	4	5	6	7
100.0	4.70	300.0	-100.0	0.0	0.0	770
100.0	4.65	308.0	- 84.0	65.0	0.25	765
100.0	4.60	312.0	- 80.0	64.0	0.4	760
100.0	4.60	320.0	- 76.0	62.0	0.6	760
100.0	4.60	320.0	- 60.0	60.0	0.8	760
100.0	4.60	328.0	- 56.0	59.0	1.0	760
100.0	4.55	332.0	- 44.0	58.0	1.2	755
100.0	4.55	336.0	- 40.0	55.0	1.4	755
100.0	4.55	340.0	- 36.0	54.0	1.6	750
100.0	4.55	340.0	- 32.0	52.0	1.8	745
100.0	4.55	348.0	- 20.0	49.0	2.05	745
100.0	4.52	352.0	- 16.0	47.0	2.25	745
100.0	4.50	356.0	0.0	43.0	2.6	740
100.0	4.48	360.0	20.0	37.0	3.1	735
100.0	4.48	360.0	28.0	35.0	3.3	735
				UNSTABLE BEYOND THIS LOAD		

TABLE (7.4)

Operating Frequency = 32.0 Hz

a) D.C. Link Current = 3.0 A

I.M. STATOR VOLTAGE (VOLTS)	I.M. LINE CURRENT (AMPS.)	WATTMETER READING W_1 (WATTS)	WATTMETER READING W_2 (WATTS)	D.C. GENERAT R ARMATURE VOLTAGE (VOLTS)	D.C. GENERAT R ARMATURE CURRENT (AMPS.)	SPEED (R.P.M.)
1	2	3	4	5	6	7
86.0	2.85	31.0	-10.0	0.0	0.0	910
86.0	2.70	34.0	- 5.0	39.0	0.3	900
86.0	2.70	35.0	- 4.0	37.5	0.5	900
				UNSTABLE BEYOND THIS LOAD		

b) D.C. Link Current = 4.0 A

100.0	3.80	51.0	-20.0	0.0	0.0	910
100.0	3.60	55.0	-15.0	38.0	0.3	908
100.0	3.60	57.0	-11.0	37.0	0.5	905
100.0	3.60	59.0	-10.0	36.0	0.7	900
100.0	3.60	60.0	- 7.0	34.5	0.9	900
100.0	3.60	61.0	- 5.0	33.5	1.1	900
100.0	3.60	63.0	- 4.0	32.5	1.3	898

contd...

1	2	3	4	5	6	7
100.0	3.60	64.0	- 3.0	31.5	1.5	895
100.0	3.55	64.0	0.0	30.0	1.7	890
100.0	3.55	64.0	3.0	29.5	1.9	888
100.0	3.58	62.0	8.0	28.5	2.1	885
				UNSTABLE BEYOND THIS LOAD		
c) D.C. Link Current = 5.0 A						
108.0	4.45	73.0	-23.0	0.0	0.0	910
108.0	4.45	77.0	-20.0	37.5	0.3	905
108.0	4.45	78.0	-17.0	36.5	0.5	905
108.0	4.45	80.0	-15.0	35.5	0.7	905
108.0	4.45	83.0	-14.0	34.5	0.9	900
108.0	4.45	84.0	-11.0	33.5	1.1	900
108.0	4.45	85.0	-10.0	33.0	1.3	900
108.0	4.43	86.0	- 9.0	32.0	1.5	900
108.0	4.43	87.0	- 8.0	31.0	1.7	895
108.0	4.41	87.0	- 5.0	30.0	1.9	895

contd.....

1	2	3	4	5	6	7
108.0	4.40	88.0	- 4.0	29.0	2.1	890
108.0	4.40	88.0	- 2.0	27.5	2.3	890
108.0	4.40	90.0	0.0	26.0	2.5	890
108.0	4.38	90.0	3.0	25.0	2.7	885
108.0	4.38	91.0	5.0	24.0	2.9	885
108.0	4.35	91.0	7.0	22.5	3.1	885
108.0	4.35	92.0	11.0	20.5	3.45	880
108.0	4.35	92.0	12.0	18.5	3.8	875
108.0	4.20	90.0	17.0	17.0	4.0	875
				UNSTABLE BEYOND THIS LOAD		

TABLE (7.5)

Operating Frequency = 34.7 Hz

a) D.C. Link Current = 4.0 A

I.M. STATOR VOLTAGE (VOLTS)	I.M. LINE CURRENT (AMPS.)	WATTMETER READING W_1 (WATTS)	WATTMETER READING W_2 (WATTS)	D.C. GENERATOR ARMATURE VOLTAGE (VOLTS)	D.C. GENERATOR ARMATURE CURRENT (AMPS.)	SPEED (R.P.M.)
1	2	3	4	5	6	7
108.0	3.60	53.0	-17.0	0.0	0.0	1030
108.0	3.55	56.0	-12.0	44.5	0.35	1025
108.0	3.55	58.0	- 9.0	44.0	0.50	1020
108.0	3.55	59.0	- 7.0	42.5	0.7	1020
108.0	3.55	60.0	- 4.0	41.5	0.9	1020
				UNSTABLE BEYOND THIS LOAD		

b) D.C. Link Current = 5.0 A

118.0	4.45	76.0	-20.0	0.0	0.0	1030
118.0	4.45	81.0	-18.0	42.0	0.3	1020
118.0	4.45	84.0	-15.0	41.0	0.5	1015
118.0	4.45	86.0	-14.0	40.0	0.7	1010

contd....

1	2	3	4	5	6	7
118.0	4.45	87.0	-11.0	39.0	0.9	1010
118.0	4.45	88.0	- 9.0	38.0	1.1	1000
118.0	4.45	89.0	- 7.0	36.5	1.3	1000
118.0	4.45	90.0	- 5.0	35.5	1.5	1000
118.0	4.45	91.0	- 4.0	34.5	1.7	1000
118.0	4.40	92.0	- 1.0	33.5	1.9	995
118.0	4.40	94.0	0.0	32.0	2.1	995
118.0	4.40	94.0	2.0	31.0	2.3	995
118.0	4.35	94.0	5.0	28.0	2.7	990
118.0	4.15	92.0	10.0	27.0	3.0	985
				UNSTABLE BEYOND THIS LOAD		

TABLE (7.6)

Operating Frequency = 38.4 Hz

a) D.C. Link Current = 3.5 A

I.M. STATOR VOLTAGE (VOLTS)	I.M. LINE CURRENT (AMPS.)	WATTMETER READING W_1 (WATTS)	W_2 (WATTS)	D.C. GENERATOR ARMATURE VOLTAGE (VOLTS)	ARMATURE CURRENT (AMPS.)	SPEED (R.P.M.)
1	2	3	4	5	6	7
104.0	3.0	172.0	-68.0	0.0	0.0	1120
104.0	2.85	180.0	-32.0	94.0	0.35	1120
104.0	2.80	180.0	-20.0	92.0	0.50	1115
104.0	2.70	180.0	-12.0	91.0	0.60	1115
				UNSTABLE BEYOND THIS LOAD		

b) D.C. Link Current = 4.5 A

124.0	4.0	268.0	-100.0	0.0	0.0	1120
124.0	3.95	300.0	- 68.0	107.0	0.4	1120
124.0	3.85	308.0	- 60.0	105.0	0.6	1115
124.0	3.80	320.0	- 56.0	102.0	0.8	1110
124.0	3.65	320.0	- 48.0	101.0	0.9	1110
124.0	3.60	320.0	- 40.0	100.0	1.0	1105
124.0	3.60	348.0	- 32.0	97.0	1.2	1105
				UNSTABLE BEYOND THIS LOAD		

c) D.C. Link Current = 5.0 A

1	2	3	4	5	6	7
140.0	4.30	340.0	-80.0	0.0	0.0	1120
140.0	4.15	360.0	-60.0	104.0	0.4	1120
140.0	4.15	364.0	-44.0	103.0	0.6	1110
140.0	4.00	372.0	-40.0	101.5	0.8	1110
140.0	3.95	376.0	-28.0	98.0	1.0	1105
140.0	3.95	376.0	-20.0	97.0	1.2	1100
140.0	3.95	388.0	- 4.0	94.0	1.4	1100
140.0	3.95	392.0	-40.0	92.0	1.5	1085
140.0	3.95	392.0	-32.0	90.0	1.6	1085
140.0	3.85	392.0	-20.0	89.0	1.8	1080
140.0	3.85	396.0	-12.0	86.0	2.0	1080
				UNSTABLE BEYOND THIS LOAD		

TABLE (7.7)

Operating Frequency = 47.0 Hz

a) D.C. Link Current = 4.5 A

I.M. STATOR VOLTAGE (VOLTS)	I.M. LINE CURRENT (AMPS.)	WATTMETER READING W_1 (WATTS)	WATTMETER READING W_2 (WATTS)	D.C. GENERATOR ARMATURE VOLTAGE (VOLTS)	D.C. GENERATOR ARMATURE CURRENT (AMPS.)	SPEED (R.P.M.)
1	2	3	4	5	6	7
94.0	3.60	320.0	-160.0	0.0	0.0	1355
94.0	3.15	296.0	-100.0	116.0	0.42	1345
94.0	3.15	308.0	- 88.0	115.0	0.50	1345
94.0	2.90	284.0	- 56.0	114.0	0.60	1345
				UNSTABLE BEYOND THIS LOAD		

b) D.C. Link Current = 5.0 A

95.0	4.02	372.0	-200.0	0.0	0.0	1355
95.0	3.85	388.0	-148.0	116.0	0.42	1350
95.0	3.80	388.0	-140.0	113.0	0.50	1350
95.0	3.77	388.0	-120.0	112.0	0.60	1350
95.0	3.60	380.0	-100.0	113.0	0.70	1350
95.0	3.60	380.0	- 96.0	111.0	0.80	1345

contd...

1	2	3	4	5	6	7
95.0	3.57	376	- 92.0	106.0	0.90	1345
				UNSTABLE BEYOND THIS LOAD		
c) D.C. Link Current = 5.5 A						
96.0	4.50	432.0	-220.0	0.0	0.0	1355
96.0	4.42	472.0	-180.0	116.0	0.45	1350
96.0	4.42	472.0	-172.0	115.0	0.55	1345
96.0	4.40	476.0	-160.0	113.0	0.70	1345
96.0	4.38	480.0	-140.0	111.0	0.90	1340
96.0	4.32	480.0	-124.0	109.0	1.10	1340
96.0	4.15	472.0	-100.0	106.0	1.30	1340
96.0	4.00	456.0	- 80.0	103.0	1.50	1340
				UNSTABLE BEYOND THIS LOAD		

[Table (7.2) to (7.7)], motor performance is calculated at different sets of operating conditions and are plotted in Fig. (7.13) to Fig. (7.46) with respect to load torque.

In order to investigate the speed control of induction motor with current-source-inverter, a particular value of load on induction motor is fixed and operating frequency is varied gradually by adjusting 100 K potentiometer [Fig. (3.7)]. For every value of operating frequency speed is recorded. These observations are tabulated in Table (7.8).

The oscillograms of motor voltage and current are first recorded at no load for two different frequencies and then at a fix load. These are compared in Figs. (7.61) to (7.68). Along with these, oscillograms of the voltage across different components of the power circuit are also recorded and are given in Figs. (7.54) to (7.56).

7.4 DISCUSSION ON CSI PERFORMANCE

7.4.1 At Resistive Load

If at the input of inverter there has been an ideal current source, then current in all the three phases of load resistance remains same all the time, independent of magnitude of resistance. But in present case, current source is not an ideal one because its input impedance is not infinite. This is why, the current in the d.c. link

TABLE (7.8)

OPERATING FREQUENCY (Hz)	MOTOR SPEED (R.P.M.)
10.4	250
12.8	310
13.8	350
16.0	400
18.9	485
21.4	550
24.5	645
27.7	750
32.0	900
34.7	1000
38.4	1100
41.6	1150
46.2	1290

as well as in all the three phases of load resistance falls sharply as their magnitudes are increased.

The capacitors used in the configuration of CSI play the main role in the commutation process of all the six SCRs. The charging of these capacitors is dependent on the load current which in fact is affected by the load resistance. Thus it is clear that the commutation capability of the CSI configuration is load current dependent. This is the reason for the distortion of current waveform at higher value of load resistance and loss of commutation at a critical value of load resistance.

7.4.2 CSI Fed IM Without Current Feedback

From the torque-slip characteristics shown in Fig. [6.3(a)] and [6.3(b)], it is clear that starting torque in current source inverter fed induction motor is very low. This is why induction motor can not be normally started even with 1 p.u. current in the d.c. link. As soon as we increase the current in the d.c. link to 1.5 p.u. for short time, motor starts and picks up speed because the torque being proportional to square of d.c. link current also increases sufficiently to start the motor. This can also be seen in the above theoretical curves.

The operating frequency range in the present case is found to be 10 - 47 Hz. The upper frequency limit

is fixed by the time for which the outgoing thyristor is to be kept reverse biased. This upper limit can be increased by decreasing the value of commutating capacitance, which in turn requires the use of high voltage thyristors. To enable use of available thyristors, capacitors are so selected that upper limit of operating frequency is 47 Hz.

It can also be noted from the theoretical curves of Fig.[6.3b]that as the operating frequency increases, stable zone decreases and its slope becomes more and more sharp making operation of induction motor difficult. The lower limit of operating frequency is fixed by the permissible torque pulsations. These are produced by the interaction between harmonics of stator and rotor flux linkages. At low frequencies the amplitude of pulsating torque is more because of the harmonics in the rotor flux linkages at low frequencies. As we try to load the motor with current in the d.c. link adjusted to 1.0 p.u., d.c. link current decreases because current source itself is not able to maintain current constant. As a result motor torque being proportional to square of d.c. link current decreases very much and motor becomes unstable coming to almost standstill. When the current in the d.c. link is increased ($\geq$ 1.5 p.u.) then at light loads d.c. link current fixes itself to about 1.0 p.u. and motor is stable. At low frequencies, stable zone of torque-slip characteristic [Fig6.3(b)] is less steep and thus has better operating

slip range. This is why at lower frequencies motor is able to take a little more load.

The quick heating of the motor can be explained because of harmonics and higher losses due to excessive saturation in the machine.

7.4.3. CSI Fed I.M.With Current Feedback

From the observation tables (7.2) to (7.7) of the load test, it can be seen that current in the d.c. link remains strictly constant at the set value independent of the loading of the motor which shows the effectiveness of the current loop.

In Chapter 5, we have seen that motor line current is directly proportional to the d.c. link current. Therefore motor line current should also be constant but observation tables show that for lower frequencies motor line current remains nearly constant and at higher frequencies motor line current starts decreasing slowly as we increase the load on the motor. The explanation for this discrepancy is given by Joshi and Dewan [10]. They have shown that at frequencies higher than a critical value, the series diodes are forward biased for a short interval other than the usual conduction period of $2\pi/3$ radian. The conduction of diodes shunts a part of the input current through the inverter leg without passing through the machine.

7.4.3.1 Stator Voltage Vs Power Output

It can be seen from the observation tables [(7.2) to (7.7)] that as the motor is loaded from no load to maximum possible extent, stator voltage remains throughout constant, which is contrary to the theoretical characteristic[Fig.6.8(a)], where wide changes take place in the stable zone. The discrepancy arises from the fact that saturation has been neglected in the analysis. The magnetising reactance which has been used for the calculation was a saturated value obtained from a conventional no load test at nominal voltage. This value was then maintained constant in the analysis. Although the assumption of a constant (saturated) magnetising reactance is reasonable when the motor is excited from a voltage source. In case of current source, operation with a fixed magnitude current results in operation over a wide range of flux conditions. Hence the magnetising reactance changes widely and plays a more dominant role in motor behaviour.

7.4.3.2 Speed Vs Power Output

The characteristics for a particular d.c. link current at different operating frequencies are shown in Fig. (7.13). The characteristics have a very small slope and agree very well with the stable zone of their theoretical counterpart[Fig. 6.4]. Since the change in speed with increase in load is too small to record it correctly,

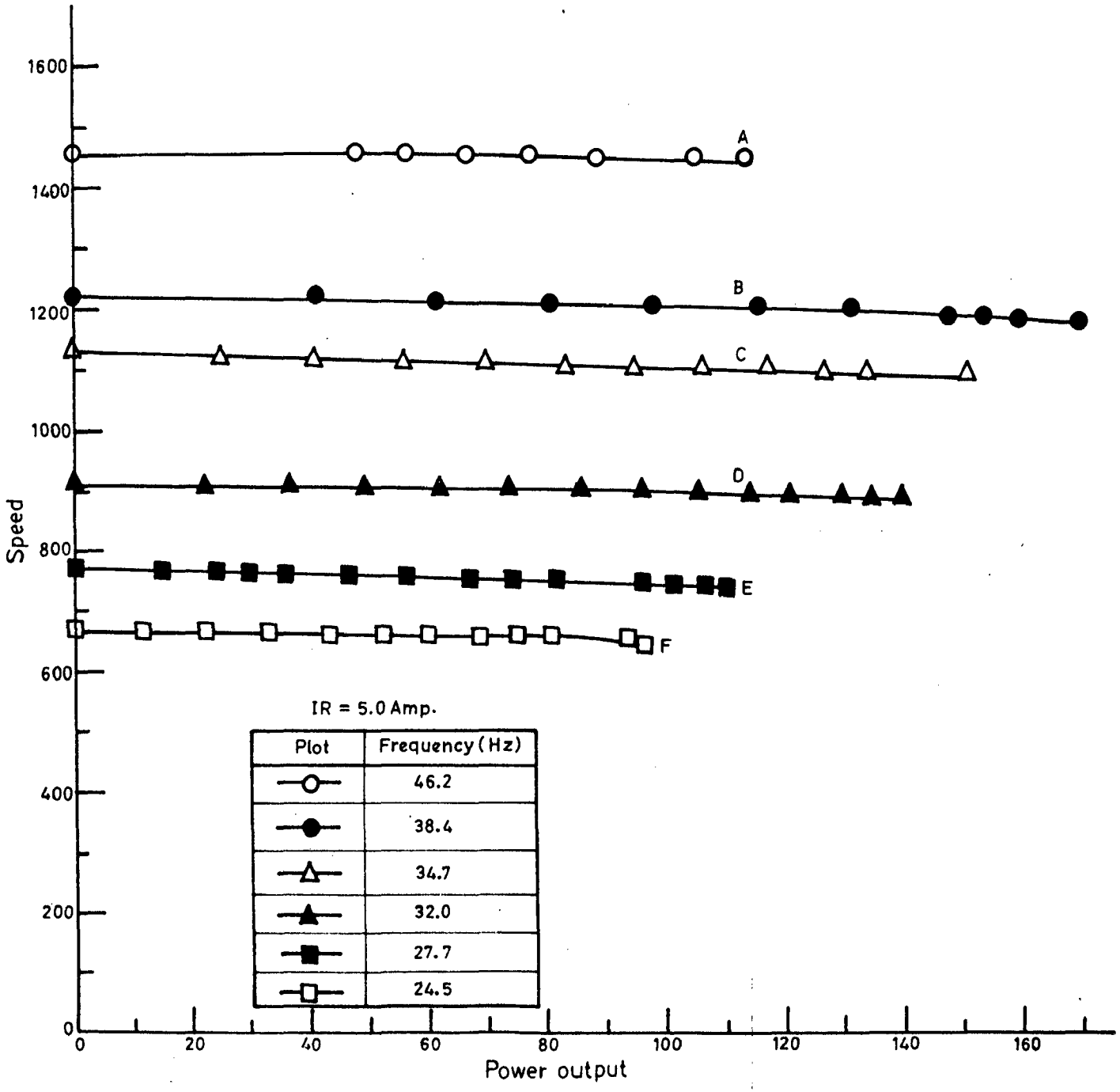

Fig. 7.13_ Speed vs. power output characteristics.

therefore motor performance like power factor, efficiency, total losses, stator voltage are plotted against power output instead of slip.

7.4.3.3 Total Losses Vs Power Output

The characteristics are shown in Fig. (7.14) to Fig. (7.25) for different sets of operating frequency and d.c. link currents. The characteristics start from a finite value at no load and then increases slowly as we increase the load on the motor. Since we are always operating in the stable zone of torque-slip characteristic therefore machine is operating under highly saturated condition. Total losses in the drive consist of mainly iron losses copper losses and friction and windage losses. At no load, total losses mainly consists of iron and friction and windage losses which remains more or less constant for a given frequency and d.c. link current. As we increase the load on the motor, rotor copper losses increase on account of decreased value of r_2/s which explains the rising nature of characteristic with load. Total losses are more for higher d.c. link currents at a fix power output and operating frequency. This is because stator and rotor copper losses being proportional to square of current increases rapidly resulting in a upward shift of the characteristic.

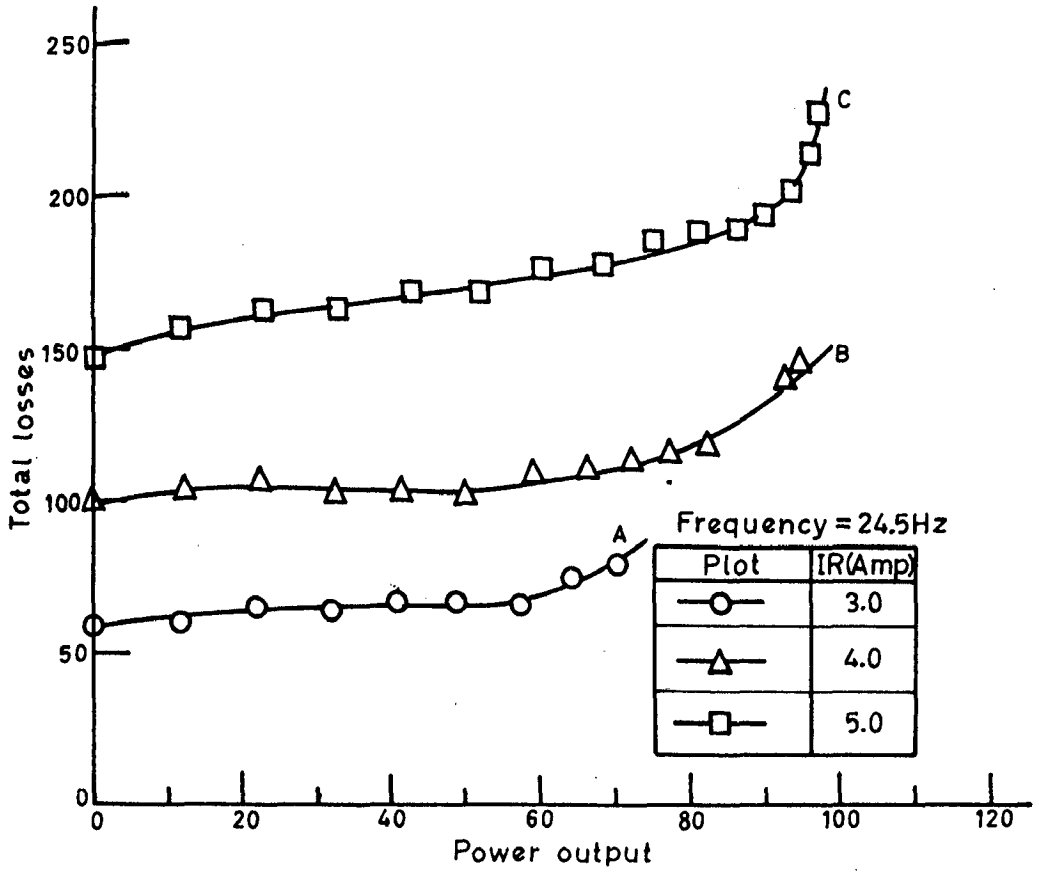

Fig.7.14_ Total losses vs. power output characteristics.

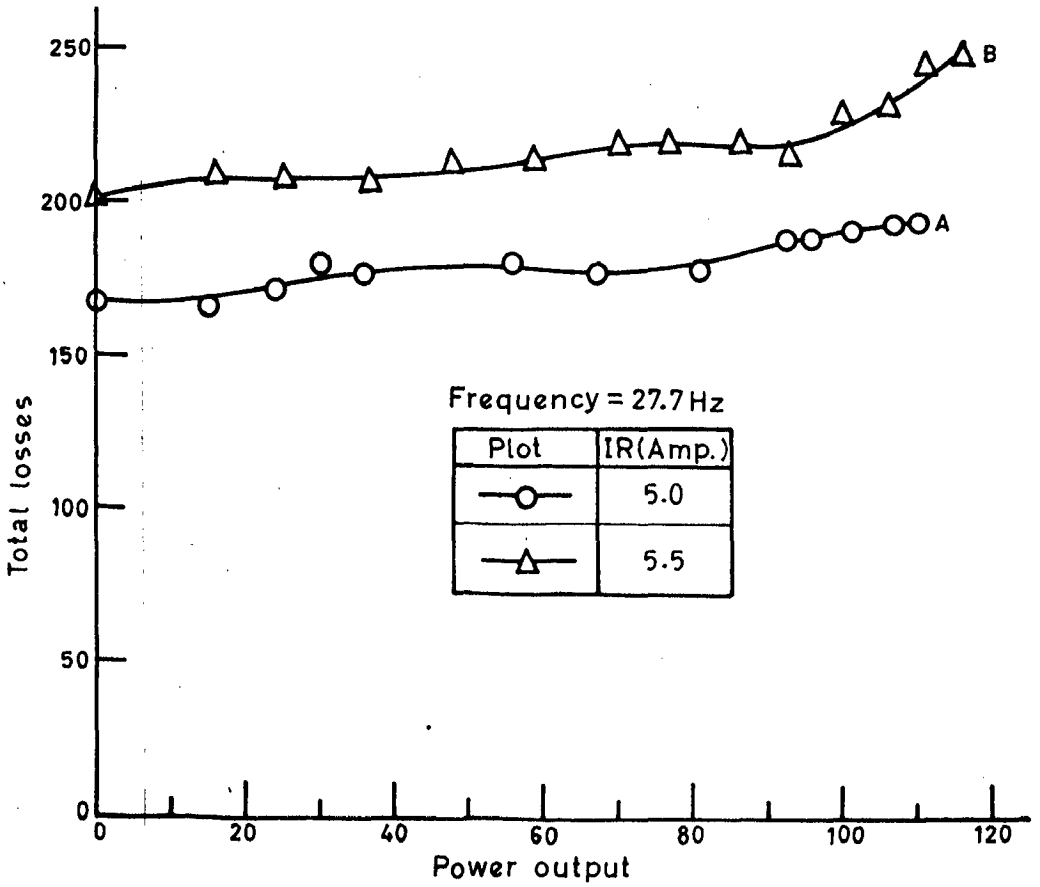

Fig.7.15_Total losses vs. power output characteristics.

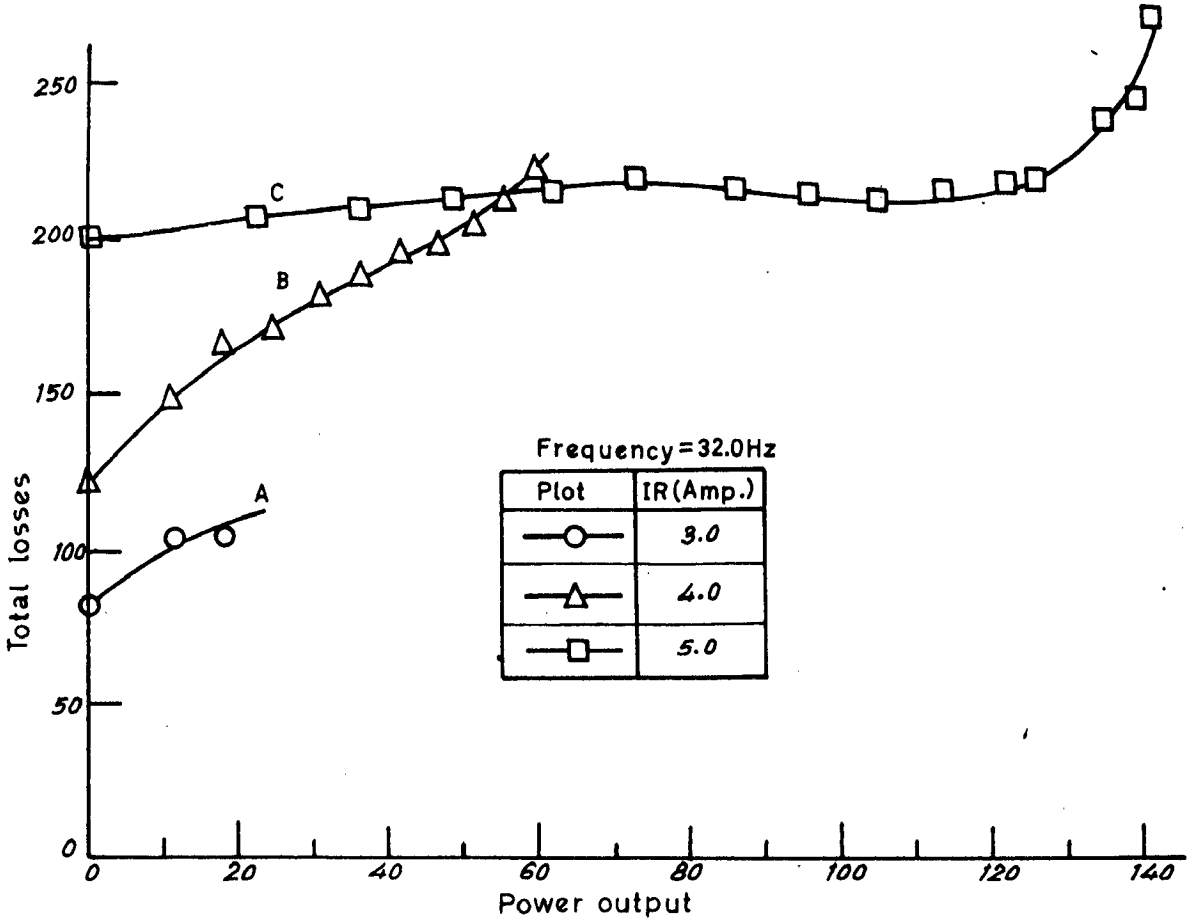

Fig.7.16_Total losses vs. power output characteristics.

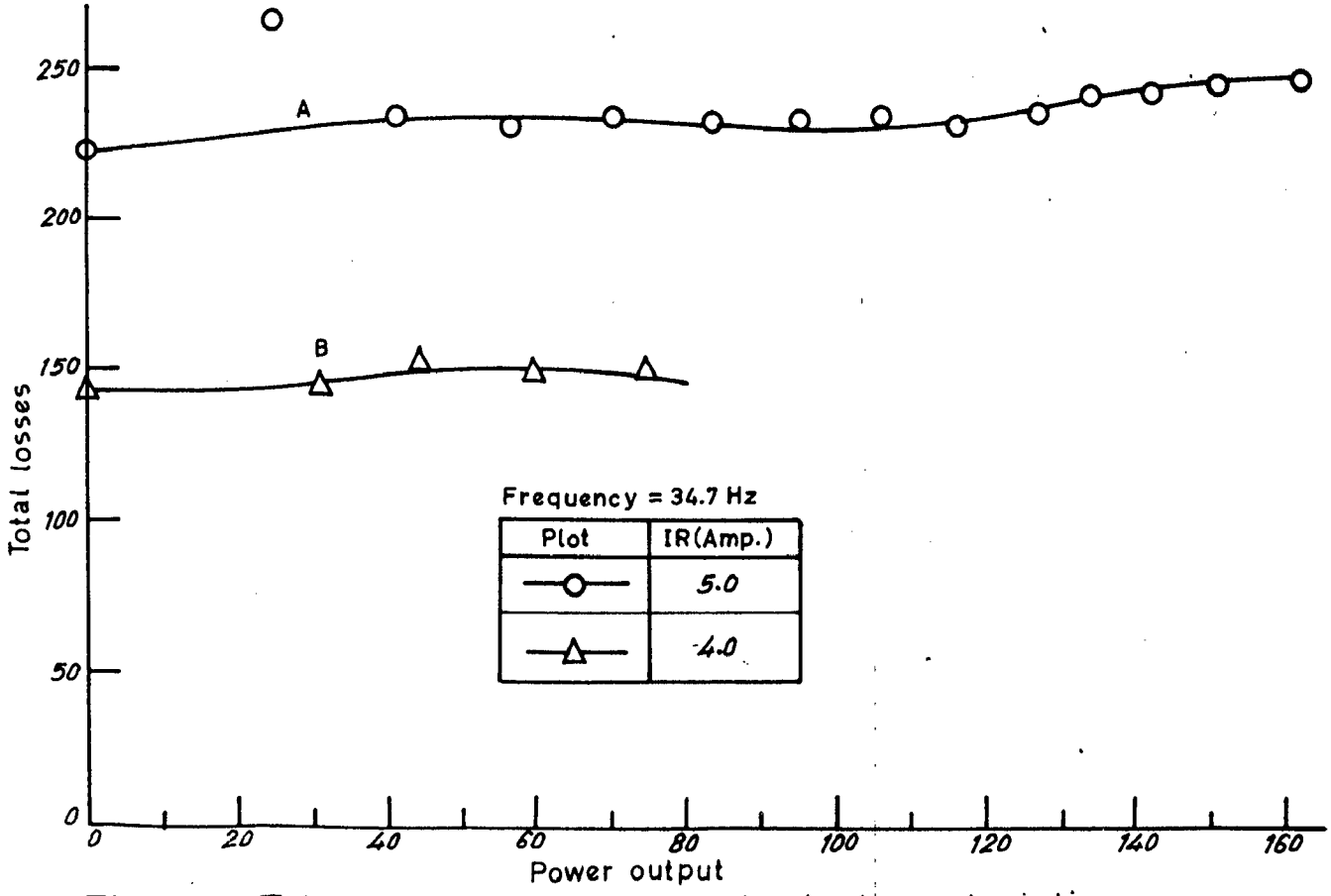

Fig.7.17_Total losses vs. power output characteristics.

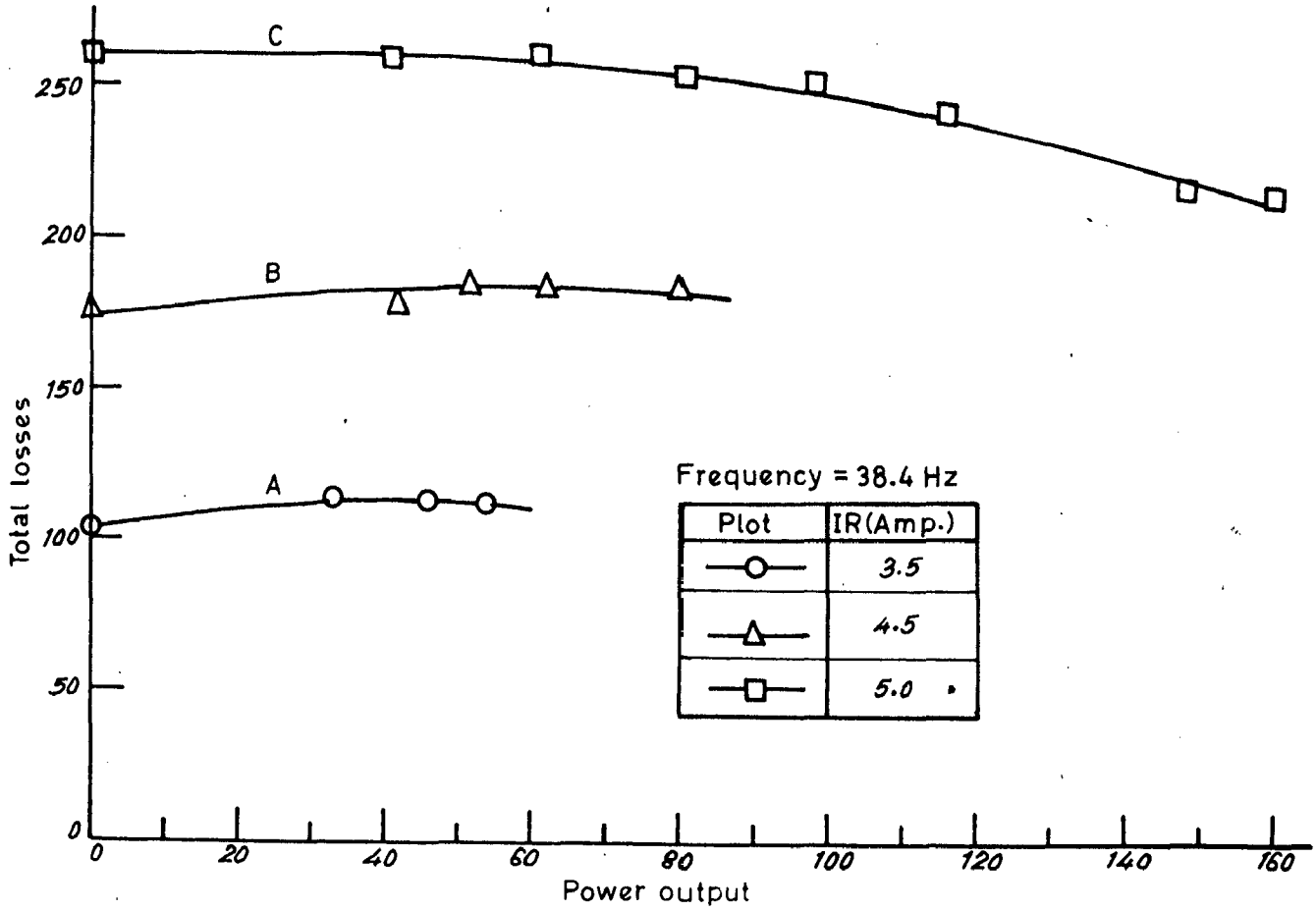

Fig. 7.18 – Total losses vs. power output characteristics.

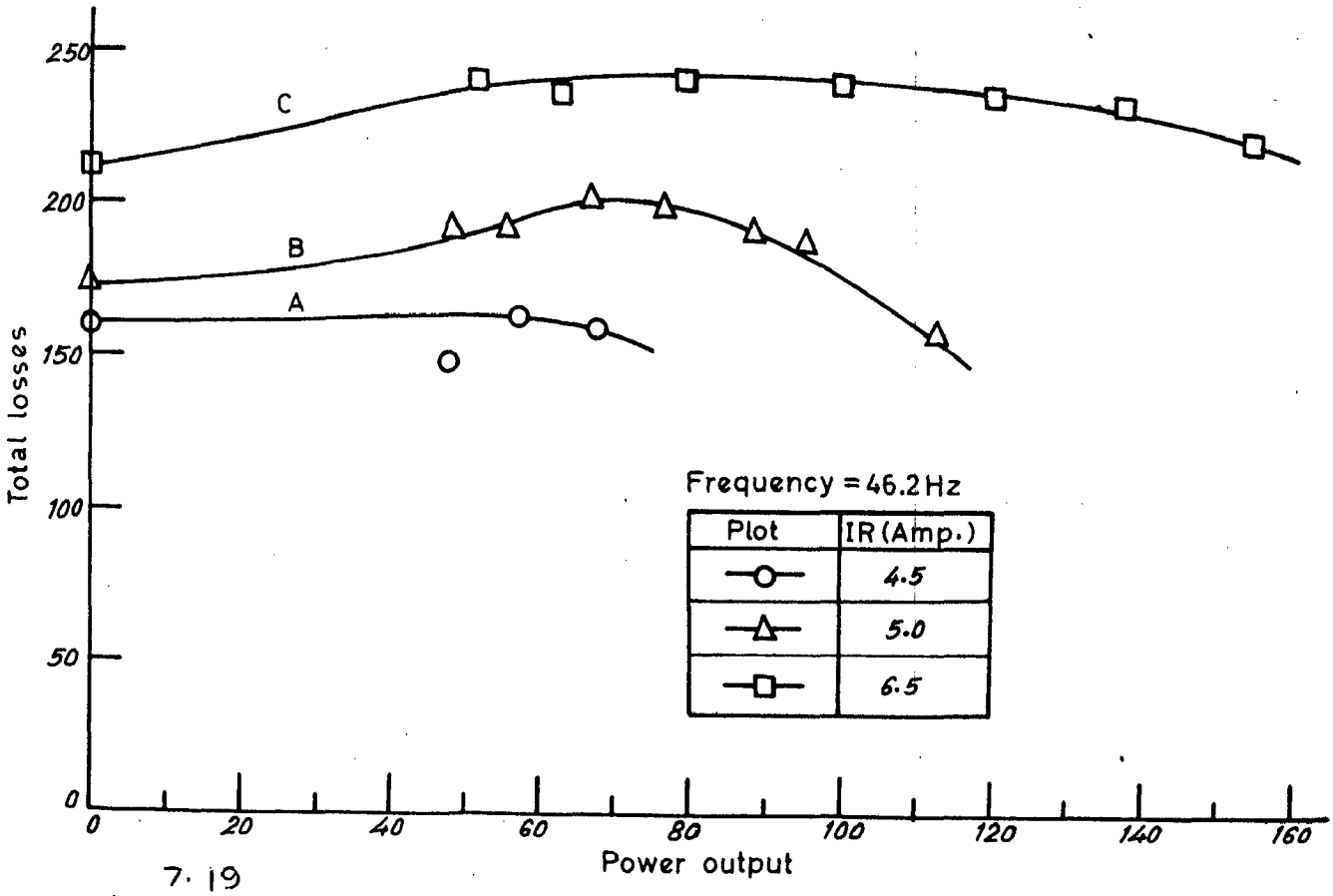

7.19

Fig. ~~7.25~~ – Total losses vs. power output characteristics.

For a given power output and d.c. link current, total losses are higher for higher frequencies because iron losses being proportional to frequency increase sharply. As the operating frequency is increased, the characteristic becomes more and more flat and even bend downward for a particular d.c. link current and operating frequency (I_R = 5.0 Ampere, f = 38.4 Hz). At higher frequencies iron losses being proportional to frequency increases considerably. On the other hand, at large frequencies rotor reactance will be more therefore rotor induced currents will be less resulting in decreased rotor copper losses. As a result of combined effect of both factors, proportion of iron losses as compared to other losses increase in the total losses resulting in relatively flat characteristics.

7.4.3.4 Efficiency Vs Power Output

The relevant curves are shown in Fig. (7.26) to Fig. (7.31) for different sets of d.c. link currents and operating frequencies. It can be seen from the curves that efficiency increases with increase in the power output and after reaching a maximum value efficiency starts decreasing because of increased losses. For the same power output, efficiency is higher for lower value of d.c. link current because total losses are less with less d.c. link current[Fig. (7.14) to Fig. (7.25)]. Since total losses increase substantially with increase in frequency

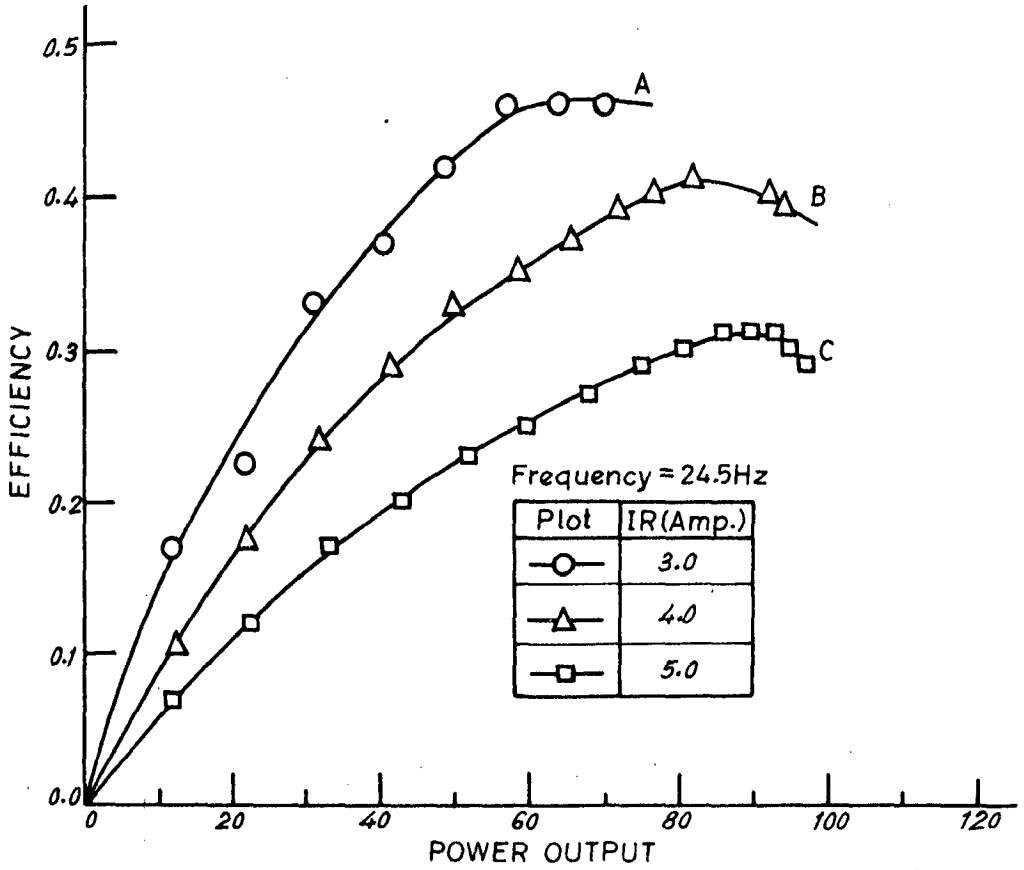

Fig. 7.26_Efficiency vs. power output characteristics.

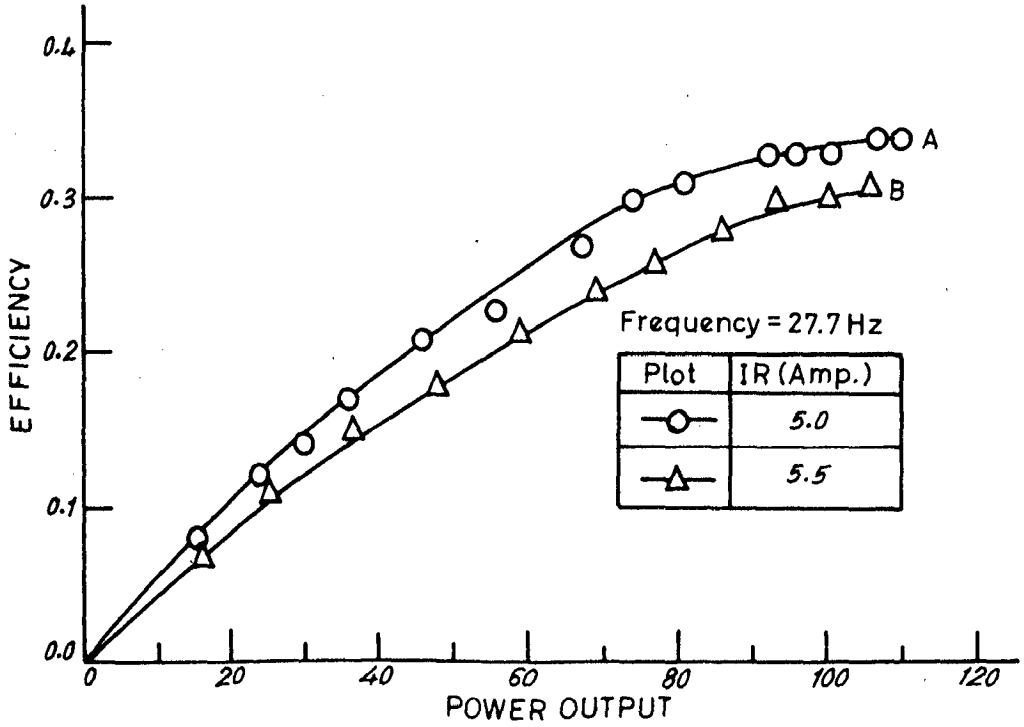

Fig. 7.27_Efficiency vs. power output characteristics.

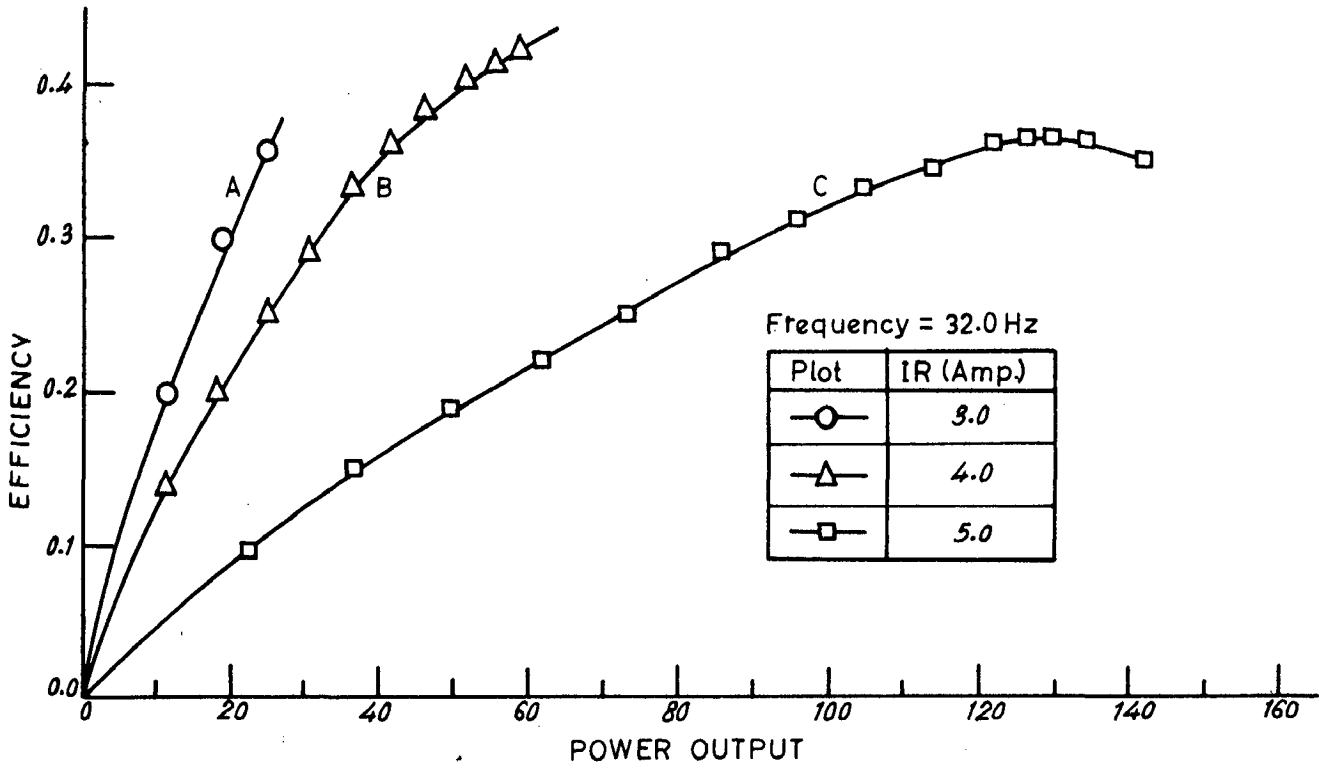

Fig.7.28_Efficiency vs. power output characteristics.

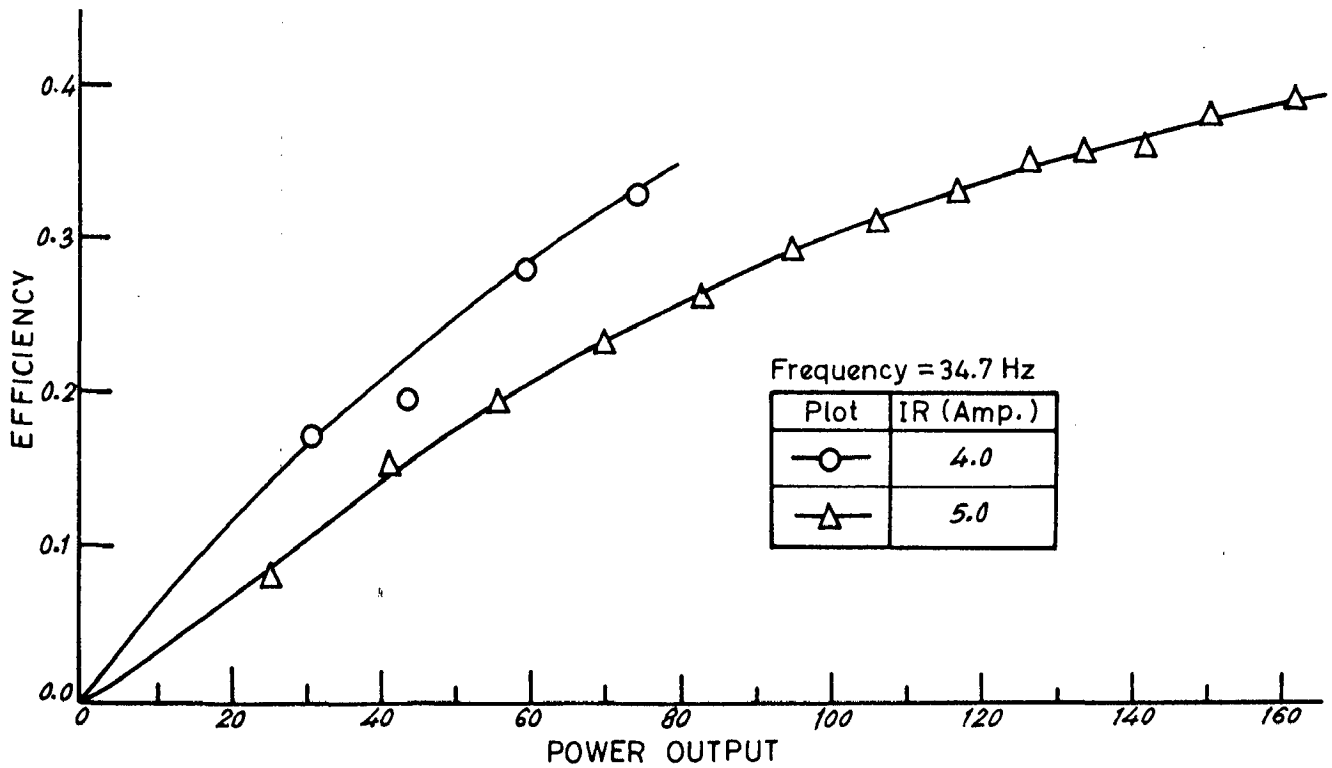

Fig.7.29_Efficiency vs. power output characteristics.

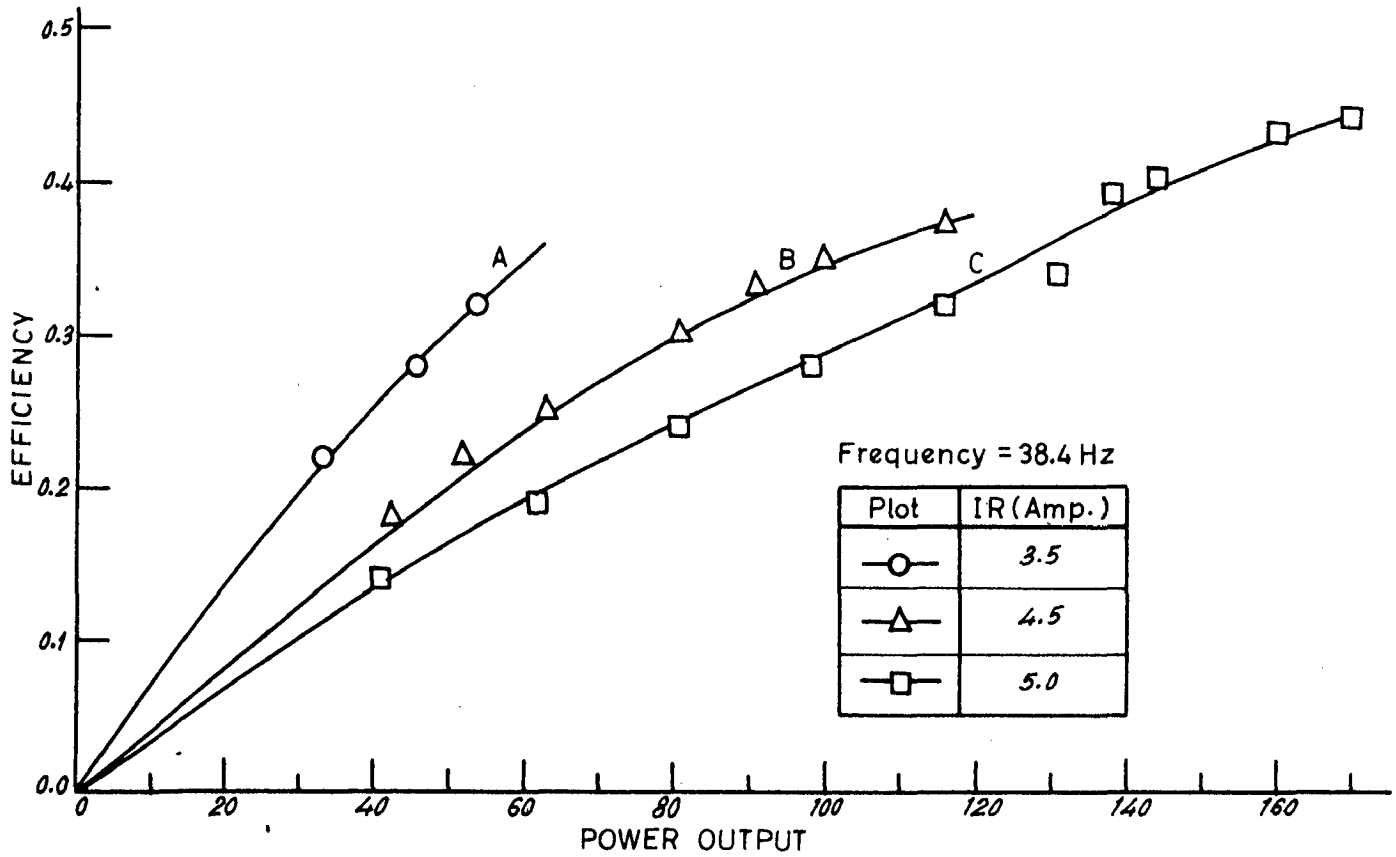

Fig. 7.30_ Efficiency vs. power output characteristics.

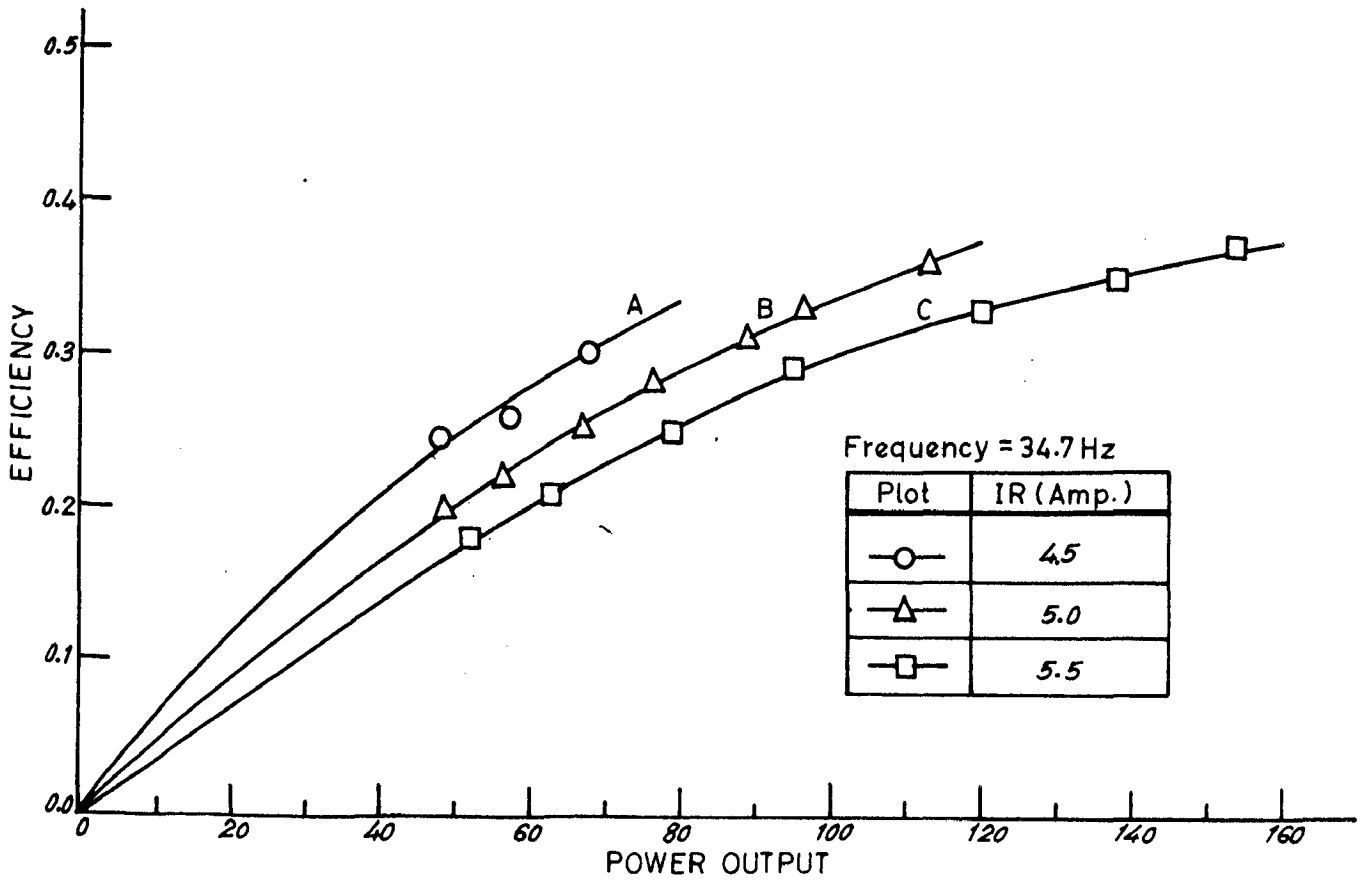

Fig. 7.31_ Efficiency vs. power output characteristics.

[Fig. (7.14) to Fig. (7.25)], this is why for the same power output and d.c. link current, efficiency decreases with increase in frequency.

7.4.3.5 Power Input Vs Power Output

The characteristics shown in Fig. (7.32) to Fig. (7.37) starts from a finite value Y-axis which equals the no load losses of the drive. As power output increases, power input also increases almost linearly. The above linearity is lost at low frequencies and higher power outputs. For the same power output, power input is more for higher d.c. link currents because total losses are higher. For same d.c. link current and power output, power input increases as frequency increases because of increased losses.

7.4.3.6 Load Torque Vs Power Output

The relevant curves are shown in Fig. (7.38) and Fig. (7.39). As we have seen in Speed Vs Power output characteristic that variation in speed with change in load is very very small. This is why Load torque Vs Power output characteristics are straight lines. As expected, power output is more for a given electrical torque at higher frequency of operation. The change in the d.c. link current does not have any effect on the above characteristic.

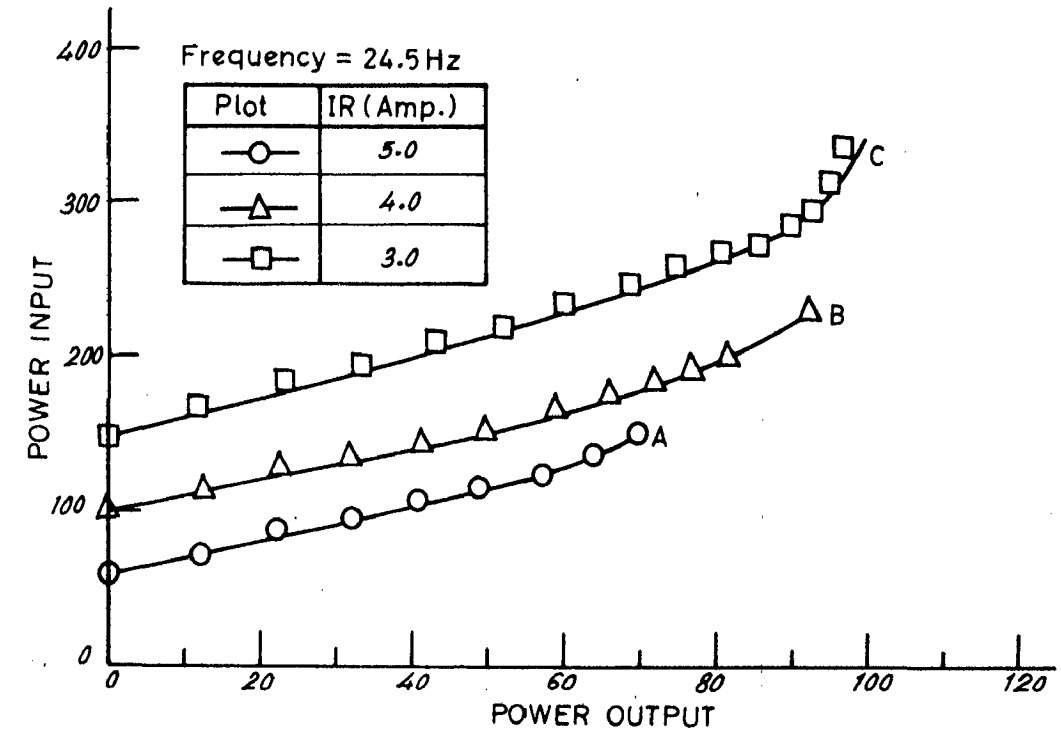

Fig. 7.32_ Power input vs. power output characteristics.

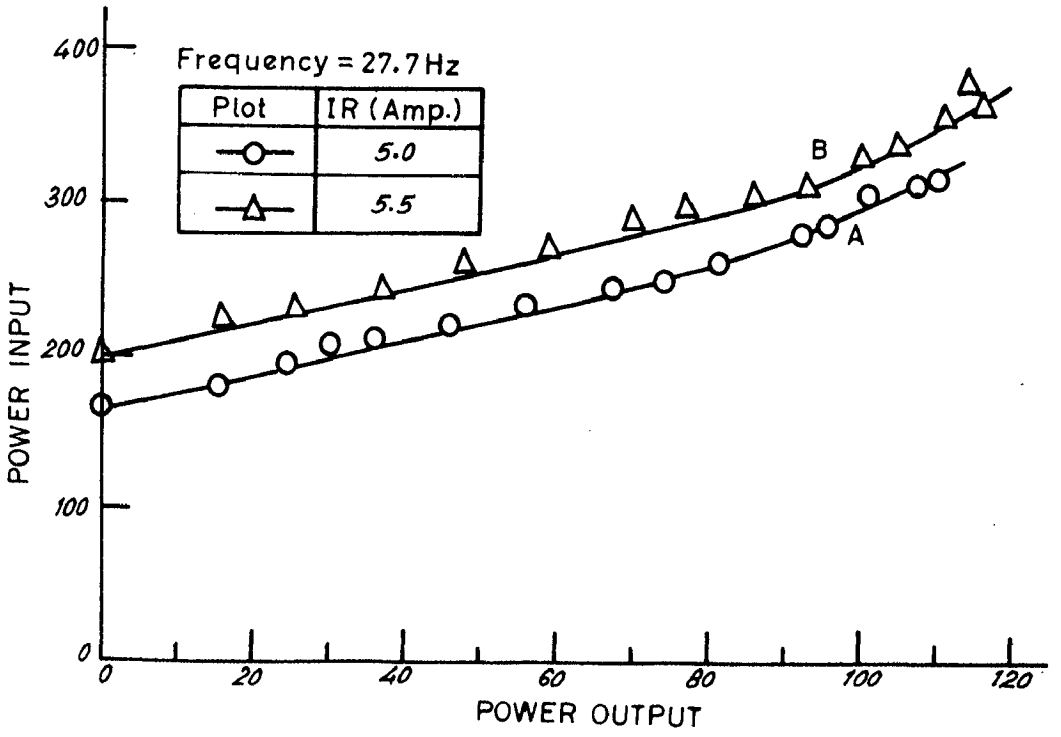

Fig. 7.33_ Power input vs. power output characteristics.

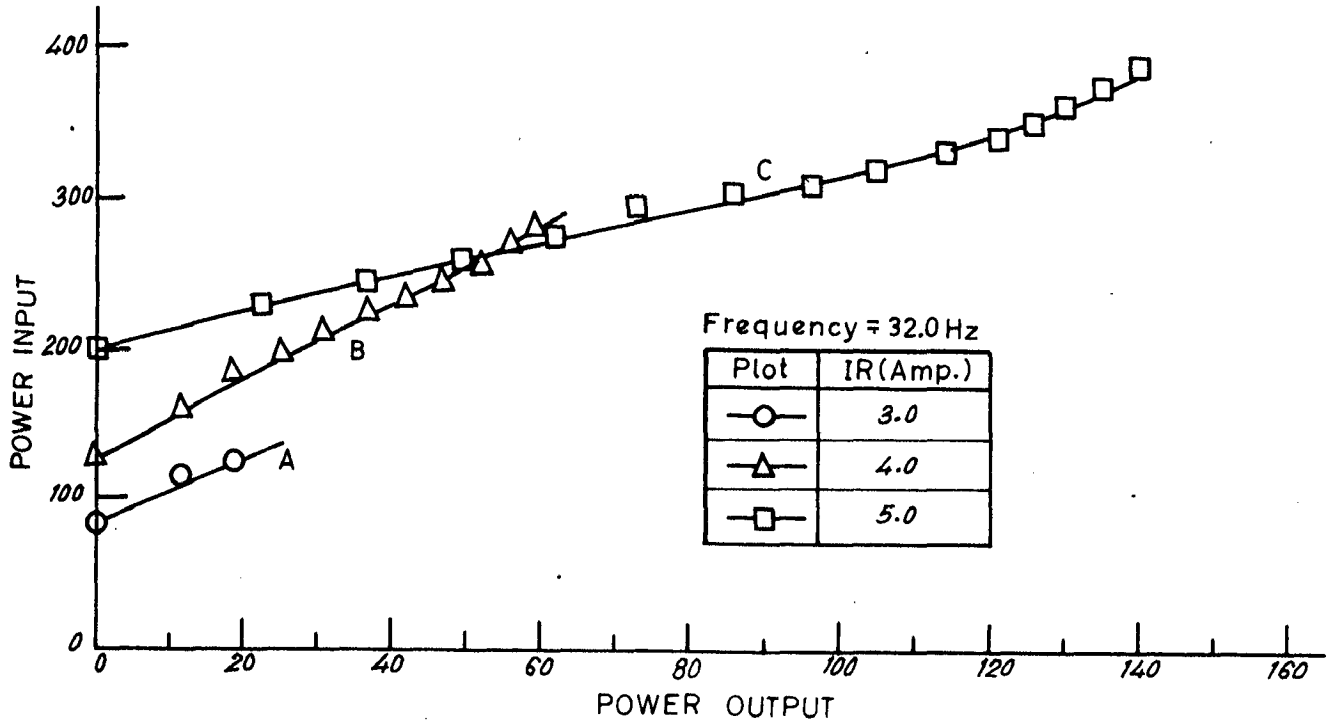

Fig. 7.34_ Power input vs. power output characteristics.

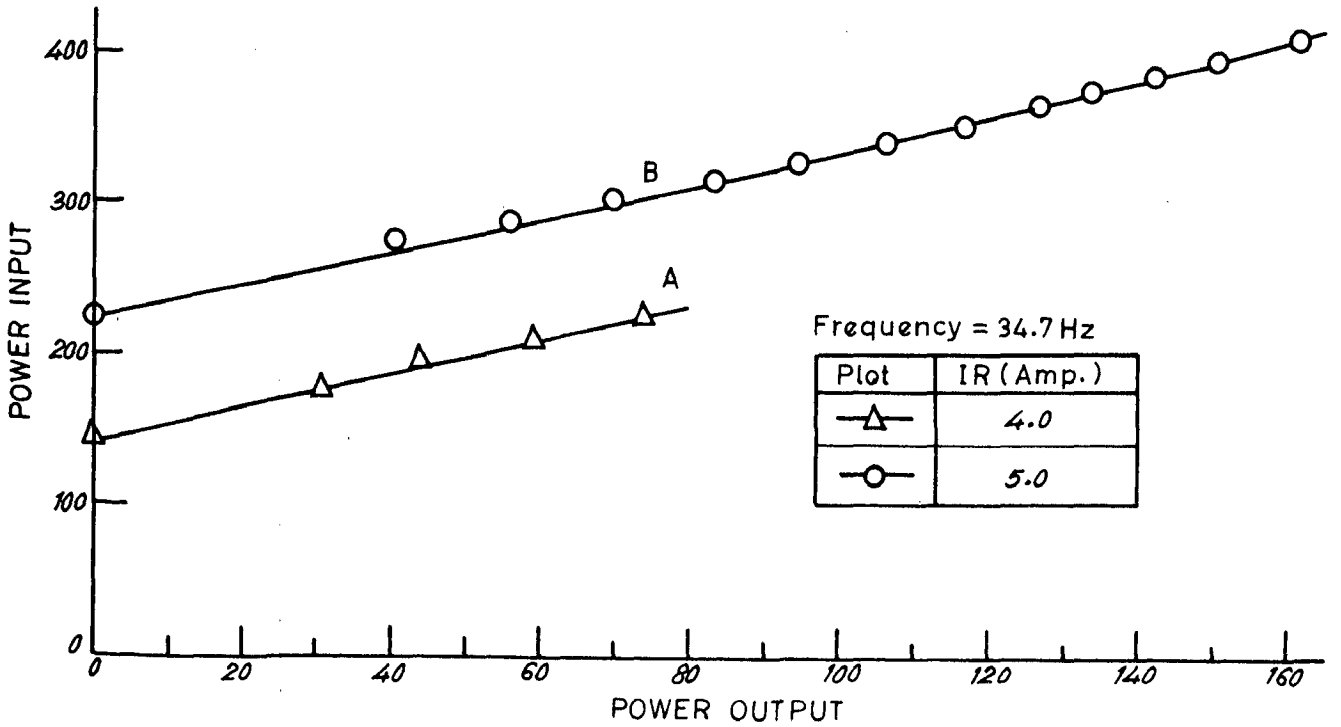

Fig. 7.35_ Power input vs. power output characteristics.

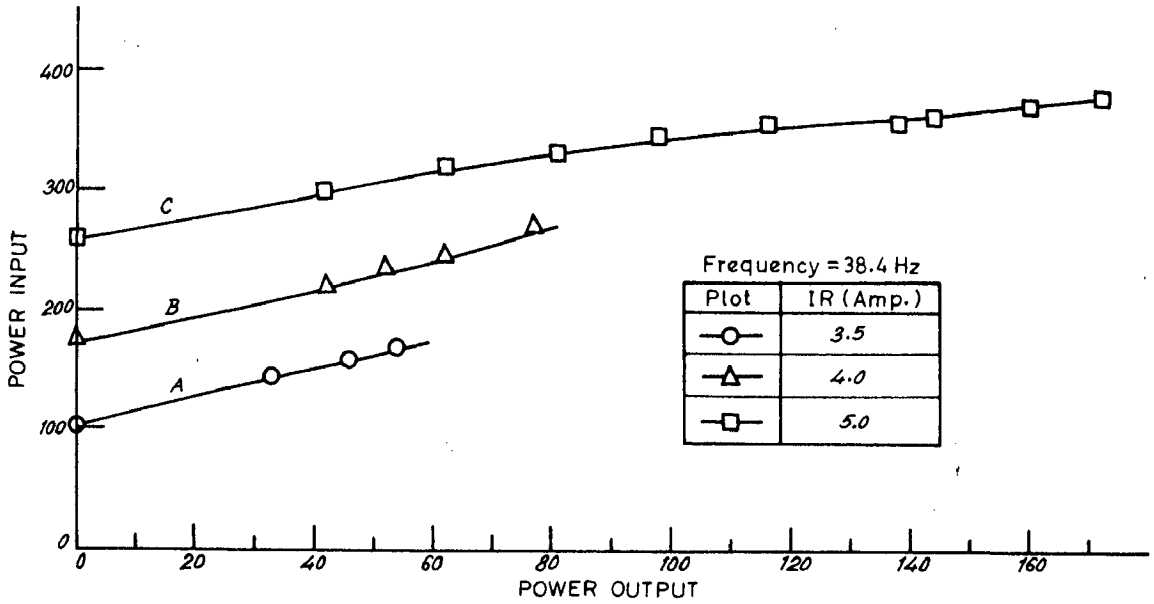

Fig. 7.36_ Power input vs. power output characteristics.

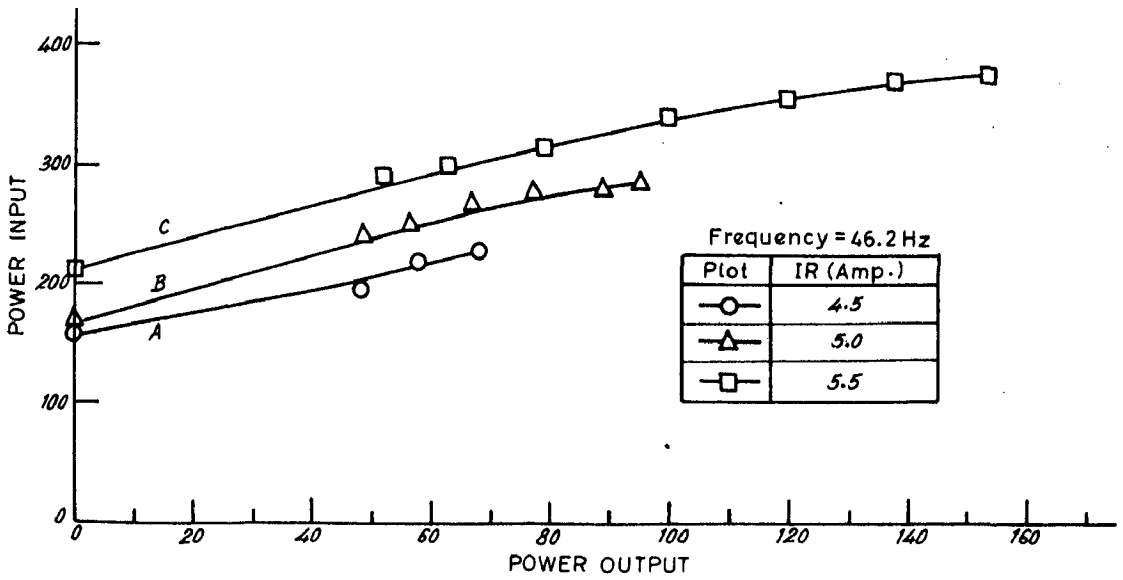

Fig. 7.37_ Power input vs. power output characteristics.

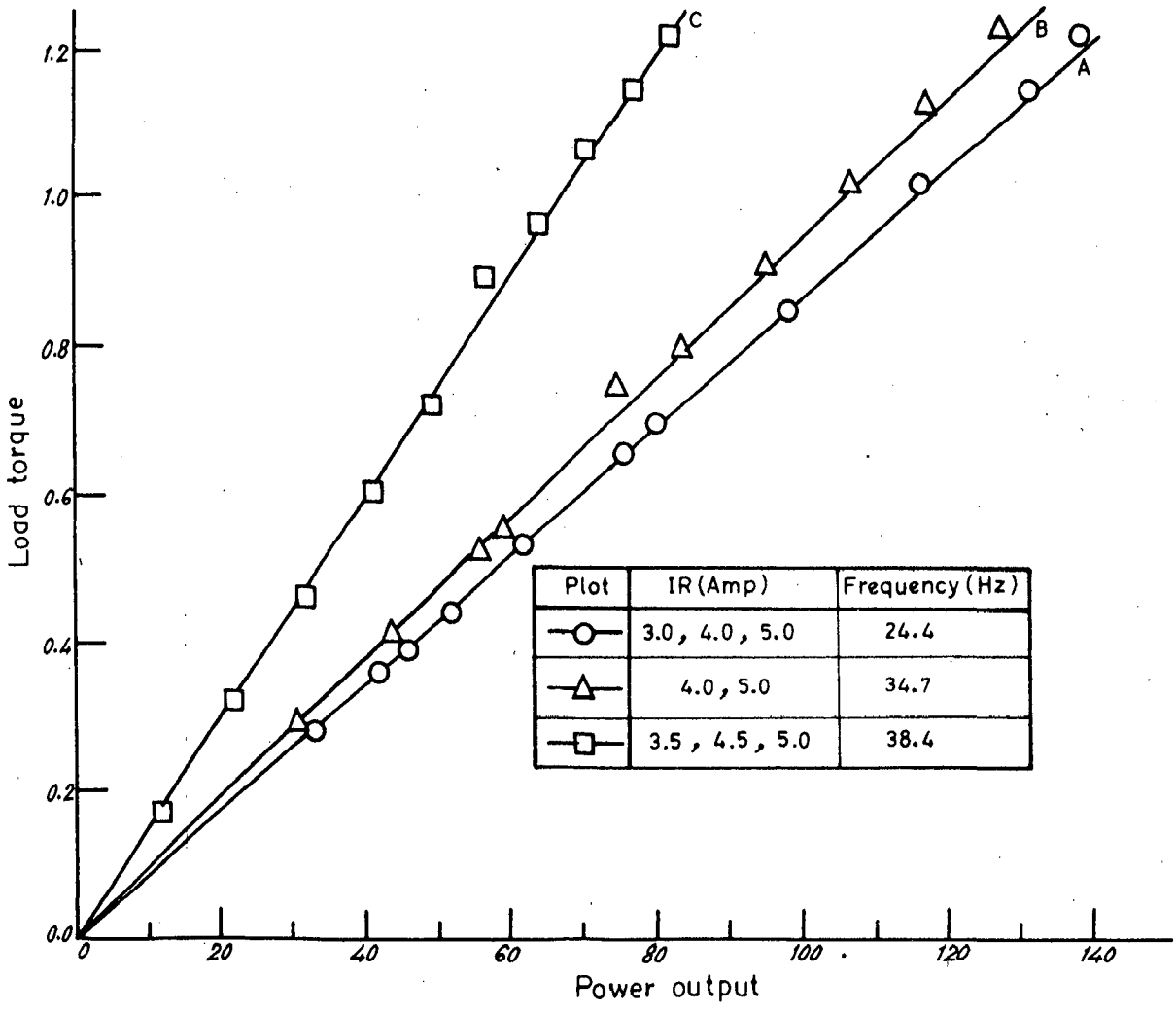

Fig. 7.38 – Load torque vs. power output characteristics.

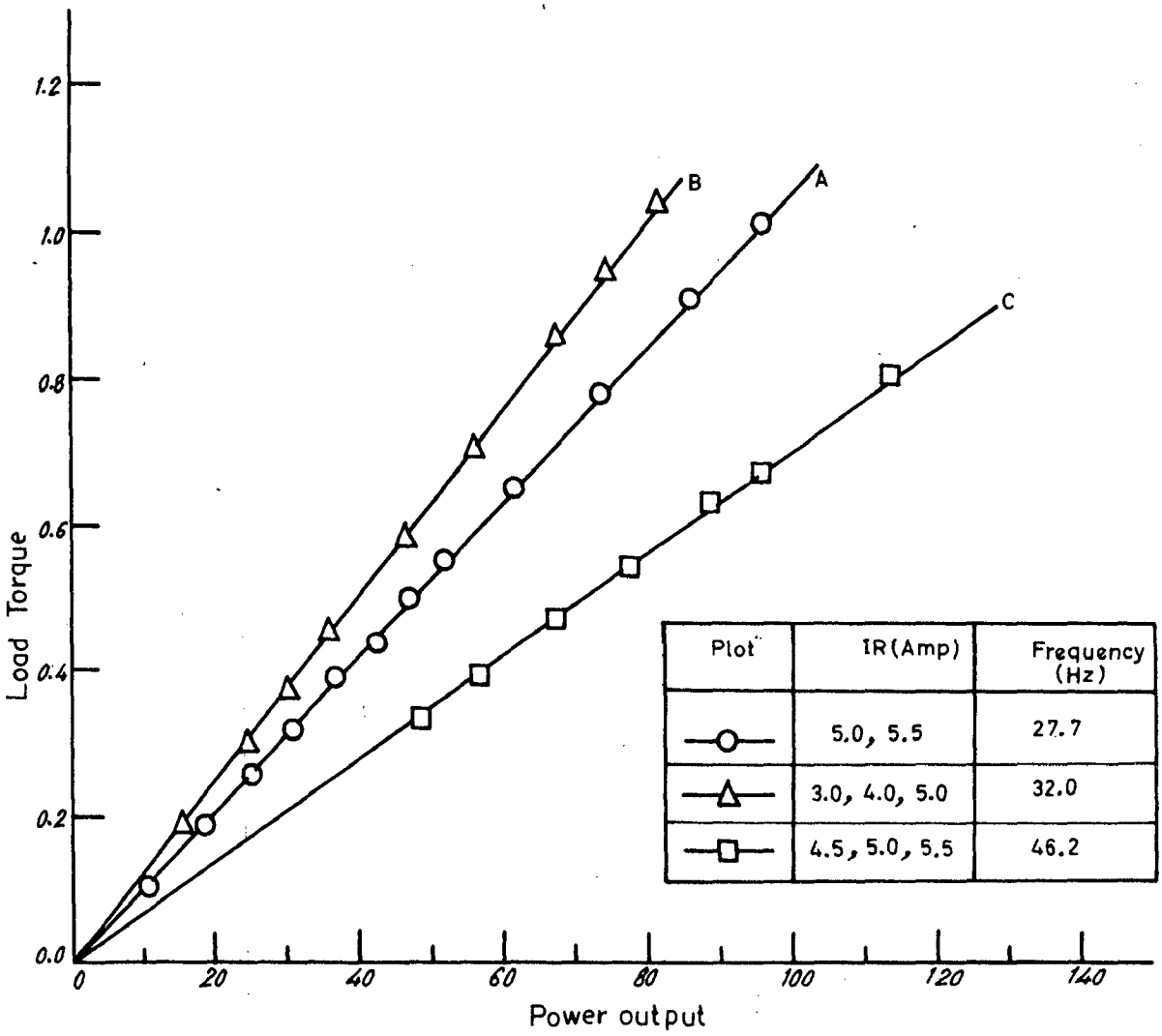

Fig. 7.39 _ Load torque vs. power output characteristics.

7.4.3.7 Power Factor Vs Power Output

The relationship between power factor and power output is shown in Fig. (7.40) to Fig. (7.45). It can be seen from the characteristics that at no load the power factor is worst but it improves with increase in the power output. At no load power factor is better for larger d.c. link current because of higher losses in the machine. The change in the operating frequency does not seem to have any specific effect.

7.4.3.8 Speed Vs Frequency

The characteristic is shown in Fig. (7.46) for a particular d.c. link current and load. The characteristic is almost linear as expected and shows effectiveness of speed control from 250 to 1350 R.P.M.

7.5 EXPERIMENTAL OSCILLOGRAMS

The various oscillograms which are shown in Fig. (7.47) to (7.68) consist of four sets. The first set of oscillograms[Fig. (7.47) to Fig. (7.52)]are at resistive load while the rest three are at induction motor load. The first set consists of waveforms of phase current, line current, d.c. link current and inverter input voltage. The effect of increase of resistance on line current and line voltage waveforms is also shown.

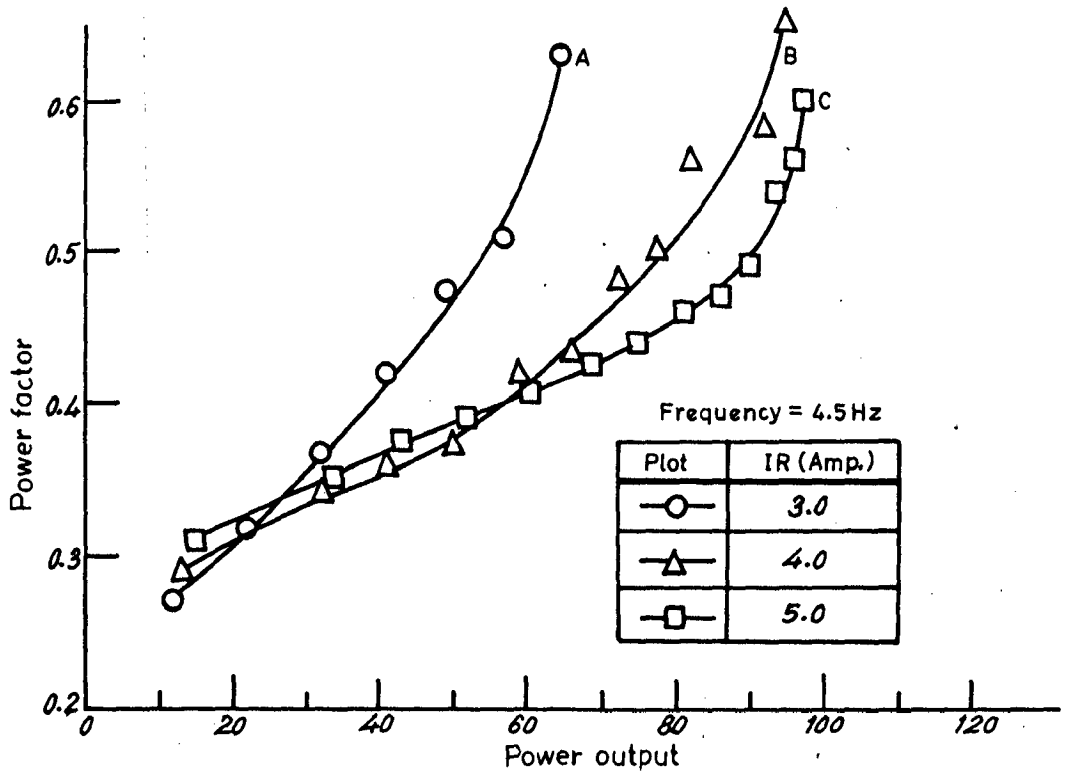

Fig.7.40_ Power factor vs. power output characteristics.

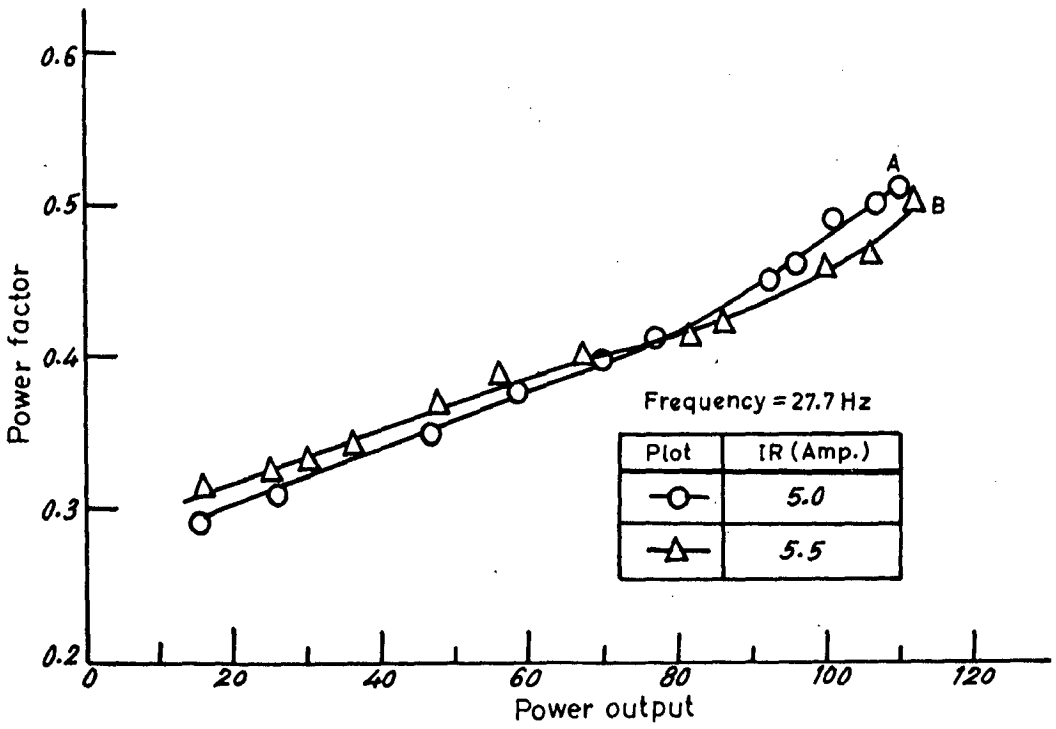

Fig.7.41_ Power factor vs. power output characteristics.

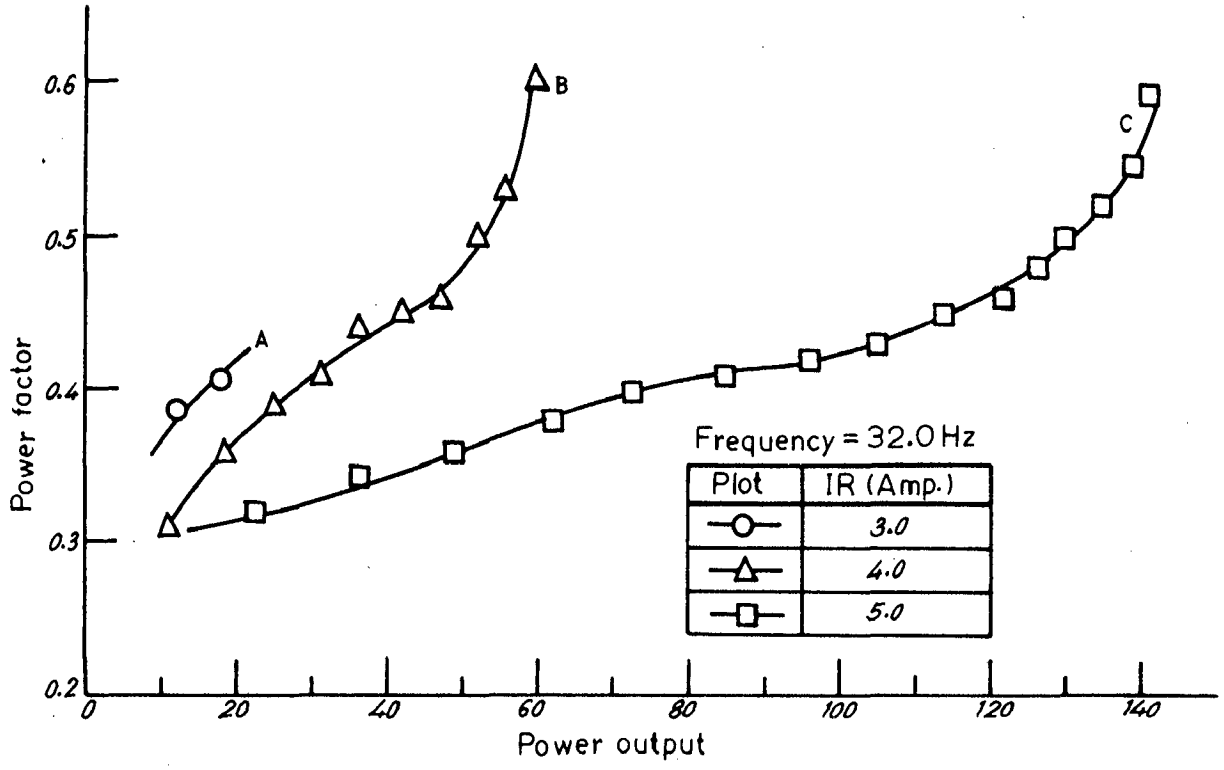

Fig.7.42_Power factor vs. power output characteristics.

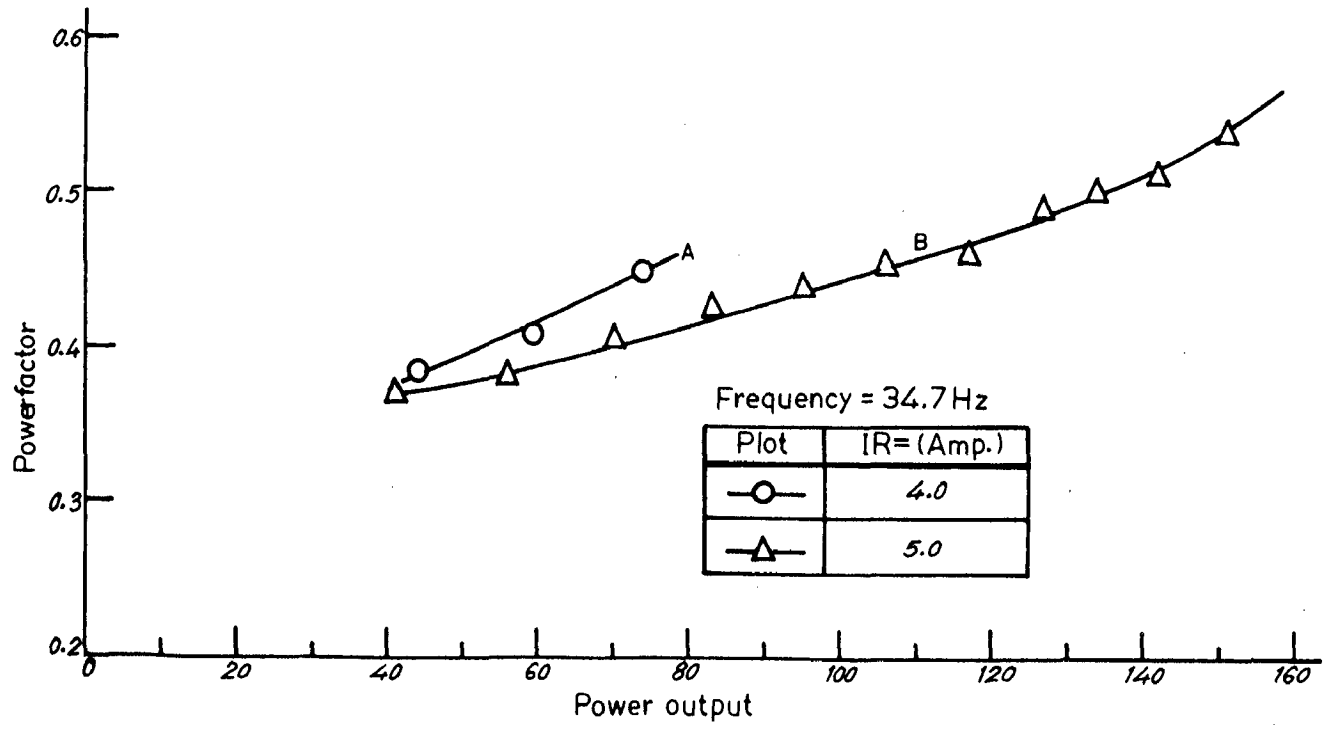

Fig.7.43_Power factor vs. power output characteristics.

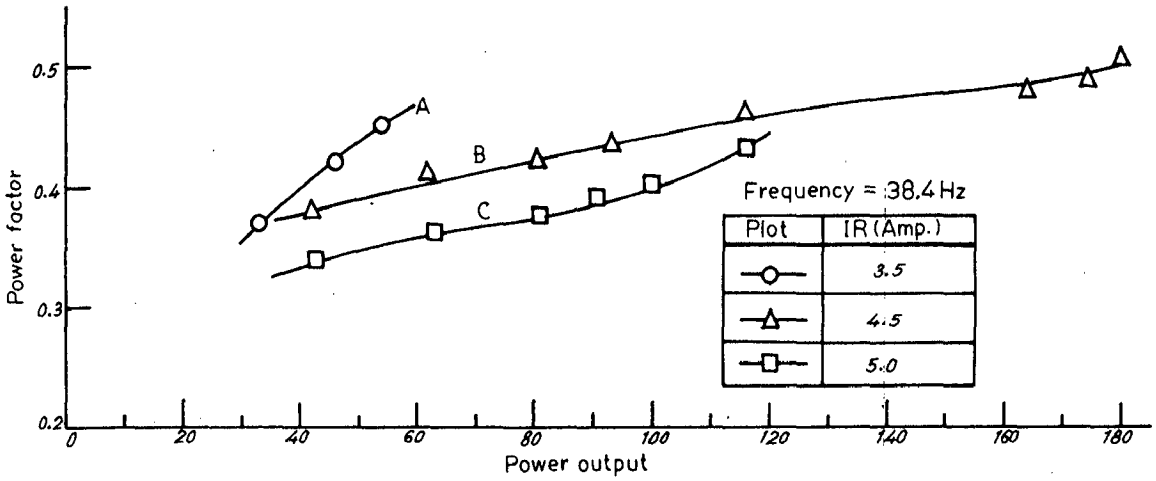

Fig. 7.44_ Power factor vs. power output characteristics.

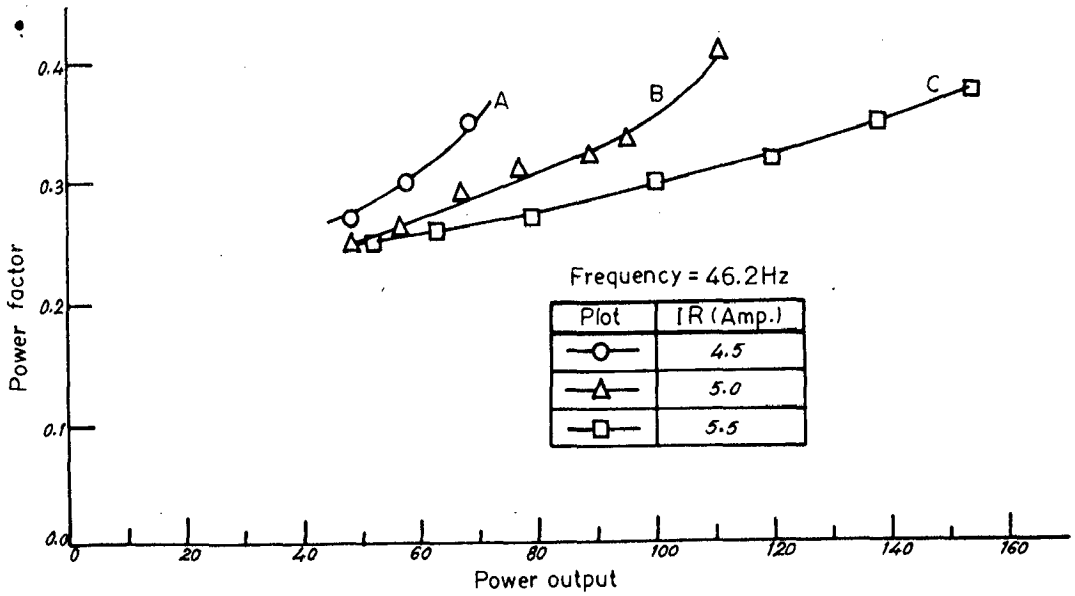

Fig. 7.45_ Power factor vs. power output characteristics.

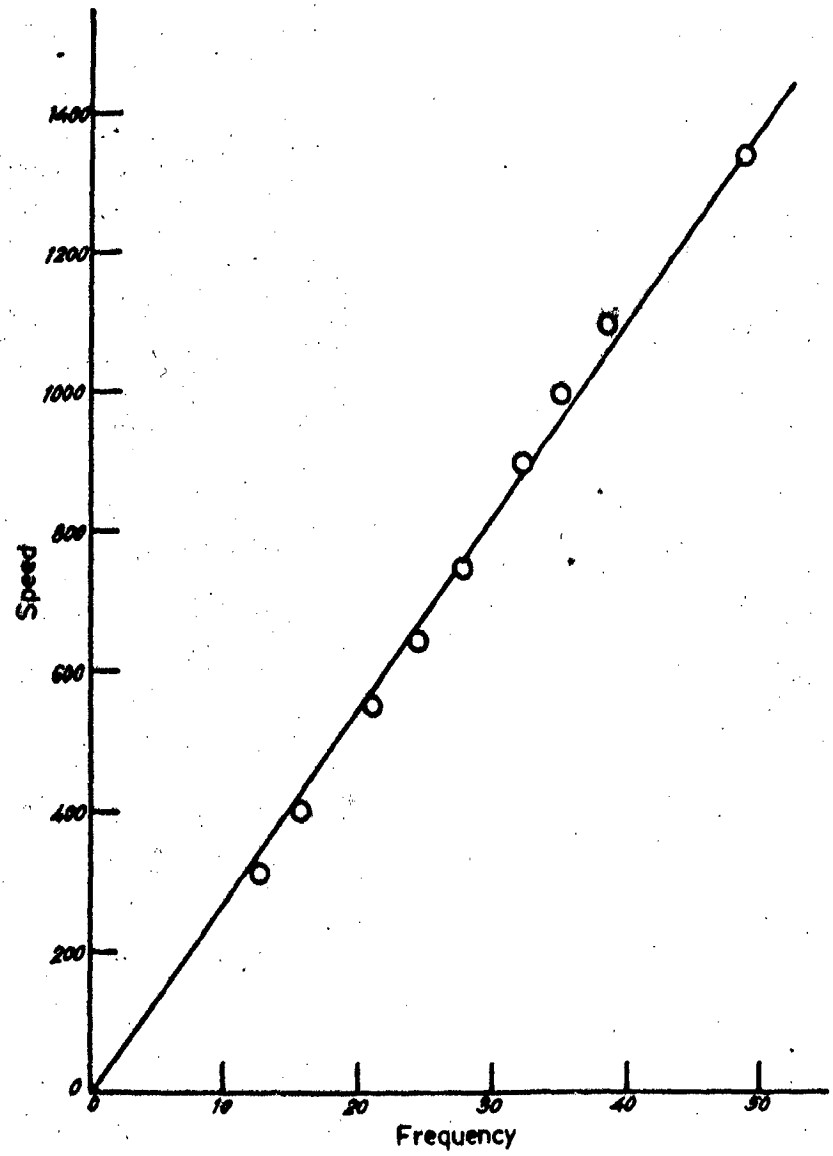

Fig.7.46_ Speed vs. frequency characteristic.

The second set Fig. (7.53) to (7.58) consists of motor line current and line voltage waveforms alongwith the waveforms of voltage drop across different components of the inverter at no load condition of the motor with the d.c. link current and frequency so adjusted as to give the best motor performance.

For the third set[Fig. (7.59) to (7.64)],d.c. link current is kept constant but operating frequency is almost doubled and the oscillograms of motor line current and line voltage are recorded to study the effect of change of operating frequency on voltage and current waveforms.

For the fourth set of oscillograms[Fig. (7.65) to (7.68)],d.c. link current and operating frequency are maintained same as in the third set but load is now applied to the motor and again line voltage and line current oscillograms are recorded to study the effect of loading on voltage and current waveforms.

7.5.1 Oscillograms At Resistive Load

Oscillogram (1)[Fig. (7.47)]shows the phase current and (2)[Fig. (7.48)] shows the line current waveforms for small value of load resistance. Both the waveforms are of six step and closely match with the ideal one shown by the side of the oscillogram.

Oscillograms At Resistive Load (1)

1

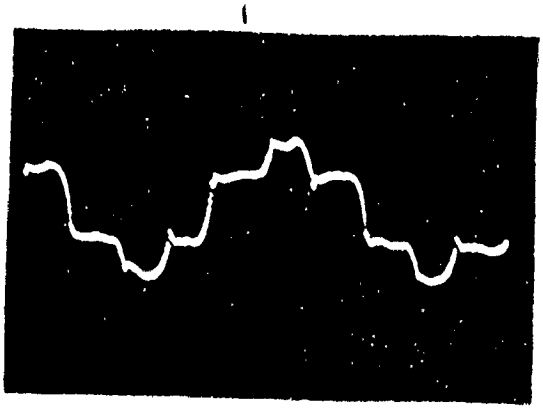

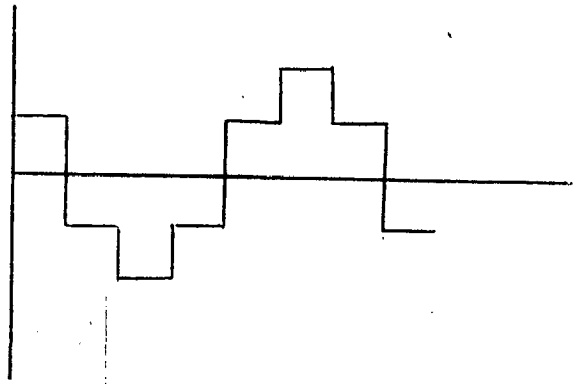

Fig. 7.47

2

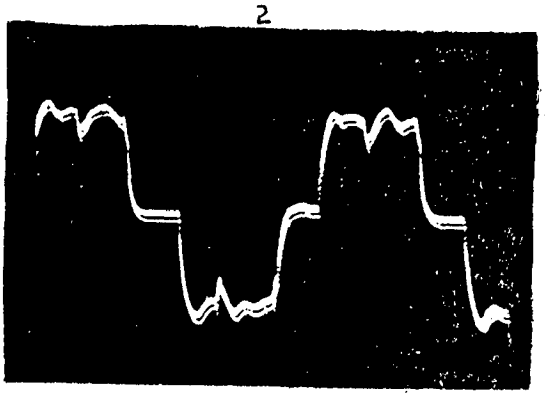

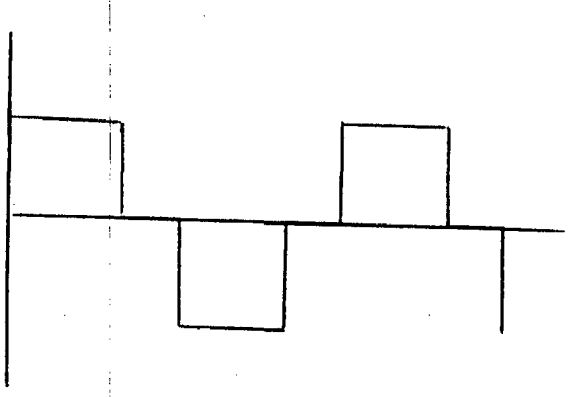

Fig. 7.48

3

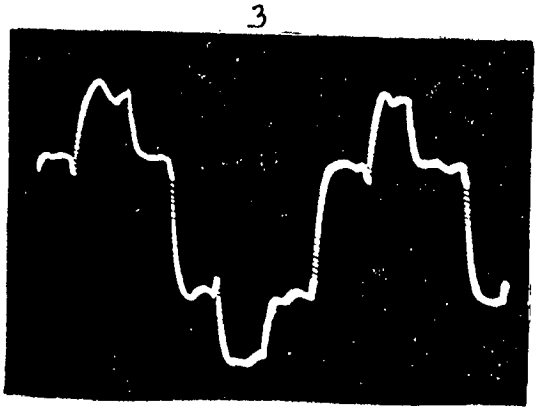

Fig. 7.49

4

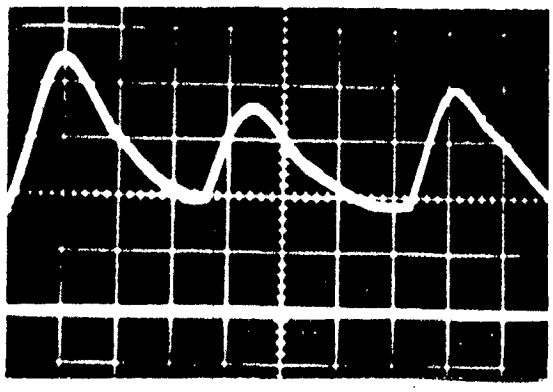

Fig. 7.50

6

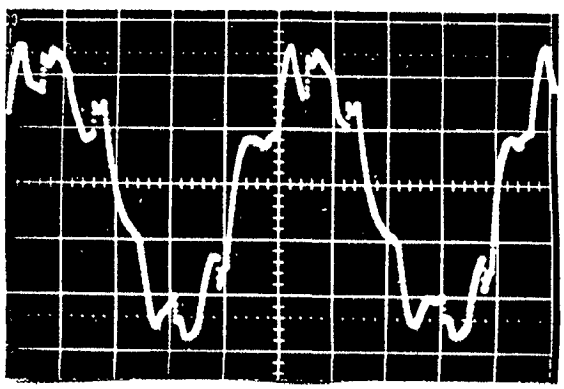

Fig. 7.52a

5

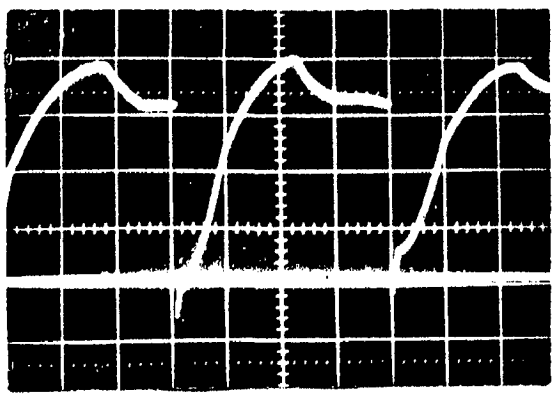

Fig. 7.51

7

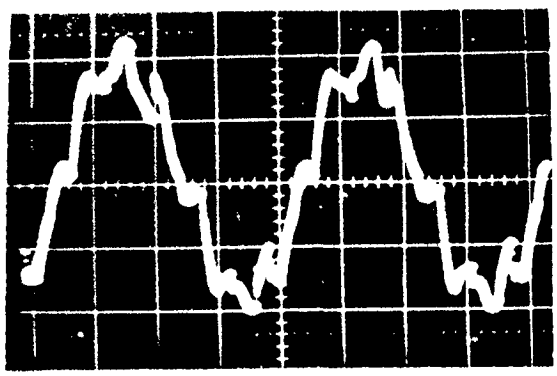

Fig. 7.52b

Oscillogram (3)[Fig. (2.49)]shows the line to line voltage waveform for delta connected load which is same as phase current since load is of resistive nature.

Oscillogram (4) and (5)[Fig. (7.50) and (7.51)] shows the waveform of d.c. link current and inverter input voltage. Large harmonics are present in the d.c. link current because the inductor in d.c. link is not very high.

Oscillogram (6) and (7)[Figs. (~~7.52~~ 7.52a) and (~~7.53~~ 7.52b)] shows the distortion in line current and line voltage waveforms when the load resistance is increased.

7.5.2 Oscillograms at No Load Operation of Induction Motor

All the oscillograms[Fig. (7.53) to Fig. (7.66)] are subjected to the following operating conditions of the motor:

INDUCTION MOTOR = NO LOAD

INVERTER INPUT = 38 VOLTS

I.M. LINE TO LINE VOLTAGE = 60 VOLTS

D.C. LINK CURRENT = 3.4 AMPERES

INDUCTION MOTOR LINE CURRENT = 2.85 AMPERES

3-ϕ Power = 84 Watts

SPEED = 470 RPM, FREQUENCY = 16.66 Hz.

Oscillogram (8)[Fig. (7.53)]shows the waveform of the d.c. link current which is rich in harmonics. These harmonics are present because of small d.c. link choke.

Oscillogram (9)[Fig. (7.54)]shows the waveform of the voltage at the input terminals of the inverter which on the average is d.c. The voltage spike on the negative side is due to commutation transient.

Oscillogram (10)[Fig. (7.55)]shows the waveform of the voltage drop across the SCR NO 6[Fig. (5.1)]of negative group. From the oscillogram it can be seen that the SCR conducts only for 120° during each cycle. In the oscillogram, voltage spikes due to commutation transient can be seen at the begining and midway of 120° conduction period. The slight difference in the voltage level of two 60° conduction period is due to small unbalancing in the capacitors of the negative group.

Oscillogram (11)[Fig. (7.56)]shows the waveform of the voltage across the commutation capacitor NO 6 [Fig. (5.1)]of negative group. In each cycle capacitor remains charged for 120° only. For the first 60°, capacitor remains charged in one direction and for the next 60° in other direction. The charging and discharging of the capacitor depends upon the RC time constant where R mainly consists of the stator winding resistance. Since R is very small therefore time constant is very small and

Oscillograms At No Load Operation Of Induction Motor

8

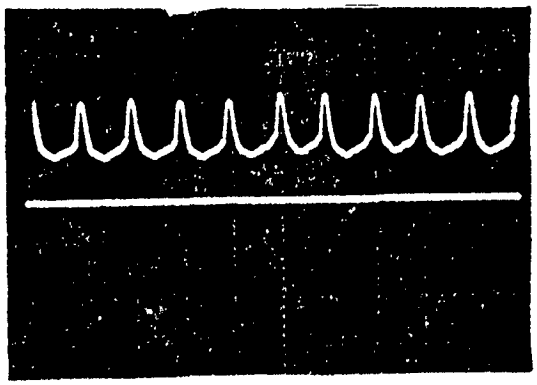

Fig. 7.53

9

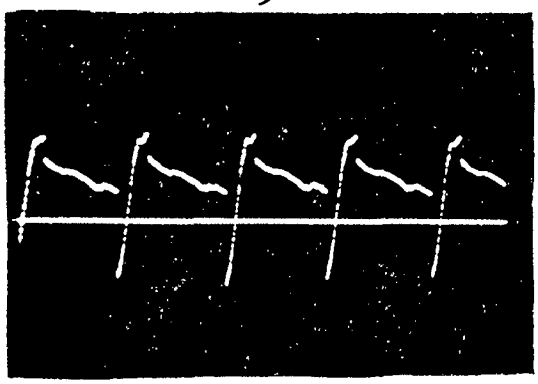

Fig. 7.54

10

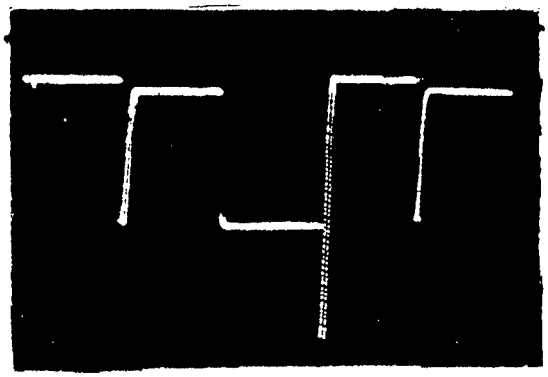

Fig. 7.55

11

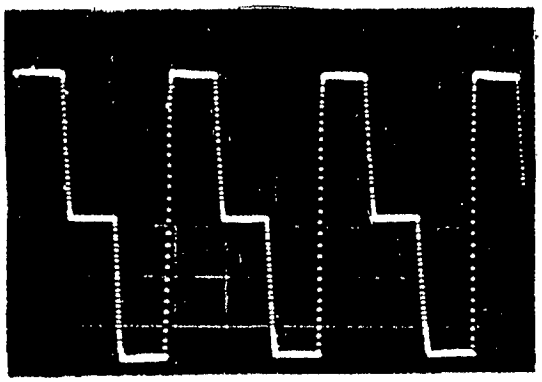

Fig. 7.56

12

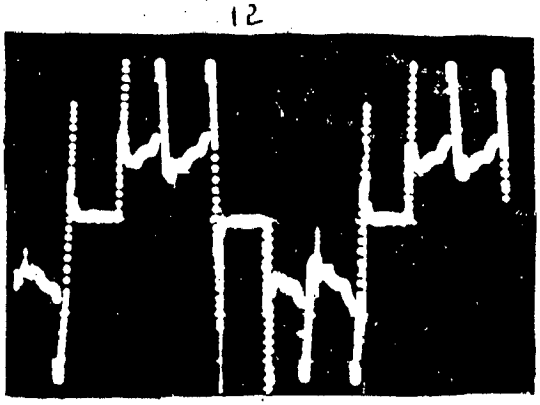

Fig. 7.57

13

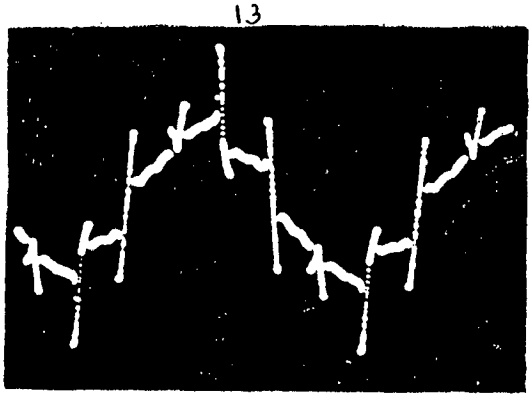

Fig. 7.58

charging and reversal of the charge takes place almost instantaneously. This explains the almost vertical nature of charging and discharging portions of the oscillogram (11).

Oscillogram (12) [Fig. (7.57)] shows the line current waveform of the induction motor. The waveform is six step quasi-square but rich in harmonics. These harmonics are present as a result of harmonics in the d.c. link current and commutation transients.

Oscillogram (13) [Fig. (7.58)] shows the waveform of line to line voltage at the input of induction motor. The voltage waveform is almost sinusoidal with transient over voltage spikes super-imposed upon it. The slight distortion in the voltage waveform is caused by stator resistance drop. The transient over-voltage spikes are formed as a result of resonant overlap angle in the current waveform [Fig.7.58(a)], which is determined by the magnitude of d.c. link current, commutation capacitance and subtransient inductance of the machine.

7.5.3 Effect of Change of Frequency on Motor Current and Voltage Waveform

Oscillograms (14) and (15) [Fig.(7.59) and (7.60)]

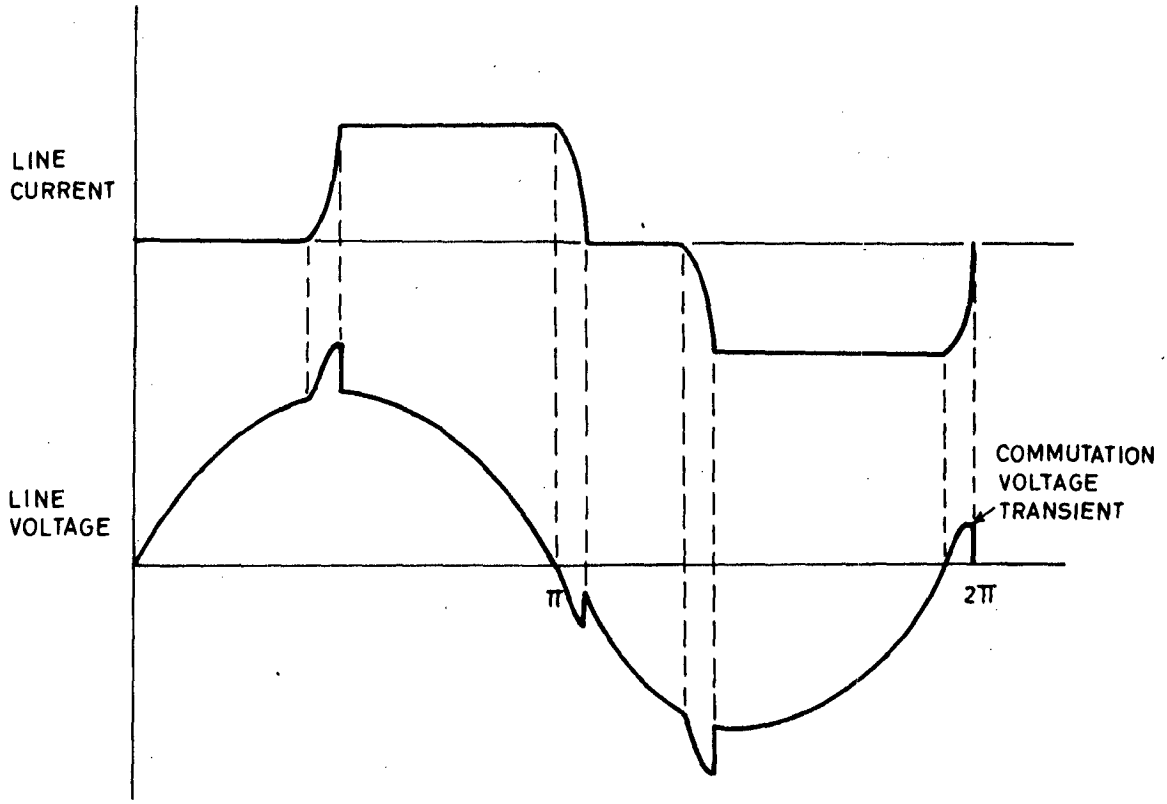

Fig. 7.58 (a) _ Nature of machine line voltage and current waveforms.

Effect Of Change Of Frequency On Motor Current And Voltage Waveform

14

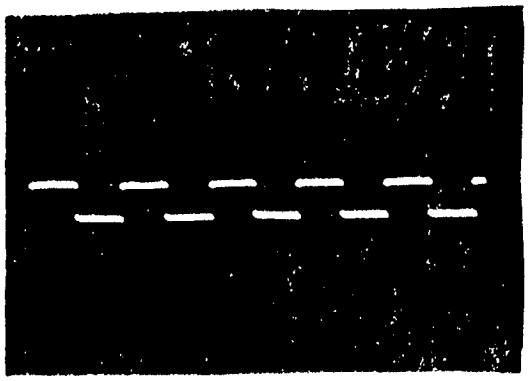

Fig. 7.59

15

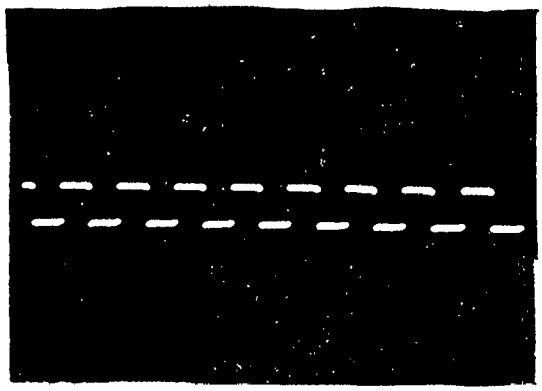

Fig. 7.60

16

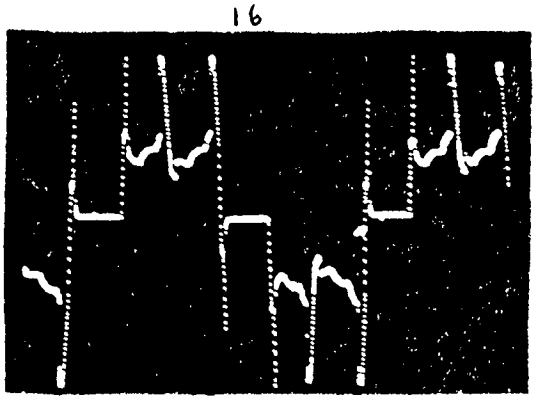

Fig. 7.61

17

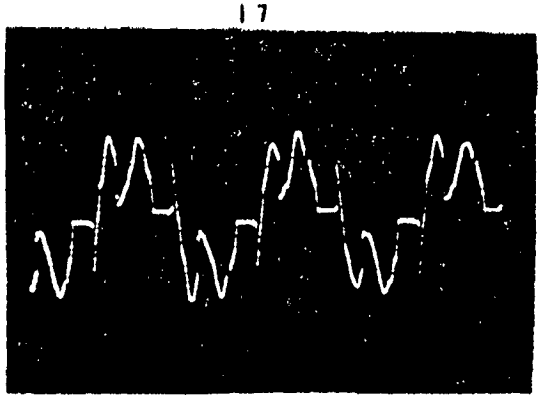

Fig. 7.63

18

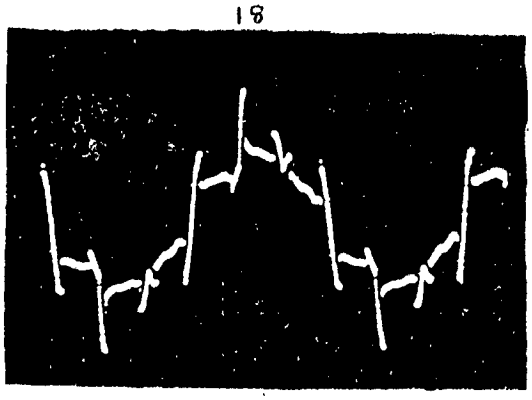

Fig. 7.62

19

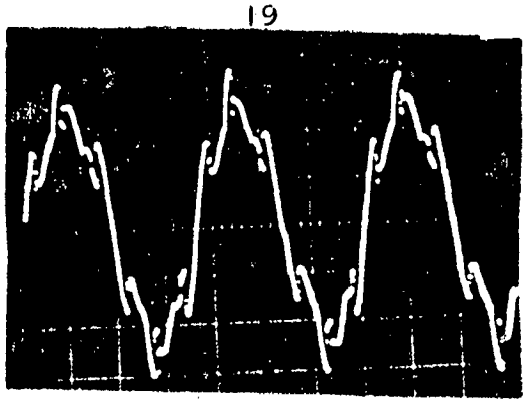

Fig. 7.64

show the output of the Johnson Counter. Oscillogram (14) represents 16.66 Hz while (15) represents 33.32 Hz.

Oscillograms (16) and (17)[Fig. (7.61) to (7.63)] and Oscillograms (18) and (19)[Fig. (7.62) to (7.64)] show the waveforms of line current and line voltage of induction motor running at no load and at the above two operating frequencies.

It is noted from the oscillogram (16) and (17) that at lower frequency (16.66 Hz) the commutating transients are predominant resulting in the over current spikes at each instant of commutation. A very small value of inductance must be used in series with each thyristor to limit $\frac{di}{dt}$ to a safe value. At large frequency (32.32 Hz) the commutation transients are present only at the instant of the reversal of the current. The waveform at large frequency is more near to the ideal one which is shown side by side, except for a dip in between the 120° conduction period which is also due to commutation.

After comparing oscillogram (18) and (19) we find that over voltage spikes due to commutation transient are present at low as well as high frequency but distortion of the voltage waveform due to these transients is more at highe frequency.

7.5.4 Effect of Change of Load on Motor Current and Voltage Waveforms

Oscillograms (20) and (21)[Fig. (7.65) and (7.67)] and (22) and (23)[Fig. (7.66) and (7.68)] show the waveforms of line current and line voltage at no load and at moderate load respectively.

After comparison we find that line current waveform improves at load because the dip in between the 120^{o} conduction period decreases. The voltage waveform at load is also better than at no load because over voltage spikes due to commutation transients are suppressed to a large extent.

7.6 CONCLUSION

In the present chapter, the performance of the constant current-source inverter at resistive and cage induction motor load is investigated experimentally. The current in the d.c. link is kept constant with the help of a current loop.

The observations at resistive load show that current-source-inverter is not suitable for resistive loads because commutation is dependent on load current which is affected by increase in resistive load.

The induction motor was operated in the stable zone of torque-slip characteristic with the help of current

Effect Of Change Of Load On Motor Current And Voltage Waveform

20

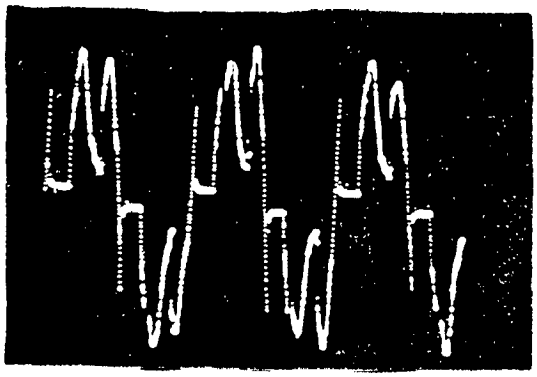

Fig. 7.65

21

Fig. 7.67

22

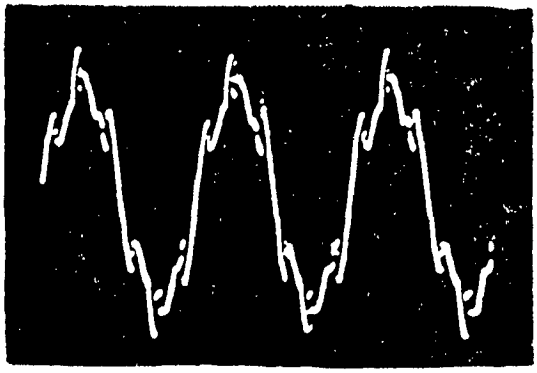

Fig. 7.66

23

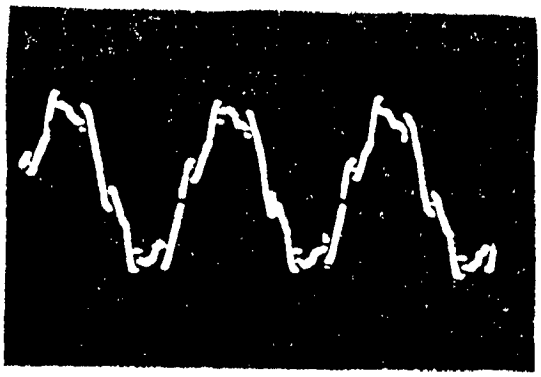

Fig. 7.68

loop and load test was performed at different operating frequencies and d.c. link currents. The observations of the load test are tabulated in tables (7.2) to (7.7).

The operating frequency range for the satisfactory operation of the drive is found to be between 10 to 47 Hz. The upper limit of operating frequency is fixed by the choice of capacitance which in turn is based on the rating of the SCR voltage. The lower limit is fixed by the permissible torque pulsations. The observation tables also show that loading capability of the motor increases with the d.c. link current. The slight decrement in the motor line current at higher frequencies because of the phase shift of the fundamental component of the line current due to finite commutation interval can also be noticed from the observations.

The performance of the drive as obtained from the observations is shown as a function of load torque in Figs. (7.13) to (7.46).

The experimental curves show that losses in the drive are high, power-factor and efficiency are poor. This is so because induction motor is always operating in the highly saturated stable zone of torque-slip characteristic. Total losses which mainly consist of iron and copper losses increase sharply with increase in d.c. link current and operating frequency resulting in more power

input and hence in the poor efficiency of the drive. The effect of change of d.c. link current on power-factor is very peculiar. At light loads power-factor is better with high d.c. link current while at high loads power-factor is better with low d.c. link current. The operating frequency does not seem to have any specific effect on power factor. The Load torque Vs Power output curve is linear because of very small change in speed with load. It is also seen that for a fix power output, load-torque is more at higher frequencies. The speed regulation of the drive is very good[Fig. (7.13)]. The speed control by change in operating frequency is almost linear as is clear from Speed Vs Frequency plot[Fig. (7.46)].

The line current and phase current oscillograms at resistive load are found very much similar to the ideal one shown side by side[Fig. (7.47) and (7.48)]. The oscillograms of line voltage, line current and of voltage drop across different components of inverter circuit at induction motor load closely matches with those given in different papers [15, 18, 30]. The change of operating frequency and load are also found to have an impact on the line current and line voltage waveforms.

CHAPTER VIII

CONCLUSION

This dissertation concerns steady-state analysis of current-source inverter fed induction motor drive. The configuration of current-source inverter in auto-sequential commutation mode is selected. The constant current source is realized with the help of a reactor connected in series with a controlled rectifier and a current loop which continuously monitors the current in the d.c. link, compares it with a reference input and adjusts the firing angles of the SCRs so as to maintain constant current. The guide lines for the selection of the ratings of various components of inverter are presented and discussed, which form a basis for the design of the inverter. The inverter designed on the above guide lines is fablicated and satisfactory performance realised.

For the auto-sequential current-source inverter, a suitable firing scheme is developed using Johnson counter as the basic block for generating three phase variable frequency square wave pulses. The outputs of the Johnson counter are manipulated to produce six sets of continuous firing pulses of 120° duration with a phase difference of 60° from one another. This firing circuit satisfactorily operated the current-source inverter made of 16A, 1200 PIV rating SCRs feeding a 3ϕ cage induction motor of 375 W size.

The commutation process in the inverter is divided into three stages. In the first stage the current transfer takes place from one SCR to the other. In the second, current modifies the capacitor voltages. The machine currents do not change in these two stages. The current transfer from one phase to the other takes place in the third stage. The transfer is also affected by the machine resistance, inductance and commutating capacitance of the inverter.

A mathematical model which completely represents the used drive scheme is developed in p.u. and an analytical method for determining steady-state performance has been set forth. The analytical results of the steady-state performance of the drive are presented as a function of slip. Complete performance is also summarised in the form of curves as a function of load torque.

The experimental results of the steady-state performance of the drive were obtained by performing load test under five sets of operating conditions. The observations of the load test are given, and performance curves plotted as a function of power output.

The analytical results show that the torque-slip characteristic consists of two zones, one with a positive slope and the other with a negative slope. The negative sloped zone is unstable. The negative sloped zone is

comparatively very small and has a very steep slope. The stable and unstable zones can also be identified in other characteristics with the help of torque-slip characteristic. The machine can be operated either in the stable zone or in the unstable zone for the same torque demand. However when operating in the unstable zone, feed backs are necessary.

The analytical results show that operation in the stable zone will result in more power output, less losses and better efficiency than the unstable zone. However power-factor will be poor and stator voltage will be dangerously high. On the other hand the experimental results which are obtained only for operation in the stable zone show that losses in the drive are high, efficiency and power-factor are poor which results in the reduction of the loading capacity of the machine by a considerable amount. The stator voltages are also not found high while operating in the stable zone.

The big difference between the theoretical and experimental results is only because of saturation which is neglected in the analysis. Since the flux level in the machine will be very high while operating in the stable zone therefore saturation must be properly accounted for in the analysis.

The operation in the unstable zone corresponds to normal flux level in the machine and therefore will result in better performance as compared to stable zone in practical case. Though operation in unstable zone requires stabilising feed backs, even then it should always be preferred.

The speed regulation of the present drive is found to be very good. The speed can be smoothly controlled from 250 R.P.M. to 1350 R.P.M. by changing operating frequency. The effect of the phase shift of the fundamental component of the line current due to finite commutation interval resulting in slight decrease in the motor line current at higher frequencies is also noticed.

The various oscillograms are found to compare very well with the standard ones, available in the literature. The operating frequency and load are seen to have an effect on line voltage and current waveforms.

8.2 SCOPE OF FURTHER WORK

Further work can be done on this topic under following aspects:

(i) A rectifier inverter source has been considered here to feed variable current and frequency

supply to the induction motor. An alternate form of the supply source like the inverter operating in the pulse width modulation mode, may be considered.

(ii) In this dissertation drive operation in sub-synchronous speed range only has been studied. Drive operation in super-synchronous speed range can also be studied.

(iii) The present work ignores commutation time of the inverter. Inverter with finite commutation time should be considered and its effect on drive performance may also be studied.

(iv) The present fabrication work has only the torque control loop (current loop) which keeps the current in the a.c. link constant. In the future work, slip control loop (speed loop) should be incorporated. The above two loops may also be combined to yield speed reference as a single variable.

(v) The firing circuit developed in the present work is suitable for two quadrant operation of the drive. The firing circuit capable of four quadrant operation of the drive should be developed in future work.

(vi) In the present work only steady-state performance has been obtained theoretically neglecting saturation and all the harmonics. The effect of harmonics (6th and 12th) and the saturation on the steady-state performance of the motor should be studied in future.

(vii) The effects of variation of parameters on the performance of the system should also be studied so that a proper choice of thyristors and commutating elements can be made.

(viii) Since in the current-source-inverter fed drives stability is the main problem, therefore stability studies should be carried out to design the system so that system is not only stable but possesses a certain minimum degree of stability.

BIBLIOGRAPHY

REFERENCES

1. Andersen, E.C., and Bieniek, K., "On the torques and losses of Voltage and Current source inverter drives", IEEE Trans.(IA), Vol.20, pp. 321, March/April, 1984.

2. Bose, B.K., "Adjustable speed A.C. drives - A Technology status review", IEEE Proc., Vol.70, pp. 116, Feb.1982.

3. Bose, B.K., "Adjustable speed A.C. drive systems", NEW YORK: IEEE Press, 1981.

4. Cormell, E.P., and Lipo, T.A., "Modelling and design of controlled current induction motor drive systems", IEEE Trans. (IA), Vol.13, pp-321, July/August, 1977.

5. D.A. Paice, "Induction motor speed control by stator voltage control", IEEE Trans. Power App. Syst., Vol.PAS-87, pp.585-590, Feb. 1968.

6. Douglas Scholey, "Induction motors for variable frequency power supplies", IEEE Trans. (IA), Vol.18, No.4, July/Aug. 1982.

7. Fekete, G, and Szentirmai, L., "Current-source inverter fed induction motor drive for four quadrant operation", International Conference on electrical machines 84, Lausanne, Switzerland.

8. Farrer, W., and Miskin, J.D., "Quasi-sine wave fully regenerative inverter", IEEE Proc., Vol.120, pp.969, Sept. 1973.

9. Friedrich, W., and Mueller, A., "Control Methods for reducing the inductance in the d.c. link of current-source inverters", IEEE Trans. (IA), Vol.19, pp.699, Sept./Oct. 1983.

10. Joshi, Avinash, and Dewan, S.B., "Modified steady-state analysis of the current-source inverter and squirrel cage motor drive", IEEE Trans. (IA), Vol.17, pp.50, Jan./Feb. 1981.

11. Jones, B.L., "Electrical variable-speed drives", IEE Proc., Vol.131, pp.516, Sept. 1984.

12. Jain, Manju, "Stability and performance analysis of a variable speed controlled slip induction motor drive", M.E. dissertation 1982, Dept. of Electrical Engg., U.O.R., Roorkee.

13. Krause, P.C., and Thomas, C.H., "Simulation of symmetrical induction machinery", IEEE Trans.(PAS), Vol.84, pp. 1038, Nov. 1965.

14. Lipo, T.A., and Cormell, E.P., "State-variable steady-state analysis of a controlled current induction motor drive", IEEE Trans. (IA), Vol. 11, pp. 704, Nov./Dec. 1975.

15. Lipo, T.A., "Simulation of a current-source inverter drive", IEEE Trans.(IECI), Vol. 26, pp. 98, May 1979.

16. Malvino, A.P., "Electronic Principles", Tata Mcgrow Hill, New Delhi 1983.

17. Murphy, J.M.D., "Thyristor Control of A.C. Motors", Pergamon press Ltd., Oxford, 1973.

18. Nelson, R.H., and Radomski, T.A., "Design method for Current-Source Inverter, induction motor drive system," IEEE Trans. (IECI), Vol.21-22, pp. 141, May,1975.

19. Nobuhiko, S. and Noriaki, S., "Steady-state and stability analysis of induction motor driven by current-source inverter", IEEE Trans. (IA), Vol.13, pp. 244, May/June, 1977.

20. Osman, R.H., "An improved circuit for accelerating commutation in current-source inverter", IEEE Trans. (IA), Vol.20, pp.742, July/Aug. 1984.

21. Phillips, K.P., "Current-source converter for A.C. Motor Drives", IEEE Trans. (IA), Vol.8, pp. 679, Nov./Dec., 1972.

22. Revankar, G.N., and Bashir, A., "Effect of circuit and induction motor parameters on current source inverter operation", IEEE Trans. (IECI), Vol.24, pp. 126, Feb. 1977.

23. Ramamoorty, M., "An introduction to thyristors and their applications," Affiliated East-West Press Pvt. Ltd., New Delhi - Madras.

24. Revankar, G.N., and Pillai, S.K., "Effect of feed inductance on current-source inverter operation," Journal of the Institution of Electronics and Tele-communication Engineers, Vol.28, pp.30, Jan. 1982.

25. Rasappa, G.R.P., "Voltage clamping circuits for CSI/IM drives," IEEE Trans. (IA), Vol.21, Part I, pp. 429, March/April 1985.

26. Revankar, G.N., and Pillai, S.K., "Reduction of commutation period in current source inverters", Journal of the Institution of Engineers, Vol.62, pp. 198, Feb. 1982.

27. Revankar, G.N., and Havanur, S.S., "Controlled slip variable flux induction motor drive system", Journal of the Institution of Engineers, Vol.63, pp.45, Oct. 1982.

28. Sen, P.C., "Thyristor D.C. Drives", Willey, NEW YORK 1981.

29. Sharma, M.C., "555 Timer and its applications", (Business Promotion Publication, Delhi 1978.

30. Subrahmanyam, V., "A method for the analysis and design of current-source inverter induction motor drive," International Conference on electrical machines 84, Lausanne, Switzerland.

31. Venkatesan, K., and Lindsay, J.F., "Comparative study of the losses in voltage and current source inverter fed induction motors", IEEE Trans. (IA), Vol.18, May/June 1982.

32. Ward, E.E., "Inverter suitable for operation over a wide range of frequency", IEE Proc., Vol.111, pp. 1423, Aug. 1964.

33. Yuvrajan, S., "Analysis of a current controlled inverter fed induction motor drive using digital simulation", IEEE Trans. (IECI), Vol. 27, pp.67, May 1980.

ADDITIONAL LITERATURE ON APPLICATION AND ANALYSIS OF CURRENT SOURCE INVERTER

1. Bashir, A., and Pradhan, B.D., "Alternative configuration for Nabae's multiple current-source inverter", Journal of the Institution of Engineers, Vol.64, pp.148, Dec. 1983.

2. Gordon, R.S., "Synchronous Motor drive with current-source inverter", IEEE Trans. (IA), Vol.10, May/June 1974.

3. Krishnan, R., and Lindsay, J.F., "Design of Angle-Controlled current source inverter fed induction motor drive", IEEE Trans. (IA), Vol.19, pp. 370, May/June 1983.

4. Lipo, T.A., and Walker, L.H., "Design and Control techniques for extending high frequency operation of a CSI induction motor drive", IEEE Trans. (IA), Vol.19, pp.744, Sept./Oct. 1983.

5. Ong. C.M., and Lipo, T.A., "Steady-state analysis of a current-source inverter/reluctance motor drive-I", IEEE Trans.(PAS), pp.1145, Vol.96, 1977.

6. Ong. C.M., and Lipo, T.A., "Steady-state analysis of a current source inverter/reluctance motor drive-II", IEEE Trans.(PAS), Vol.96, pp. 1145, 1977.

7. Palaniappan, R., and Vithayathil, J., "The current fed twelve step current source inverter", IEEE Trans.(IECI), Vol.25, pp.377, 1978.

8. Palaniappan, R., and Vithayathil, J.,"Principle of dual current source inverter for a.c. motor drives", IEEE Trans.(IA), Vol.15, pp. 451, 1979.

9. Revankar, G.N., and Havanur, S.S.,"Pulsating torque calculations in CSI fed induction motor drive system", Journal of the Institution of Engineers (India), Vol.62, pp. 262, 1982.

10. Ranganatha Rao, K.,"Current-fed induction motor analysis using boundary value approach", IEEE Trans. (IECI) Vol.24, pp. 178, May 1977.

11. Steigerwald, R.L.,"Characteristic of a current-fed inverter with commutation applied through load-neutral point", IEEE Trans. (IA), Vol.15, pp.538, 1979.

12. Salvador, M.,"Current-source double d.c. side forced commutated inverter", IEEE Trans.(IA), Vol.14, pp.581, 1978.

13. Suzuo, S., and Nakagawa, T.,"New application of current-type inverter", IEEE Trans. (IA), Vol.20, pp. 226, Jan./Feb. 1984.

14. Turton, R.A.,"Stability of synchronous motors supplied from current source inverters", IEEE Trans. (PAS), Vol.98, Jan./Feb. 1979.

15. Teruo, K., "Steady-state characteristics of a CSI/Double-wound synchronous machine system for A.C. power supply", IEEE Trans. (IA), Vol. 16.

16. Yasuhiko, D., "Stabilization of controlled current induction motor drive systems via non-linear state observer", IEEE Trans. (IECI), Vol.27, May 1980.

17. Ziogas, P.D., and Manias, S., "Application of current source inverters in UPS system", IEEE Trans.(IA), Vol.20, pp.742, July/Aug. 1984.

APPENDIX 'A'

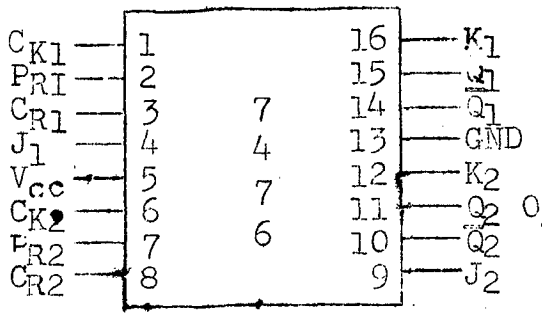

DUAL LEVEL TRIGGERED
MASTER SIAVE J.K. F/F

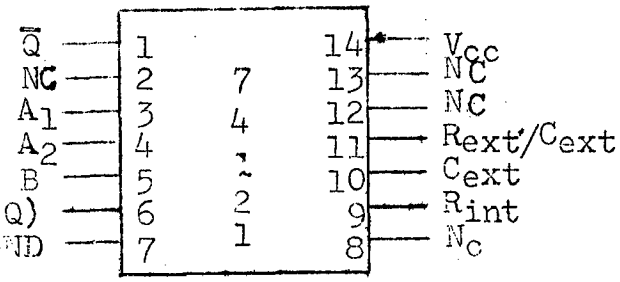

MONOSTABLE MULTIVIBRATOR

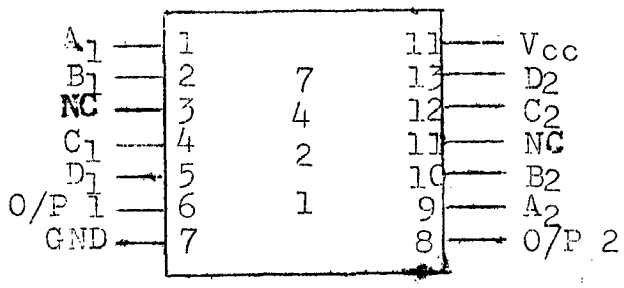

DUAL 4-INPUT POSITIVE-AND
GATES

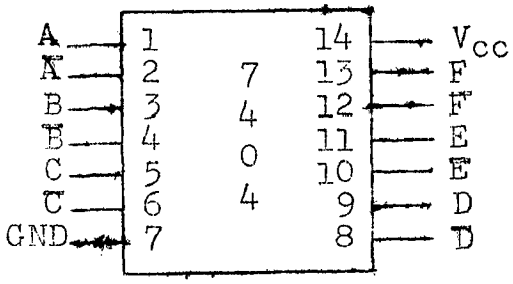

HEX INVERTER

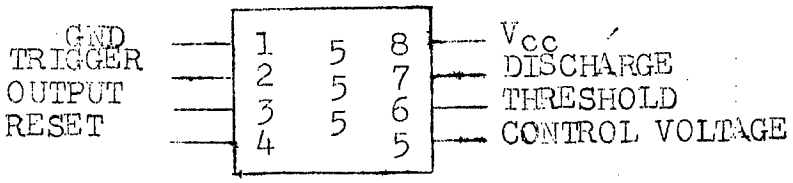

TIMER

Pin Details of Different I.C. Chips

APPENDIX B

CONNECTION DIAGRAMS OF DIFFERENT I.C. CHIPS

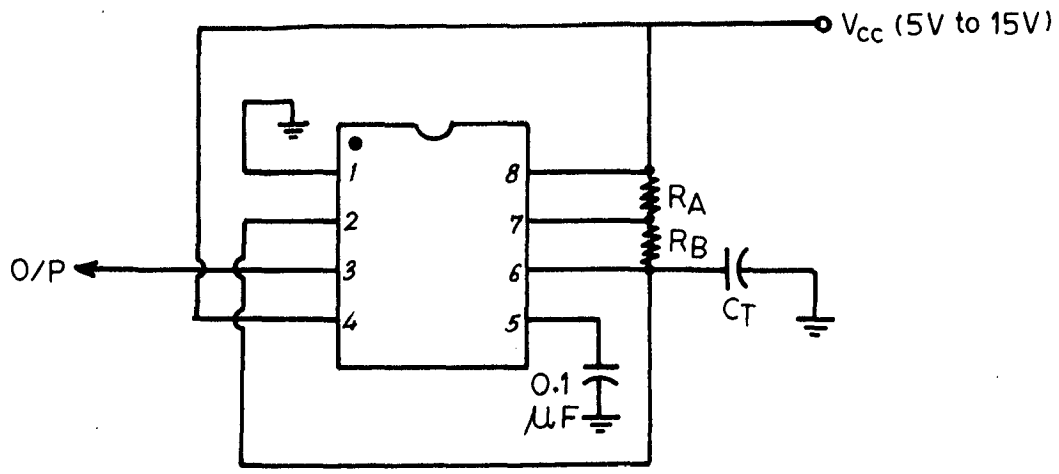

Astable operation of 555 timer

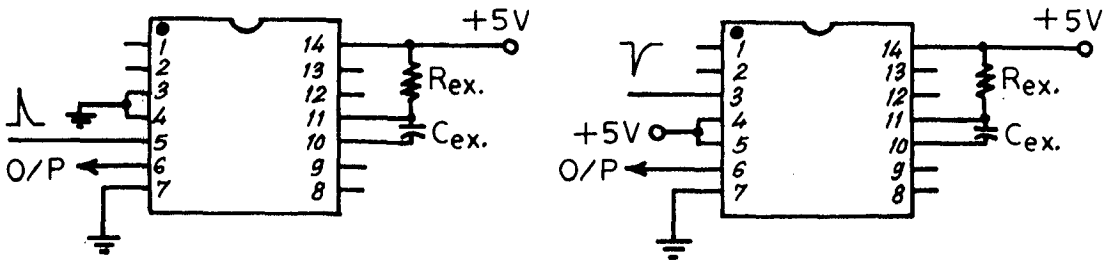

Monostable operation of IC 74121 for rising and falling edge

APPENDIX 'C'

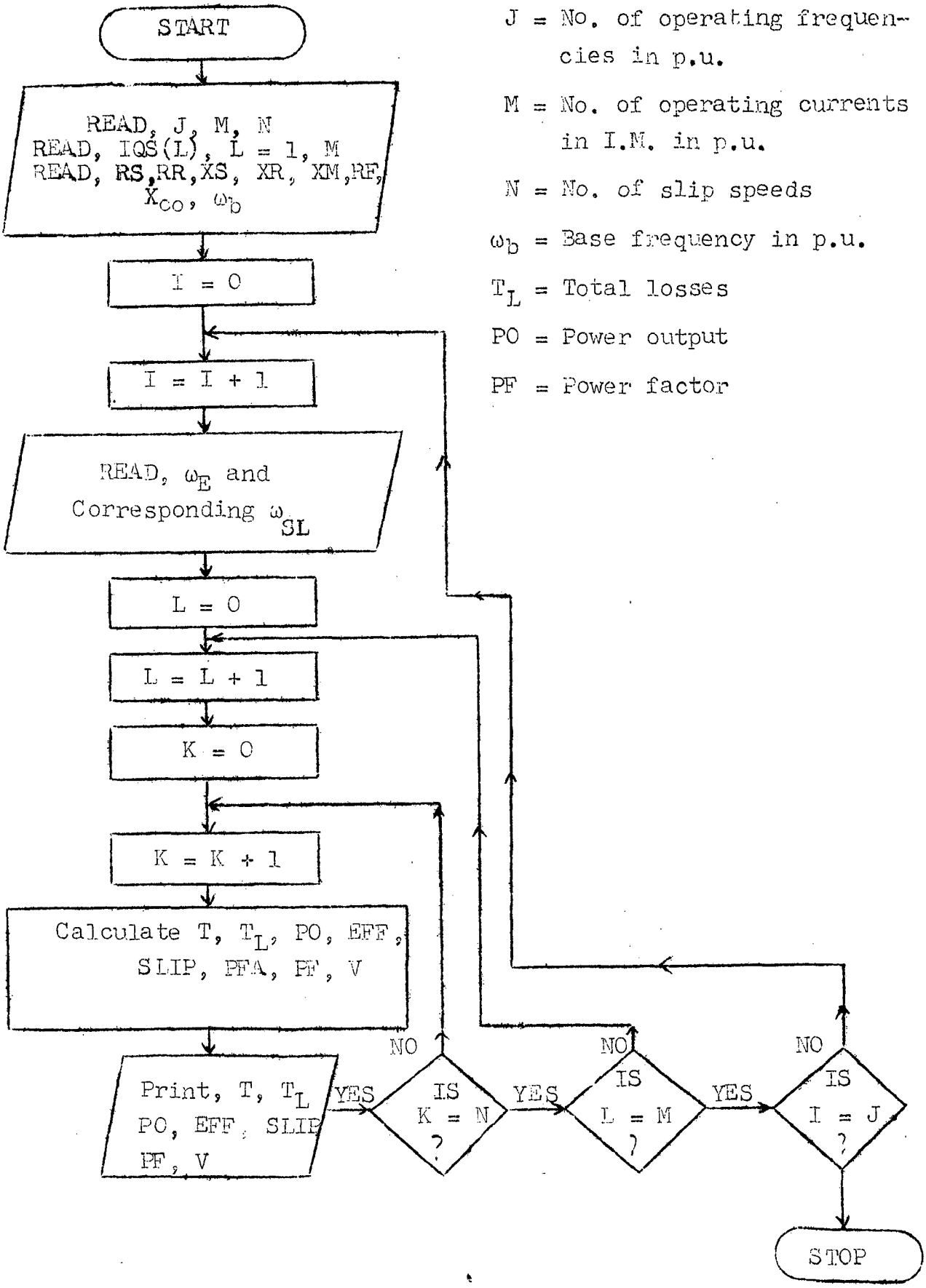

J = No. of operating frequencies in p.u.

M = No. of operating currents in I.M. in p.u.

N = No. of slip speeds

ω_b = Base frequency in p.u.

T_L = Total losses

PO = Power output

PF = Power factor

Flow Chart For Steady-State Analysis

APPENDIX 'D'

PROGRAM NO 6

```
C     ************************************************************
C        STEADY STATE ANALYSIS OF  CSI FED SQ.CAGE INDUCTION MOTOR
C     ************************************************************
C     WE = OPERATING  FREQUENCY  IN  P.U.
C     FIQS = D.C.  LINK  CURRENT  IN  P.U.
C     WSL = SLIP  SPEED  IN  R.P.M.
C     U  = SLIP  SPEED  IN  P.U.
C     WB = SYNCHRONOUS  SPEED  OF  INDUCTION  MOTOR  IN  R.P.M.
C     AT  BASE  FREQUENCY
C     RS = PER  PHASE  STATOR  RESISTANCE  IN  P.U.
C     RR = PER  PHASE  ROTOR  RESISTANCE  IN  P.U.
C     XS = PER  PHASE  STATOR  SELF  INDUCTANCE  IN  P.U.
C     XR = PER  PHASE  ROTOR  SELF  INDUCTANCE  IN  P.U.
C     XM = MUTUAL  INDUCTANCE  BETWEEN  STATOR  AND  ROTOR  INP.U.
C     RF = D.C. LINK  INDUCTOR  RESISTANCE  IN  P.U.
C     XCO = COMMUTATING  REACTANCE  IN  P.U.
C     ************************************************************
      DIMENSION WE(4),FIQS(8),WSL(100),U(100)
      OPEN(UNIT=1,DEVICE='DSK',DIALOG)
      OPEN(UNIT=12,FILE='TS1.DAT',DEVICE='DSK')
      OPEN(UNIT=4,FILE='TS2.DAT',DEVICE='DSK')
      OPEN(UNIT=3,FILE='TS3.DAT',DEVICE='DSK')
      OPEN(UNIT=2,FILE='TS5.DAT',DEVICE='DSK')
      OPEN(UNIT=7,FILE='TS6.DAT',DEVICE='DSK')
      OPEN(UNIT=8,FILE='TS4.DAT',DEVICE='DSK')
      READ(1,*),J,M,N
      READ(1,*),(FIQS(L),L=1,M)
      READ(1,*),RS,RR,XS,XR,XM,RF,XCO,WB
      PRINT*,J,M,N
      PRINT*,(FIQS(L),L=1,M)
      PRINT*,RS,RR,XS,XR,XM,RF,XCO,WB
      A=XR*XR
      B=RR*RR
      C=XM*XM
      DO5I=1,J
      READ(1,*) WE(I),(U(K),K=1,N)
      PRINT*,WE(I),(U(K),K=1,N)
```

```
      PROGRAM  NO  6
      DO5L=1,M
      PRINT10,WE(I),FIQS(L)
10    FORMAT(30X,'PU OPERATING FREQUENCY =',F8.3,5X,'FIQS='F12.8)
      DO5K=1,N
      WSL(K)=U(K)/WB
      D=WSL(K)*WSL(K)
      E=D*A+B
      FIDR=WSL(K)*XM*RR*FIQS(L)/E
      T=XM*FIQS(L)*FIDR
      TL=FIQS(L)*FIQS(L)*(RS+RF+D*C*RR/E)
      PO=T*(WE(I)-WSL(K))
      EFF=PO/(PO+TL)
      SLIP=WSL(K)/WE(I)
      VQS=(RS+WE(I)*WSL(K)*C*RR/E)*FIQS(L)
      VDS=WE(I)*FIQS(L)*(-XS+C*D*XR/E)
      PFA=ATAN(-VDS/VQS)
      PF=COS(PFA)
      V=SQRT(VQS*VQS+VDS*VDS)
      Z=PO+TL
      PIN=VQS*FIQS(L)
      WRITE(12,*),SLIP,EFF
      WRITE(4,*),SLIP,PO
      WRITE(3,*),SLIP,T
      WRITE(8,*),SLIP,TL
      WRITE(2,*),SLIP,V
      WRITE(7,*),SLIP,PF
C        PRINT*, SLIP,T,PO,TL,EFF,V,PF,C,PIN,X
5     PRINT*,SLIP,PO,V,PF,VQS,Z,PIN
      STOP
      END
```

APPENDIX 'E'

Measured Values of P.U. Parameters of the I.M. and D.C. Link Inductor

R_s	Stator resistance per phase	= 0.049
R_r	Rotor resistance per phase	= 0.0656
X_s	Stator self reactance per phase	= 1.913
X_r	Rotor self reactance per phase	= 1.913
X_M	Magnetising reactance per phase	= 1.84
R_F	D.C. link inductor resistance	= 0.025
X_F	D.C. link inductor reactance	= 3.95